AN ABSTRACT OF THE THESIS OF

Homam Mohammed-Zahid Al-Baroudi for the degree of Doctor of Philosophy
in Nuclear Engineering presented on March 30, 1993.
Title: Experimental Simulations of a Rotating Bubble Membrane
Radiator for Space Nuclear Power Systems

Redacted for Privacy

Abstract Approved:_____
Andrew C. Klein

A rotating, flat plate condensation experiment has been developed to
investigate the heat of the Rotating Bubble Membrane Radiator (RBMR). The
RBMR is a proposed heat rejection system for space applications which uses
working fluid condensation on the inside surface of a rotating sphere to
reject heat to space. The flat plate condensation heat transfer
experiment simulates the microgravity environment of space by orienting
the axis of rotation parallel to the gravitational vector and normal to
the surface of the plate. The condensing surface is cooled to simulate the
rejection of heat to cold surface. The working fluid is a super heated
steam.

The results obtained include relationships between the overall heat
transfer coefficient as a function of the temperature difference between
the working fluid and a cold environment, both placed in dimensionless
groups, and plate angular rotational speeds. This empirical relationship
is useful for choosing the optimum rotational speed for the flat plate

radiator given a desired heat rejection load.

A RBMR prototype, using full sphere shell, was designed and built completely in this research efforts and ready to be tested in future planned experiments in microgravity environment. This RBMR is the first one ever built to investigate the RBMR concepts experimentally.

This study also provides the basis for designing new heat rejection systems utilizing centrifugal forces and condensation phenomena in both space and ground applications.

Experimental Simulations of a Rotating Bubble
Membrane Radiator for Space Nuclear Power Systems

by

Homam Mohammed-Zahid Al-Baroudi

A THESIS

submitted to

Oregon State University

in partial fulfillment of
the requirements for the
degree of

Doctorate of Philosophy

Completed March 30, 1993

Commencement June 1993

APPROVED:

Redacted for Privacy

_____
Associate Professor of Nuclear Engineering in charge of major

Redacted for Privacy

_____
Head of Department of Nuclear Engineering

Redacted for Privacy

_____
Dean of Graduate School

Date thesis is presented ____March 30, 1993_____

Typed by_____Homam M. Al-Baroudi_____

ACKNOWLEDGMENT

TABLE OF CONTENTS

LIST OF FIGURES

LIST OF TABLES

Experimental Simulations of a Rotating Bubble Membrane
Radiator for Space Nuclear Power Systems

I. BACKGROUND

I.1 Brief Review Of The United States Space Nuclear Power Program :

The use of nuclear energy in space applications was considered almost as early as the first nuclear reactor was built. In 1948, the Air Force commissioned the Rand Corporation to recommend development work for reconnaissance satellite programs known as Project Feedback. The growing need for a reliable power source for space applications was addressed. Specialized studies on nuclear-electric sources for space applications were done under the Pied Piper Program conducted in 1954[1].

From 1952 to 1955 the Atomic Energy Commission (AEC), now known as Department of Energy (DOE), performed an analysis of nuclear power sources and evaluated them on their feasibility to be used with future spacecraft. In 1955, a joint Air Force-AEC committee established specifications for nuclear power in space[1].

The Space Nuclear Auxiliary Power (SNAP) program was initiated in 1955 and terminated in 1973. The objective of the AEC's SNAP program was the development of compact, light-weight, reliable atomic electric devices for space, sea, and land uses. During that period approximately $850 million then-year dollars were spent to develop nuclear power sources capable of producing from 500 W up to 1000 kW of electricity. The technology encompassed a wide range of materials and power conversion systems. The SNAP reactor program was the beginning of the development of compact nuclear reactor systems for space applications, which are capable

of producing high power levels at a small specific weight, this is defined as the total mass of the system, in Kg, divided by the amount of electrical power output of this system, in KW_e[1].

In the 1960's, there was considerable interest in the use of radioisotopes for propulsion systems. One of the most successful nuclear space programs in the U. S. is the development of Radioisotope Thermoelectric Generators (RTGs) where the heat generated from the alpha particle decay of Pu-238 is used. Some RTGs could reach power levels as high as multi hundred Watts. The efficiency of these RTGs is roughly 5 to 7%. Several improvements and new designs have been going on for several years. The production cost of Pu-238 fuel has risen over the past few years. Also Pu-238 availability, whenever it is needed, to support the isotope power systems is another concern. These two considerations have led to development of alternate power system concepts to provide better utilization of this limited resource [2,3,4,5].

In March 1983 the United States initiated the SP-100 program to develop a Space Reactor Power System (SRPS) capable of providing the increased power levels required to support new horizons in the exploration of space, and in the maintenance of national security against threats into the next century. During the first three years of the program, system studies were performed and critical feasibility issues were addressed. The result was the selection of a concept using a fast spectrum reactor coupled to thermoelectric energy conversion units by magnetically pumped liquid lithium which, in turn, is coupled to individual heat pipe radiator panels to reject the waste heat to space. Since that time, considerable progress has been made in developing the space reactor power system. The

program is presently in the detailed design and component development phase. Extensive testing of the power systems' critical components is underway. Liquid metal testing of the heat transport, energy conversion and heat rejection components and subsystems is planned for the period 1995 to 1998, while testing of the Nuclear Assembly (reactor,shield,and controls) is planned for early FY 2003[6].

Nuclear Propulsion has been identified as a key technology by several groups that have studied how to go back to the Moon, establish a human presence on Mars, and explore space beyond Mars[7].

On 20 July 1989, President George Bush provided a new strategic focus to the United States civil space program called the Space Exploration Initiative (SEI). The SEI has as its goals the completion of space station Freedom, the return to Moon, and then humans to Mars. In response to the president's space policy speech of July 1989, the National Aeronautics and Space Administration (NASA) conducted a series of studies to synthesize the results of several years of exploration mission studies and to define feasible mission options and their requirements. It has been noted in several recent NASA studies that the use of nuclear-powered systems offers a number of potential advantages. One of these is providing power for a round trip in Mars of less than one year[8,9].

For the last few decades extensive work has been done to find reliable concepts and ways to effectively reject heat generated by space systems to space. These studies have ended up with a few concepts that have been studied intensively since then. One of the most reliable one is Heat Pipes. Heat pipes are highly reliable and efficient energy transport devices which operate passively in vacuum and zero-gravity. In power

systems and space platforms, such as the space station, heat pipes are used either as the main energy transport device or in the radiator for heat rejection. Heat pipes operating at temperatures in excess of 700 K employ liquid metal working fluids such as potassium, sodium and lithium while those operating at lower temperatures may employ nonliquid-metal fluids, such as water or ammonia[10]. Several improvements are being made to heat pipe concepts to meet other space mission criteria such as low system mass. Replacement of components of a space system heat pipe by Advanced Ceramic Fabrics (ACF) will decrease system mass considerably.

I.2 Description of the Rotating Bubble Membrane Radiator :

Since the figure of merit used in defining any space power system is the specific power (in electrical power output per unit power system mass), the decrease in the mass of any reactor system component will yield a tremendous benefit to overall system performance. This has certainly been the case for the SP-100 space nuclear reactor program during the SP-100 minimization project that has been underway over the last few years, and likely will continue until an acceptable reactor system is completed. Also, since the heat rejection system of any power system can make up a large portion of the total system mass, any reduction in the mass of the heat rejection radiators will significantly affect the performance of the power system.

Recently, composite materials which combine the high strength, flexibility, and low mass characteristics of ceramic fabrics with the attractive compatibility and heat transfer features of metallic foils,

have been proposed for use in a number of space radiator applications. Thus, the weave of the fabric and the high strength capability of the individual fibers can be combined with the high thermal conductivity and chemical stability of a metallic liner to provide a light weight, flexible alternative to heavy, rigid, metallic radiator structured containers[12].

The Rotating Bubble Membrane Radiator (RBMR) concept was developed specifically to take advantage of the developments in fabric material technology which are combined with the change of phase in a working fluid to provide a significant reduction in radiator mass. Emissivity tests of the composite material have shown recently that significant improvements can be made which will greatly enhance the radiation of waste heat to space. Further studies of these developments, both analytical as well as experimental, are required in order to quantify the potential application of this attractive radiator concepts[12]. The RBMR, shown in Figure (I.1), is an enclosed two-phase direct contact heat exchanger.

In this system, the two-phase working fluid enters the radiator via feed lines incorporated within the central axis of rotation. The working fluid is then ejected from the central spray nozzle as a combination of liquid droplets and vapor into the radiator envelope. Within this envelope, both convection and radiation heat transfer occur between the droplets, the vapor, and their cooler surroundings, with the dominant mode

Return Pump
Collection
Trough

Return Piping/
Structural

Central
Rotation
Shaft

Radiating
Surface

Central
Spray
Nozzle

Rotation Platform

Attachment Boom

Feed/Return
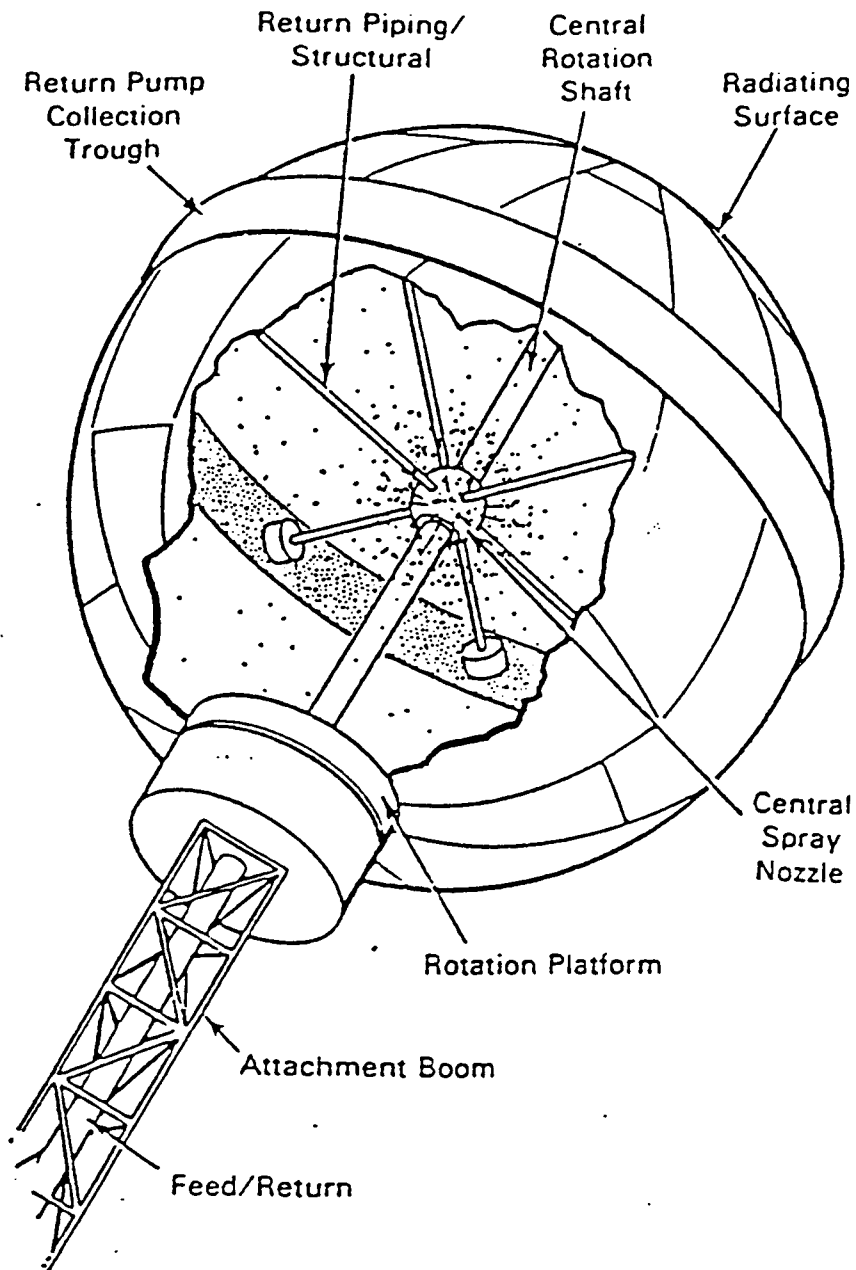
Figure (I.1) Schematic Diagram of the Rotating
Bubble Membrane Radiator.

of heat transfer being radiation. As the droplets move radially outward, they grow in size by the condensation of vapor upon their surface and by collision with other droplets before striking the thin liquid film on the inner surface of the radiator. Once assimilated into the thin surface film, the working fluid begins to flow from the poles of the sphere toward the equator due to the rotationally induced artificial gravity. Heat transfer between the fluid and bubble radiator then becomes a combination of conduction and convection. As the fluid reaches the equator of the sphere, it is collected in gravity wells (troughs) and pumped back to repeat the process. Some other geometries of the RBMR are also proposed. Figure (I.2) shows some of these configurations.

To operate effectively in space, the RBMR will include design features to minimize damage and mitigate coolant losses that may result from meteoroid and space debris impact. In addition, design options are being considered that would seal membrane penetrations and reduce coolant losses from micro-meteoroids[13].

I.3 RBMR Simulations :

In order to begin to understand the fluid and heat transfer phenomena associated with the RBMR, a condensation experiment has been developed which reduces the problem of gravity. It is obvious that it is very difficult to simulate a spherical radiator for a space application (where the gravity is negligible) on the earth (where the gravity plays a large role). Any ground based experiment needs to take into account the force exerted by gravity on the fluid droplets to the equator of the
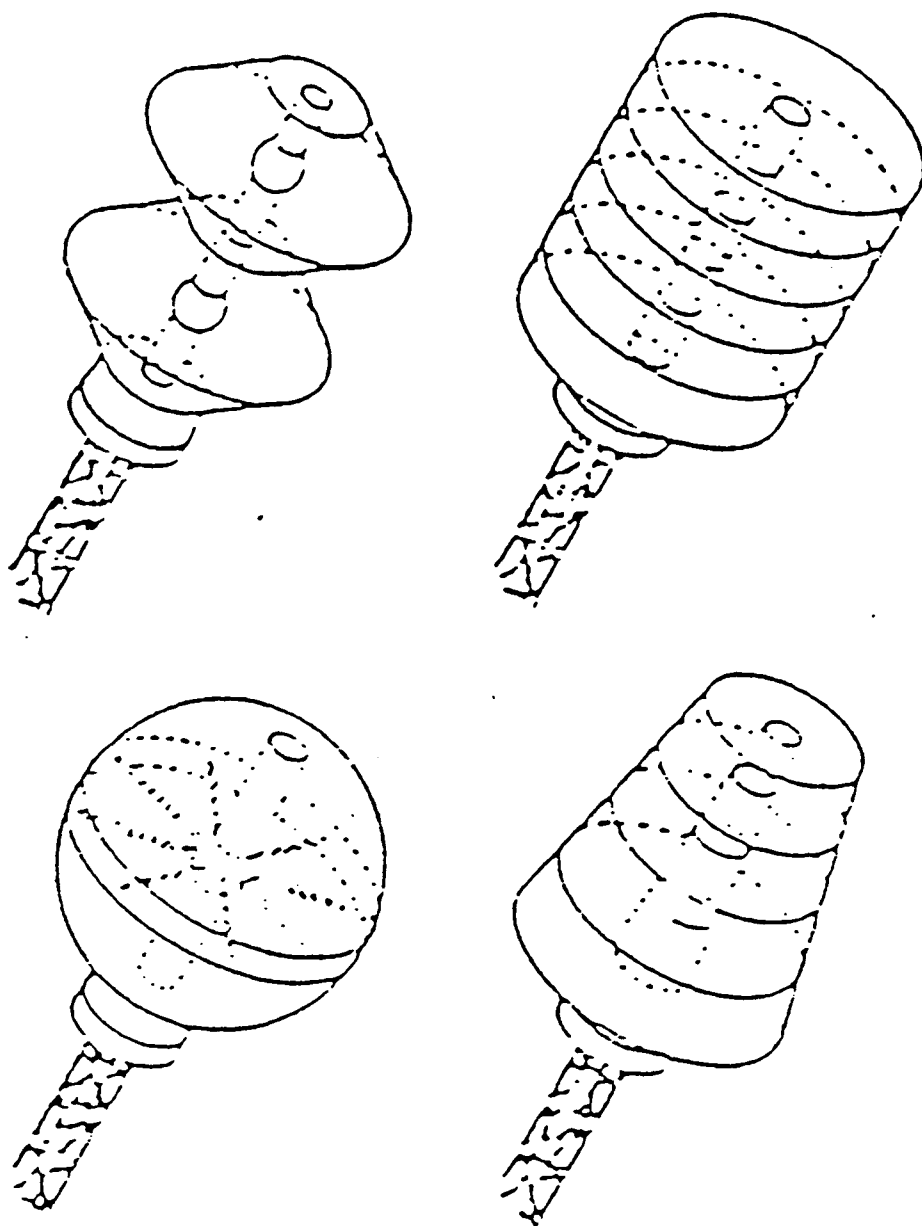
Figure (I.2) Proposed RBMR Configurations.

sphere. The effect of the gravitational field can be minimized by using a flat plate in which its axis of rotation is parallel to the gravity vector. As the working fluid condenses, the centrifugal force will pump the droplets towards the edge of the plate and gravitational force does not play as important a role. As a result, it is expected that the pumping capability, fluid transport phenomena, and thermal behavior which would be expected in a spherical RBMR in zero gravity can be simulated in the flat plate experiment in normal gravity. The main part of this study is devoted to investigate the thermal behavior of the condensation phenomena on a rotating flat plate experiment in normal gravity.

The construction of a full sphere simulation, i.e. an RBMR prototype, will be necessary for the purpose of comparing results of both tested configurations, flat and sphere, on the ground based tests. Since the flat plate experiment was assumed to describe the behavior of the full sphere in microgravity, this will show the effect of the gravity on the RBMR. The RBMR prototype will be, also, the first one ever built to test the RBMR's concepts experimentally and will be ready for the proposed future testing in microgravity.

I.4 Research Objectives :

The specific objectives of this study are : 1) To design, construct, operate and demonstrate a heat rejection system using condensation on a rotating flat plate, this radiator may be used in space power systems as well as in ground systems.

2) To find the relationships between heat transfer parameters, system temperatures, and rotating speeds for the system mentioned in 1).

3) Recording the condensate thickness at different system's temperatures and rotating speeds, and the condensate flow patterns at different speeds; both experimentally.

4) To design, construct, operate and demonstrate a full RBMR prototype.

I.5 Nomenclature :

The following nomenclature is used throughout the thesis

A	=	Disk surface area, m^2
Cp	=	Specific heat of condensate, J/Kg.°C
$\overset{.}{G}$	=	Condensate volumetric flowrate, m^3/sec
h	=	Local convective heat transfer coefficient, $W/m^2/°C$
h_{avg}	=	Average condensate convective heat transfer coefficient, $W/m^2/°C$
h_{fg}	=	Latent heat of condensate, J/Kg
R	=	Disk radius, m
k_{Al}	=	Aluminum plate thermal conductivity, W/m/°C
k_{ss}	=	Stainless Steel plate thermal conductivity, W/m/°C
$\overset{.}{m}$	=	Condensation mass flow rate, Kg/sec
N	=	Number of temperature measures over a certain period of time at a specific location.
Pr	=	Prandtl number, $C_p\mu/k$
q	=	Heat transfer rate due to condensate, W

q/A = Heat flux, W/m^2

t_{Al} = Aluminum plate thickness, m

t_{ss} = Stainless Steel plate thickness, m

T_1 = Average thermo-couple temperature readings connected to channel one of data logger, °C

T_2 = Average thermo-couple temperature readings connected to channel two of data logger, °C

T_3 = Average thermo-couple temperature readings connected to channel three of data logger, °C

T_4 = Average thermo-couple temperature readings connected to channel four of data logger, °C

T_{Alo} = Average aluminum plate outer surface temperature, °C

T_{Ali} = Average aluminum plate ice-contacted (inner) surface temperature, °C

T_{av} = Average temperature of N number of readings over a certain period of time at a specific location, °C

T_c = Average cold (condensing) surface temperature, °C

T_i = Sample temperature reading at certain time and a specific location, °C

T_{wv} = Saturated water vapor temperature at given pressure, °C

U1 = Average overall heat transfer coefficient between T_{wv} and T_{Ali}, W/m^2/°C

U2 = Average overall heat transfer coefficient between T_{wv} and T_{Alo}, W/m^2/°C

ν = Kinematic viscosity of condensate, m^2/sec

ω = Angular velocity, #/sec

μ = Absolute viscosity of condensate, Kg/m.sec

σ^2 = The average value of the squared deviation of each data point from the true value; it is called variance.

σ = The positive square root of the sample; it is called the standard deviation.

δ = Thickness of condensate layer, m

II. LITERATURE REVIEW

II.1 Introduction :

Condensation phenomena are a world wide concern because of their many applications in different scientific areas. The behavior of condensation under normal gravitational fields (1 g) has been investigated extensively on stationary. However, there has been much less study on rotating surfaces. A number of interesting, primarily analytical, studies were conducted in the late 1950's through the early 1990's.

In the film-wise condensation of vapor, the latent heat of condensation passes through a film of liquid on its way to the condensation surface. The predominant mode of heat transfer through the film is conduction. Since most liquids have a low thermal conductivity, the condensate film provides a substantial resistance to heat transfer. If the condensate film is not removed from the condensing surface, it thickens and increases the resistance to heat transfer. In most industrial condensers, the condensate continually drains away from the cooled surface by gravity. For condensation on a vertical or inclined surface, the film thickness and hence the resistance to heat transfer increases with the distance from the top of the surface[14].

It is now well recognized that centrifugal forces generated in a rotating system may be utilized to replace the gravity force in the condensation process. Rotating condensation systems appear potentially attractive for space vehicle applications, where the force of gravity is

essentially zero. In addition, rotating condensation also seems promising for earth-bound applications where higher condensation rates are desired than are obtainable with gravity[15].

A thin liquid film is quite commonly found during evaporation or condensation on a solid surface in many engineering devices such as compact heat exchangers and spin coating in metal industries where it flows along condensate surfaces. Studies on thin liquid film flows have been studied extensively. Moreover, the understanding of such flows under reduced or zero gravity, where the flow is acted on only by viscous and inertial forces, is essential for the proper design of heat exchangers and heat pumps for space applications[16].

II.2 Condensation Heat Transfer on a Rotating Flat Plate :

Laminar film condensation on a vertical plate first became a subject of analytical study in 1916 with the work of Nusselt[17]. Since then, studies on condensation heat transfer have been largely concerned with the situation of gravity-induced flow. Nusselt neglected the effects of both energy convection and fluid accelerations within the condensate layer. Over the years, there have been a number of improvements to Nusselt's analysis. The pioneering work of E. M. Sparrow and J. L. Gregg in 1959 on the boundary-layer treatment of laminar film condensation and the theory of rotating condensation[17,18] opened the door for more analytical, numerical, and experimental investigations of condensation phenomena on various rotating surfaces such as cones[15], spheres[19], drums[20], curved bodies[21], tubes with suction at the wall[22], and pinned

tubes[23]. In the absence of gravity or the generation of sufficient centrifugal force, the orientation of the plate becomes immaterial, and an identical flow condition is achieved whether the plate is horizontal, vertical, or inclined[24].

Sparrow and Gregg[17] analytically studied film condensation on a rotating disk situated in a large body of pure saturated vapor. The centrifugal field associated with the rotation of the plate sweeps the condensate outward along the disk surface, and gravity forces were not involved. The problem was formulated as an exact solution of the complete Navier-Stocks and energy equations. Numerical solutions were obtained for Prandtl numbers between 0.003 and 100 for $C_p \Delta T / h_{fg}$ in the range 0.0001 to 1.0. Results were given for the local heat transfer, as well as for the condensate layer thickness, torque moment, and temperature and velocity profiles. In this pioneering work, the following results were obtained :

1) For a particular liquid and a fixed temperature difference, the local heat-transfer rate per unit area is proportional to the square root of the disk angular velocity, or

$$q'' \propto \omega^{1/2}$$

2) It is found that the local heat transfer coefficient of the condensate verses temperature difference across the film condensate, both in dimensionless groups, is represented by Figure (II.1)
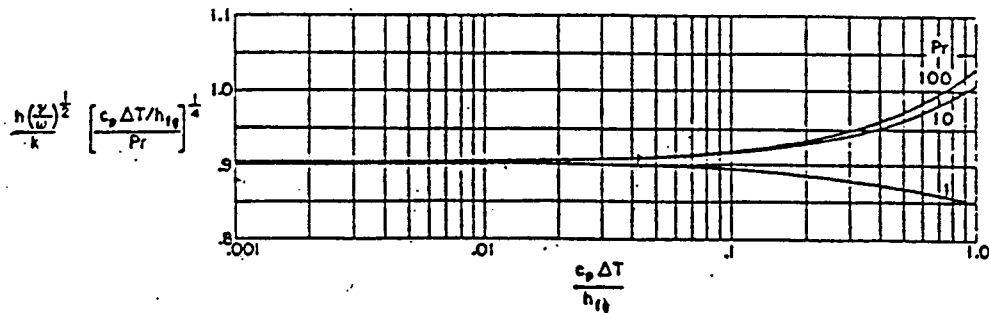
Figure (II.1) Predicted Local Heat Transfer Coefficient for Working
Fluids of Different Prandtl Numbers[17].

By inspection of this Figure, it is seen that for small values of C_p
$\Delta T / h_{fg}$, all the results are represented by

$$\frac{h(\frac{\nu}{\omega})^{1/2}}{K} = 0.904 \left(\frac{Pr}{\frac{Cp\Delta T}{h_{fg}}}\right)^{\frac{1}{4}} \qquad (2.1)$$

This equation corresponds precisely to the heat transfer result for
the situation where energy convection and acceleration terms are
negligible. Therefore, departures from this relationship represent the
effects of convection and inertia, the former tending to increase the heat
transfer and the latter tending to diminish it. For high Prandtl numbers
the effect of energy convection becomes relatively more important than
inertia effects, while for small Prandtl numbers the argument is vice
versa. The analysis shows that for thin condensate layers, the energy
convection and inertia tend to become negligible.

3) The temperature profile across the condensate layer closely approximates a straight line[17].

S. S. Nandapurkar and K. O. Beatty, Jr., in 1960 published their experimental results using methanol, ethanol, and Freon-113 all at atmospheric pressure. The centrifugal force has been shown to be an effective method for the continuous removal of condensate from a horizontal plate condenser[25].

Measured heat transfer coefficients for condensing methanol, ethanol, and Freon-113 vapors on a rotating surface have been shown to be about 25-30% below those predicted by the theory of Sparrow and Gregg. This deviation from the theory was attributed to neglecting the effect of the vapor drag on the liquid film in the theoretical analysis, which would have a force component inward along the radius of the disk, and thus would tend to retard the condensate flow and produce a thicker condensate layer on the disk. Figure (II.2) shows some of these reported results[25].
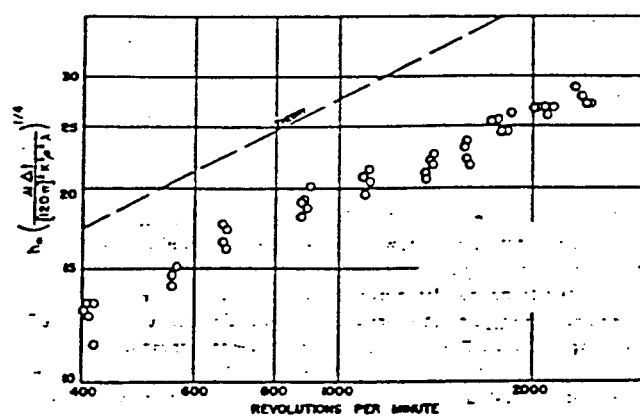
Effect of rotational speed for methanol
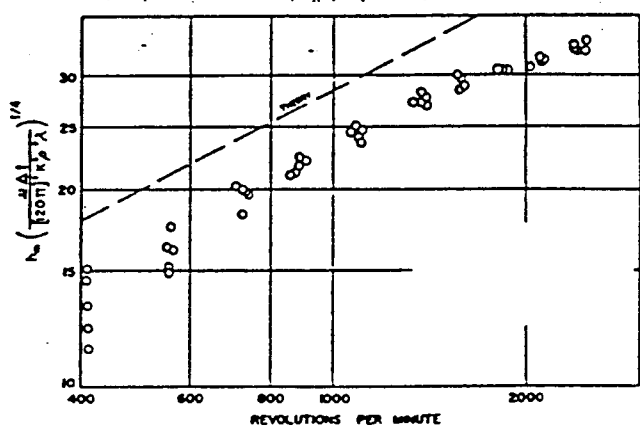
Effect of rotational speed for ethanol
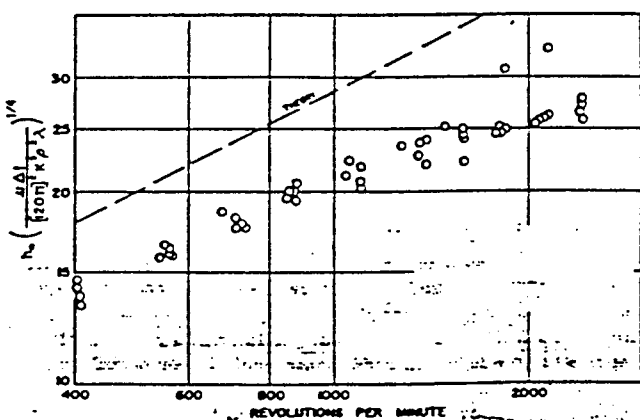
Effect of rotational speed for Freon-113.

Figure (II.2) Effect of the Rotational Speeds for Different Working
Fluids on Mean Heat Transfer Coefficient[25].

E. M. Sparrow and J. L. Gregg, in a technical briefing in February of the same year, added the effect of vapor drag to their previous analysis of heat transfer and showed that the effect was quite small. It was claimed that the deviation between theory and experiment must be laid to other causes[26].

One important experimental work was done by A. I. Butuzov and V. F. Rifert in 1972. The primary motivation for this study was to determine the heat transfer coefficients for steam condensing at a rotating surface which has the form of a disk for sea-water distillation. Their experimental study of the condensation of steam was carried out on a copper disk, 0.3 m in diameter, rotating in the horizontal plane. The experimental equipment was a closed circuit, consisting of a test condenser, electric boiler, steam super-heated and condensate collector. The experiments were carried out at disk speeds ranging from 10 to 224 rpm and heat flux densities from $2x10^4$ to $19x10^4$ W/m^2. In all the experiments the steam was forced to condense at the downward face, i. e. the bottom surface where Sparrow and Gregg analysis assumed the condensate to occur on the upward surface of the disk where gravitational forces have much less effect.

The experiments showed that at constant disk rotational speeds the average condensation heat transfer coefficient decreased with increasing heat flux or temperature difference and the average heat transfer coefficient was found to be proportional to the average temperature difference to the -0.25 power (characteristic of laminar condensate flow). In equation form this is given as

$$h_{avg} \propto (\Delta T)_{avg}^{-0.25}$$

For less than 52 rpm, the power of the angular velocity was 0.23, this was attributed to the fact that at low rpm the condensate film flow at disk segments closer to the center of rotation is affected by gravitation forces which makes for separation of individual droplets from the film; while for high rpm the condensate film flow and the heat transfer are determined primarily by the effect of centrifugal forces and the previous relationship was applicable.

Comparing experimental data with the theoretical predictions of the heat transfer parameter (the theoretical expression that was derived in this work is close to the one developed by Sparrow and Gregg[17]) showed a good agreement with the experimental points lying about 5-10% below the theoretical predictions. This was attributed to the fact that the theoretical expression derived in this work has neglected the circular motion of the condensate film on the rotating disk, which increases the film thickness and the thermal resistance to heat transfer.

The rotation of the surface aids in augmenting the heat transfer during the film-wise condensation of steam. All other conditions remaining equal (the same temperature difference and surface area) the average heat transfer coefficient for a rotating disk is 3-5 times greater than the heat transfer from steam condensing on a stationary vertical surface, where the condensate flows by gravity[24].

In 1972 P. M. Beckett, P. C. Hudson and G. Poots[27] employed regular perturbation theory methods to investigate the problem of laminar film condensation on a rotating disk in a large volume of quisencent vapor. Exact numerical solutions were obtained for the case of steam-water condensation and compared with those derived analytically. The flow

configuration was as follows. An infinite disk is held at constant temperature with controlled known angular velocity in a large volume of quiescent pure vapor at the saturation temperature, and greater than the disk temperature. A condensate film is formed on the disk and a steady state axially symmetric flow exists in which both vapor and condensate are swept radially outwards in spiral paths away from the axis of rotation. The steady renewal of condensate maintains the interface in a fixed position. The actual location being dependent on the magnitude of rotation and the rate of cooling of the disk surface. The analytical results of this work showed better agreement with experiments[25] than those proposed by Sparrow and Gregg[17].

However, despite all these arguments, the theoretical predictions of Sparrow and Gregg were verified by other analytical and numerical studies[28,29,30] and they were taken for granted and used by other investigators as a base for other studies that built on them[20,31,32].

A numerical study of the three-dimensional laminar film-wise condensation over a rotating flat plate, maintained at a uniform temperature, has shown the effect of the body force on all tested aspects of the condensate film; e.g., the velocity and temperature distributions, the local mass transfer. In addition, an increase in the body force results in control of the liquid-layer thickness and thus in the condensation heat transfer[33].

Experiments for condensation on a vertical rotating finned tube, using Methanol and Isopropanol vapors, show that the condensation film heat transfer coefficient can be significantly increased by the use of centrifugal force. The fins and the rotation decrease the condensate film

thickness and hence decrease the resistance to heat transfer. Although mechanical condensers of this type are capable of much higher heat fluxes than conventional condensers, this advantage may be offset by the additional expense required to fabricate and operate a relatively sophisticated piece of equipment. However this type of condenser is suitable where the equipment must be compact or where in space vehicles the gravitational force is not available[28].

An interesting study by V. Dhir and J. Lienhard has given an expression for the local Nusselt number on arbitrary axisymmetric bodies, including vertical plates and cylinders. This practical expression is important for condensation in non uniform body force fields, or on various surfaces whose slopes change in a uniform gravity field; e.g., in space applications, in certain heat pipe configurations, and for many bodies at earth normal gravity[28].

II.3 Condensate Thickness and Flow-Patterns :

Several studies have made to obtain, analytically, an expression for the condensate thickness of a laminar liquid film on a rotating disk[17,24,34]. A very close expression, with limitations in one of the studies[17], was reached by all investigators using different approaches. The common equation is

$$\delta = [\frac{3 \nu G}{2 \Pi \omega^2 R^2}]^{1/3} \qquad (2.2)$$

According to this equation $\delta \propto \omega^{-2/3}$ [24,34]; while according to another study, for a given fluid and a fixed temperature difference $\delta \propto \omega^{-1/2}$[17]. In most studies, the film thickness is assumed to be uniform over the disk area and does not change radially[17,25,35]. This conclusion is acceptable for a problem where the gravity force of the condensate is negligible, there is a perfectly frictionless condensing surface, and the condensed liquid forms a continuous film on the disk. Even though these assumptions are reasonable in many cases and they will facilitate attacking the problem analytically and numerically it is certainly not always the case. Sometimes it is needed to develop a wall profile with variable thickness to get a constant heat flux and hence constant film thickness[20].

There have been few reports of experimental studies of thin liquid films on rotating disks. Several methods have been tried to find the thicknesses. An optical method, based on the absorption intensity of Infra-Red (IR) radiation passing through the film on a transparent disk, which also acts as the condensing surface, was used to measure the mean thickness of a water film. It was found that the film thickness was one-half to one-third of those calculated theoretically using equation 2. It was claimed that the surface may not have been completely wetted by the liquid[34,36].

S. Matsumoto, K. Saito, and Y. Takashima have measured the thickness of a liquid film on a rotating disk using a needle. The needle was movable vertically and horizontally. The thickness of liquid film at any position on the disk was obtained from the difference between the surface position of the liquid film and that of the rotating disk. The liquid

surface was determined by observing the standing waves when the head of the needle just reached the free surface. The results showed reasonable agreement with the theoretical solutions[37].

Additional methods were used in the 1980's to measure thicknesses of liquid films. One of these methods used sensing electrodes embedded into the surface of the disk, whose resistance was a function of the film thickness[38].

The major difficulty of measuring the thicknesses of liquid films on rotating surfaces is the very small thickness, particularly when using to high rotational speeds. The thickness of a liquid film was found to be smaller in a centrifugal force field than in a gravity flow and was on the order of a few microns.

Almost all of the experimental investigations have been concerned with thin liquid films which were generated by an impinging jet onto the center of a disk, i.e., the liquid films were not generated by condensation. Measuring the condensate film thickness is much more difficult since achieving a constant film thickness over the entire disk is practically impossible. The extremely thin films, especially for high angular speeds, and the vapor environment gives poor visibility and adds complexity to the many film thickness measurement techniques mentioned above.

To study the flow patterns of a flowing fluid, one needs to add some material with the same or lighter density to the working fluid, so that it will be carried along with the fluid, but not disturb the pattern. This material should be able to be observed and recorded by a camera or video equipment. Such external material is usually added in small amounts to

keep the properties of the tested fluid unchanged as much as possible. Two techniques to accomplish this will be mentioned in this review.

The first involves, using suitable grades of aluminum powder after the liquid film is already established. In order to determine the direction of motion along the streak, a high-speed flash unit is triggered at the end of the exposure interval in order to place a more intense dot on the head of each streak. For accurate quantitative measurements of the velocity from the streak lengths, it is advantageous to determine displacements between two similar images of the particle produced by the flash illumination. To do this, a delay timer is used to fire the flash a short time after the camera shutter opens in addition to firing the flash at the end. If the speed of the particle is large enough to give well-separated images, this provides two dots from which velocity can be determined (once the time interval between the flashes is found) plus a short tail which fixes the sense in which the particle moved along the streak. In this method, considerable care is needed in the adjustment of light positions and intensities, but when these are properly set it is possible to obtain very good definition of the streaks left by the particles when they are continuously illuminated during a long enough camera exposure. Figure (II.3) shows an example of this method results[39].
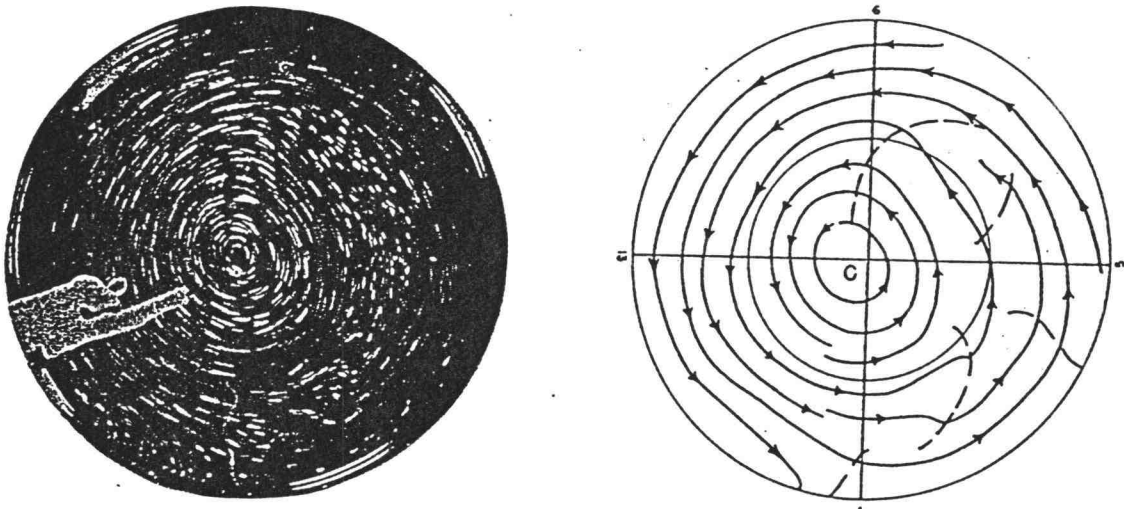
Figure (II.3) Flow Patterns Picture and Sketch Using Aluminum
Powder and Strobe Light[39].

Second, using a colored solution that has different color than the
tested fluid[25]. After the liquid film is consistently established on
the rotating disk, a solution of the working fluid and florescent powder
is introduced into the system at the plate center so they spread with the
film towards the plate edge without disturbing the film. Then the flow
patterns can be filmed by a video-camera.

II.4 Film-Wise Verses Drop-Wise Condensation :

Condensation is simply the process of conversion of a vapor to a
liquid, i.e. the reverse of evaporation. Condensation may be film-wise
when there is a continuous flow of liquid over the cooling surface, or
drop-wise when the vapor condenses in droplets and the cooling surface is
not completely covered by liquid.

After a condensate film is developed in film-wise condensation, additional condensation will occur at the liquid-vapor interface, and the associated energy transfer must occur by conduction through the condensate film. Drop-wise condensation, on the other hand, always has some surface present as the condensate drop forms and runs off. Drop-wise condensation is, therefore, associated with the higher heat transfer rates of the two types of condensation phenomena[40].

Because of the mechanism of drop-wise condensation, heat transfer coefficients can be about 4 to 20 times those of film-wise condensation. The advantages of drop-wise condensation are therefore obvious. Additives, to promote dropwise condensation by preventing the condensate from wetting the surface, are used with varying degrees of success, and are effective for limited periods of time[41]. Unlike film-wise condensation, the heat transfer coefficient in drop-wise condensation increases with the temperature difference between the vapor and the condensing surface to a maximum, then decreases because of increased condensation rates which blanket the surface and cause an approach to film-wise condensation conditions[41].

Drop-wise condensation is attractive for applications were extremely large heat transfer rates are desired; however, because of its uncertain nature and the conservative approach needed in the design of heat transfer systems, film-wise condensation heat transfer coefficients are predominately used. The condensate becomes film or drop-wise depending on whether the cooling surface is wettable[42]. Because of the difficulty of maintaining reliable drop-wise condensation in practice, film-wise heat transfer coefficients are recommended for design purposes[41].

II.5 Non-Condensable Gases Effects :

In nature and a number of technological applications, condensation of one component of a vapor in a mixture may occur in the presence of other non-condensable components. The most common example is the condensation of water vapor from air on a cold, solid surface. If the component gases are considered to be a mixture of independent substances, the condensation of one component of a vapor will occur if the temperature of the surface is below the saturation temperature of the pure vapor at its partial pressure in the mixture[43]. The presence of non-condensable gases while condensation processes are taking place may affect heat transfer coefficients very dramatically. The presence of even a small quantity of non-condensable gas in the vapor has been shown to reduce the heat transfer coefficient significantly. A very good explanation of why this happens may be understood by quoting the following paragraphs :

> "The general effects of non-condensable gases on a film condensation process can be envisioned by Figure (II.4). Once steady state is achieved, condensation occurs at the interface of a liquid film on the wall. Due to the condensation process at the interface, there is a bulk velocity of the gas toward the wall, as if there were suction at the interface. Because only the vapor is condensed, the concentration of the non-condensable gas at the interface W_i is higher than its value W_∞ in the far ambient. This, in turn, decreases the partial pressure of the vapor at the interface below its ambient value. The corresponding saturation temperature at the interface is therefore lower than the bulk temperature T_∞. At equilibrium, the interface concentration of the non-condensable gas is high enough so that the resulting diffusion and/or convection of this component away from the interface into the ambient just balances the rate at which its concentration increases due to the condensation process.
> In systems where the non-condensable gas is a low-concentration contaminant, the phenomena described above can lead to a high concentration of the non-condensable contaminant at the interface. The resulting depression of the interface temperature generally

reduces the condensation heat transfer rate below that which would result for pure vapor alone under the same conditions"[43].
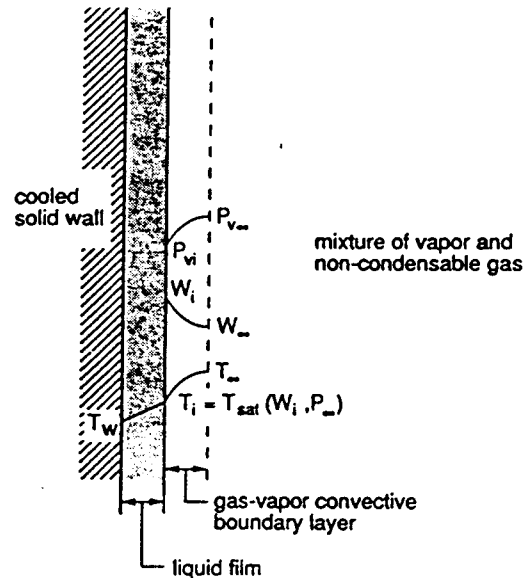
Figure (II.4) System Model for Analysis of Film Condensation in the Presence of a Non-Condensable Gas[43].

The presence of non-condensable gases affects drop-wise condensation in a manner similar to that for film-wise condensation[41].

A significant decrease in the heat transfer coefficient results in the presence of very small amounts of the non-condensable gas. One study has shown that even at a gas content in the vapor of 1%, the heat transfer coefficient decreases by 60%[44].

III. DESCRIPTION OF THE METHODS AND EXPERIMENTAL MODELS

III.1 Introduction :

The flat plate configuration was chosen initially to reduce the effects of gravity on the simulation before proceeding to the next step of testing different configurations such as spherical or ellipsoidal shells. Analysis has shown that the tangential force, at certain location and rotational speed, on a condensate droplet of a working fluid on the inner surface of a RBMR may be simulated by the same amount of force, generated by a known flat plate rotational speed, acting on the same size of droplet of same working fluid, located at some distance from the center of a flat plate. More details will be provided in Chapter V.

III.2 Experimental Setup and Equipment Functions :

The primary components of the ground based Flat Plate Condensation Experiment and their uses are shown as follows :

1) A large glass pipe section with a length of one meter and a forty five centimeter diameter. It was constructed in England by Corning Glass Works, and was designed especially to hold zero vacuum. It was used to contain the major components of the experiment as shown in Figure (III.1). A transparent glass pipe was chosen to allow the use of laser beams to be shined through it in an attempt to measure the film condensate thickness. The glass pipe is sealed on its ends by two Aluminum plates. The bottom
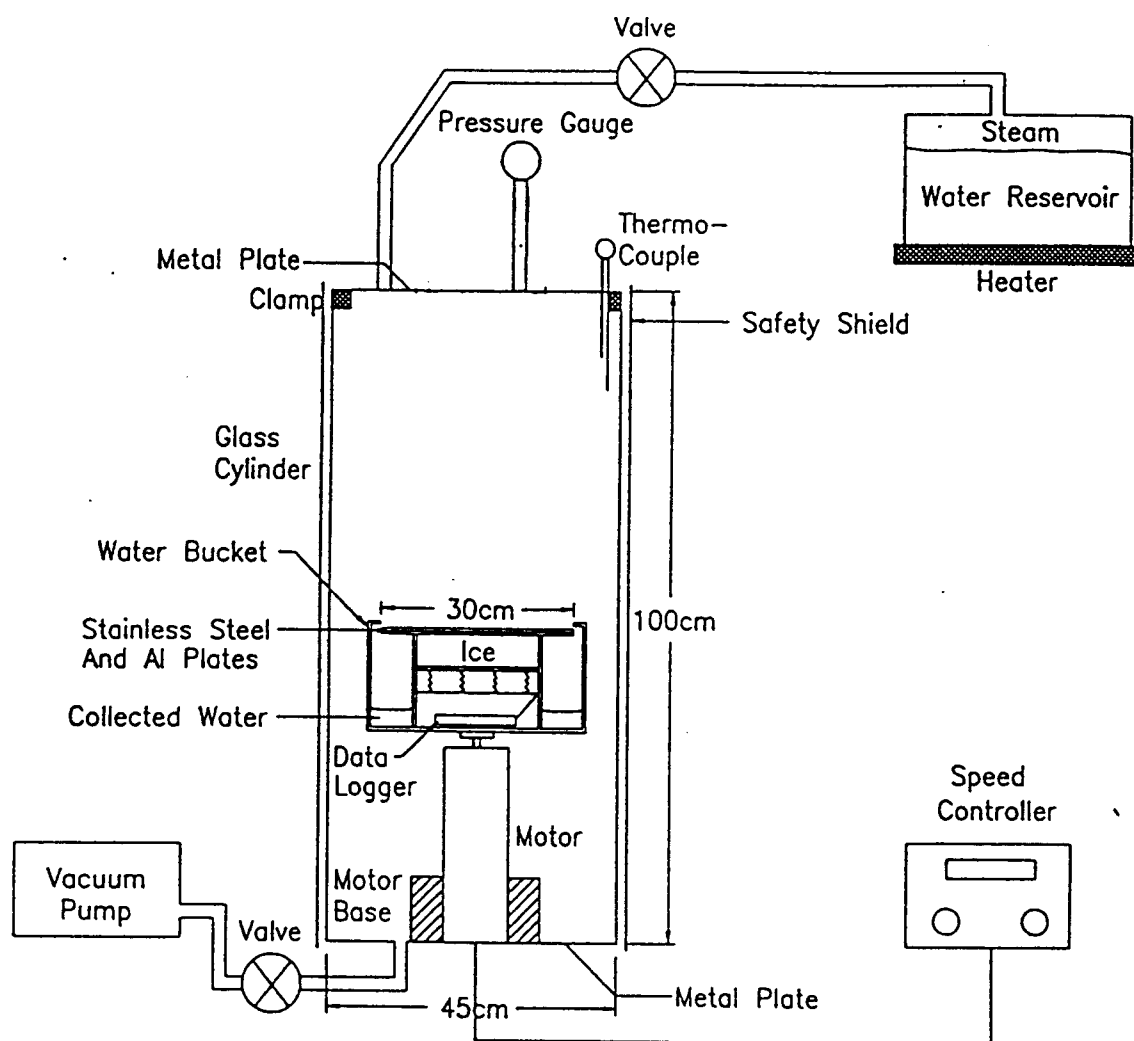
Figure (III.1) Schematic Diagram of the Flat Plate
Condensation Experiment.

plate has adjustable legs to help in leveling the glass pipe, and also has a vacuum valve that connects the glass pipe to the vacuum pump, and an electrical feed through to connect the rotating motor to a power supply and controller. The upper plate has a plastic window to allow video-taping the flow pattern. It has also a steam valve, pressure gauge, and two feed through that are used while recording the flow patterns. Both plates are attached to the glass pipe by metal flanges and built-in screws.

2) The rotating flat plate assembly, shown in Figure (III.2), consists of two parts:

* Two flat plates of metal with high thermal conductivity. The upper one is a mirror type (#8 finish) stainless steel, alloy SS304, where the condensation is designed to occur. This plate simulates the radiator's condensing surface and is 30.48 cm in diameter and 0.265 cm thickness. The mirror finish helps in smoothly sweeping the condensate to the plate edge when it is rotated, and also to, effectively, reflect the laser beam when the condensate thickness is measured. The other plate is made of Aluminum 6061-T6, with a 30.48 cm diameter and a 0.635 cm thickness. This plate is attached to the ice bucket, and is used to measure the heat flux from the stainless steel plate to the block of ice which is pressed against the lower surface of the aluminum plate. By measuring the temperature difference across the aluminum plate the heat flux can be determined.
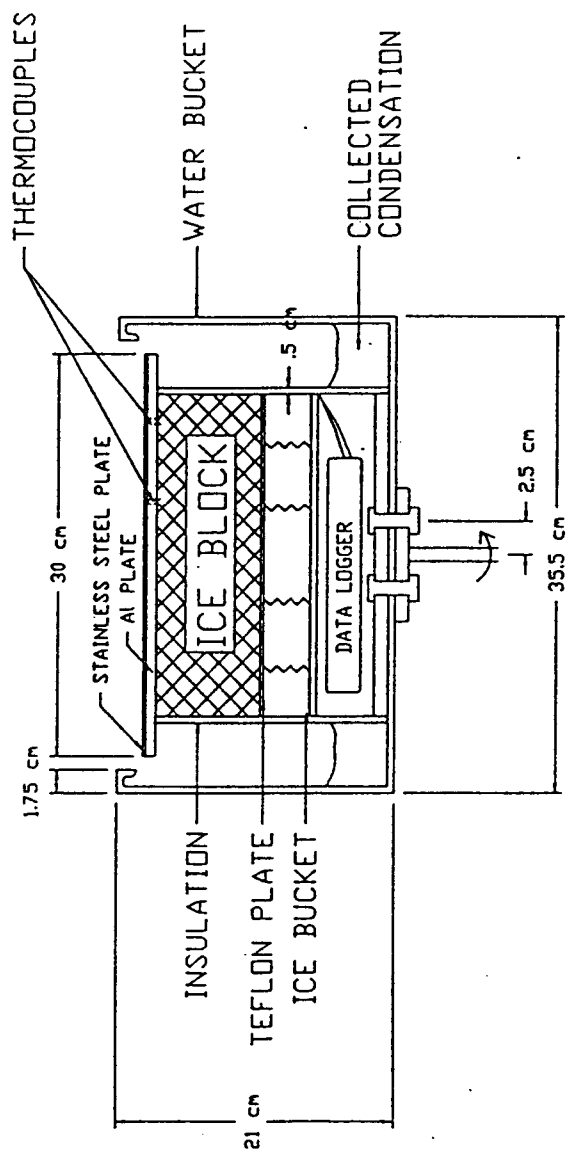
Figure (III.2) Schematic Diagram of the Flat Plate
Condensation Assembly.

* An ice bucket which provides a constant temperature heat sink for the experiment. This is achieved by attaching several springs to a teflon platform tape which pushes an ice block against gravity to keep it in contact with the bottom surface of the aluminum plate at all times. The teflon platform has some free spaces (holes) to allow the melting water to pass through. After each experiment run, the ice bucket is frozen up-side-down with the teflon platform springs pulled back to allow the formation of an ice block. The ice block then simulates the cold environment of space. The ice-bucket is thermally insulated from the sides and bottom so that only a limited amount of condensation should occur on surfaces other than the upper one.

3) The water bucket :

It consists of two Aluminum pipe sections with their bottoms fixed to an aluminum plate as shown in Figure (III.2); the inner pipe is used to hold the rotating flat assembly and the data logger while the outer one is used to collect the condensate.

4) Variable speed motor and amplifier :

A DC servo system motor, type 0642-30-017 from Robins & Myers, environmentally sealed, with maximum continuous speed of 4500 rpm is used in these experiments. This motor is connected to a matching Electro-Craft LA-5600 linear servo amplifier. The LA-5600 amplifier is designed to drive small and medium size permanent magnet DC servo motors with DC tachometers in a velocity control mode. The motor has a 14v/Krpm tachometer. This system allows the speed of rotation to be accurately controlled.

5)   Vacuum pump :

It is a mechanical high vacuum pump, model 5BA-1-G482x, GAST brand. Evacuating the system helps in getting high superheated steam at relatively low temperatures. Low steam temperatures also decrease the condensation on the other system parts, and also very few air molecules in the system for the steam to be condense on. A small amount of air in the system means less non-condensable gases which helps in getting more accurate results. It also reduces the amount of condensation on the inner surface of the glass pipe which helps in better visualizing of the condensate film.

6)   LASER beam :

Helium-Neon laser beam, model 100 series, UNIPHASE brand, was used to attempt find the thickness of the condensate. It has 632.8 nm wavelength, i.e. visible beam, with 10.0mW power, 320 MHz longitudinal mode spacing, 0.68 mm diameter, and linear polarization. This type of laser beam is classified as a Class III-medium power laser.

7)   Data logger :

A compact, portable battery-operated model 50 data logger from Cole-Parmer which has five thermocouple channels is used. The output data can be either printed on the 24-column thermal printer or loaded on a remote computer. Each individual channel of the data logger is programmable directly from the keyboard. The programming systems include: time, log interval, thermocouples type (J, K, T, or E), temperature unit ($^{\circ}$F or $^{\circ}$C), etc. T type thermocouples are used in these experiments. The data logger is used to measure the temperature of the aluminum plate at different locations.

8)   Steam supply system :

A 2000 ml beaker is used as a water reservoir. It is placed on a heating plate. The beaker has two openings; one is closed by a stopper while the other is connected to the glass pipe by a hose so that when the steam is generated, it is forced to enter the glass pipe.

9)   Black Light :

A black-ray ultraviolet lamp with 115 volt and 60 cycle, model B-100A, of Ultra-Violet Products, Inc., is used to illuminate a fluorescent solution that is added at the center of the condensing surface to watch the condensate flow patterns.

III.3 Methodologies :

The following sections explain the detailed methodologies that were used in achieving the objectives of this study.

III.3.1 Assumptions :

Several important assumptions were made that have significant effects on the results. These effects caused less accuracy in the results and the effects were measured and calculated by performing statistical analysis.

The first assumption is that the heat is transferred from the condensate to the ice in a steady state mode. The fact that was noticed from the temperature measurements that the temperature increases very fast initially and then continues to increase with a very small slope where it is assumed to be in a quasi steady state condition. It takes a few

minutes to reach the appropriate quasi steady state conditions. Printouts of the variation of the temperatures with time are shown in Chapter 4.

Secondly, the heat is transferred in one dimension, i.e. the Z-direction in the cylindrical coordinates. Very little variation in R-direction, in comparison to Z-direction, was noticed. Calculations used to justify the validity of this assumption, i.e. negligible variation with space other than Z-direction, are shown in Chapter 4.

The third significant assumption is that the aluminum plate and the stainless steel plate are in a very close contact in such a way as to neglect the effect of the gap between them. This gap is caused by placing very thin thermocouples on the aluminum surface that is in contact with the stainless steel plate. As a matter of fact, this gap serves as a resistance that should be counted in calculating the heat transfer parameters. For reasonably high temperature difference across the gap however this assumption is quite reasonable as will be shown later.

III.3.2 Heat Transfer Parameter Measurements :

A common way of expressing the heat transfer rate for a situation involving a composite material or combinations of heat transfer mechanisms is by determining the overall heat transfer coefficient (U). In cases where the condensation is involved, U1 is defined as

$$U1 = \frac{\dfrac{\dot{m}\, h_{fg}}{A}}{T_{wv} - T_{Ali}} \qquad (3.1)$$

where

$$\frac{q}{A} = \frac{\dot{m}\, h_{fg}}{A}$$

An alternative way to measure the heat flux at steady state in equation (3.1), which is due to condensation, is to measure the temperatures across the condensate. For the one dimensional steady state case, the amount of energy which crosses the condensate will be same as the amount of energy which crosses the stainless steel plate coming from the condensate, and the same as that which crosses the aluminum plate and is eventually deposited in the ice block, and thus the heat flux can be measured as

$$\frac{q}{A} = \left(\frac{K_{Al}}{t_{Al}} \right) \left(T_{Alo} - T_{Ali} \right) \tag{3.2}$$

A convenient way, using $(T_{wv}-T_{Ali})$ as a temperature difference, to find U1 is then found to be

$$U1 = \frac{\left(\frac{q}{A} \right)}{\left(T_{wv} - T_{Ali} \right)} \tag{3.3}$$

and, using $(T_{wv}-T_{alo})$ as a temperature difference, U2 to be

$$U2 = \frac{(\frac{q}{A})}{(T_{wv} - T_{Alo})} \qquad (3.4)$$

Since T_{wv}, T_{Ali}, T_{Alo}, and t_{Al} are measured, and K_{Al} is known by using Tables of physical properties for aluminum alloys, the only unknowns in equations 2, 3 and 4 are the heat flux (q/A), U1 and U2.

To find the average convective heat transfer coefficient, the following equation is used

$$T_{wv} - T_{Ali} = (\frac{q}{A}) [\frac{1}{h_{avg}} + \frac{t_{Al}}{K_{Al}} + \frac{t_{ss}}{K_{ss}}] \qquad (3.5)$$

where t_{ss} is measured and K_{ss} is known by using Tables of physical properties for stainless steel alloys, the only unknown is h_{avg}.

The average condensing surface temperature (T_c) is calculated using the following equation

$$\frac{q}{A} = h_{avg} (T_{wv} - T_c) \qquad (3.6)$$

III.3.3 Statistical Analysis :

The use of statistical methods for data analysis has become common practice in all scientific disciplines. These methods enable researchers to predict the distribution function that will describe the results of many repetitions of a given measurement[45].

III.3.3.a Main Error Parameters :

The variance, denoted by σ^2, is an important statistical parameter that measures the amount of fluctuation in the original data. It could be introduced as

$$\sigma^2 = \frac{1}{N-1} \sum (T_i - T_{av})^2 \qquad (3.7)$$

Because it is impossible to know the true theoretical temperature mean from a finite number of measurements, the value T_{av} is derived from the data set itself to calculate values for the deviations. The use of the experimental, rather than true theoretical mean value, will tend to reduce the average deviation and therefore result in a smaller than normal variance. Statistically, the number of degrees of freedom of the system has been reduced by one, and the -1 which appears in the denominator of equation 3.7 accounts for this self-minimizing effect.

Another important statistical parameter is the standard deviation, denoted as σ, which is the positive square root of the sample variance. A data set with a narrow distribution will have a small typical deviation from the mean, and therefore the value for the sample variance will be small. On the other hand, data with a large amount of fluctuation will have a wide distribution and a large value for typical deviations, and the corresponding sample variance will also be large. The significance of the standard deviation is that it is the best estimate of the deviation, i.e. error, from the mean value. Assuming that the data has a normal (Gaussian) distribution of the parent data, then using one standard deviation ($\pm \sigma$) means that this interval ($T_{av} + \sigma$ to $T_{av} - \sigma$) is expected

to contain the mean value T_{av} with a probability of 68 percent. If it is wished to increase the probability that the true mean is included, one can do so only by expanding the interval or error associated with the measurement. For example, to achieve a 99 percent probability that the true mean is included, the interval must be expanded to 2.58 σ. Figure (III.3) shows a plot of the general Gaussian curve[45]. One standard deviation is used in this study.
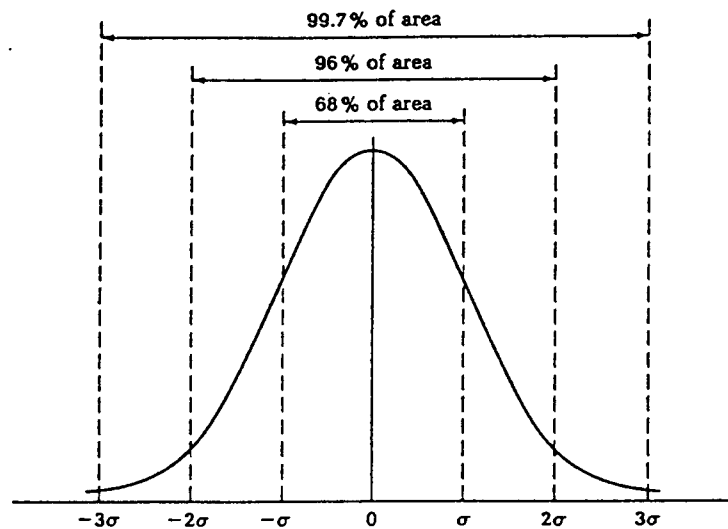
Figure (III.3) General Normal (Gaussian) Distribution.

III.3.3.b Error Propagation :

If x,y,z,... are directly measured values or related variables for which we know σ_x, σ_y, σ_z,..., then the standard deviation for any quantity u derived from these measures can be calculated from

$$\sigma_u^2 = (\frac{\partial u}{\partial x})^2 \sigma_x^2 + (\frac{\partial u}{\partial y})^2 \sigma_y^2 + (\frac{\partial u}{\partial z})^2 \sigma_z^2 + \ldots \qquad (3.8)$$

Where $u=u(x,y,z,\ldots)$ represents the derived quantity. Equation 3.8 is generally known as the "Error Propagation Formula". The use of equation 3.8 can be illustrated by applications to some cases of interest in this study[46].

Case 1. Sums or Differences :

If one defines

$$u=x+y \qquad or \qquad u=x-y$$

then

$$\frac{\partial u}{\partial x}=1 \qquad \frac{\partial u}{\partial y}=\pm 1$$

Application of equation 3.8 yields

$$\sigma_u^2 = (1)^2 \sigma_x^2 + (\pm 1)^2 \sigma_y^2$$

or

$$\sigma_u = \sqrt{\sigma_x^2 + \sigma_y^2} \qquad (3.9)$$

Case 2. Multiplication or Division by a Constant :

If one defines

$$u=Ax \qquad v=\frac{x}{B}$$

Where A and B are constant (no associated uncertainty), then application of equation 3.8 gives

$$\sigma_u = A\sigma_x \quad \sigma_v = \frac{\sigma_x}{B} \qquad\qquad 3.10$$

Case 3. Multiplication or Division :

For the case

$$u = xy \quad v = \frac{z}{t}$$

Similar way to previous cases, one can get

$$\left(\frac{\sigma_u}{u}\right)^2 = \left(\frac{\sigma_x}{x}\right)^2 + \left(\frac{\sigma_y}{y}\right)^2 \quad \left(\frac{\sigma_v}{v}\right)^2 = \left(\frac{\sigma_z}{z}\right)^2 + \left(\frac{\sigma_t}{t}\right)^2 \qquad (3.11)$$

Case 4. Multiplication by a Constant and a Variable With Power :

Assume one has the following relation

$$u = A(x)(y^n)$$

Where A is a constant and n is a constant power. Application of equation 3.8 yields

$$\left(\frac{\sigma_u}{u}\right)^2 = \left(\frac{\sigma_x}{x}\right)^2 + \left(\frac{n\sigma_y}{y}\right)^2 \qquad (3.12)$$

III.3.4 Condensate Film Thickness Measurements :

A technique to measure the condensate fluid thickness using a laser beam has been developed. A laser beam will be directed towards the disk surface (from outside the glass container), with a known angle relative to the plate surface. A part of the beam reflects from the film surface while the reminder of the beam refracts in the condensate film and then

reflects from the disk surface. A laser receiver receives these two beams, and since the shift between these beams is proportional to the thickness of the film, the film thickness can be found using the known geometry, index of refractions of the system, and basic laws of refraction and reflection. Figure (III.4) demonstrates the principles of operation of this aspect of the experiment and shows the equation that is used to find the film thickness.

III.3.5 Flow Patterns :

To record the flow patterns of the colorless condensate water, a shiny (light) or colored (dye) materials must flow with the condensate without disturbing its flow pattern. It was found that a water solution of Sodium Florocein will not disturb the flow patterns since its density is similar to the condensate and it can be introduced at the center of the condensate plate. If this is the case, this shiny solution will flow with the condensate and by using matching black light, the solution will illuminate and its motion be recorded by either a video tape camera or a photo camera. When the quasi steady state case is achieved with an established condensate film, the solution is introduced into the system. The amount of solution to be entered and the location where to introduce are controlled by a controlling value and a stick.

III.4 Procedures :

The following shows the major steps of the experiment procedures while a detailed check list is shown in Appendix I. The water bucket is

fixed on the rotating shaft, inside the glass pipe. Five thermocouple (TC) wires are connected to the Data Logger (DL), two of them on the bottom side of the Aluminum plate and two on the corresponding upper side, and one to measure the superheated steam by suspending it into the glass pipe. The DL is started in the print data mode, to read the temperature to assure that the TC's are working properly. The flat plate surface is treated with some detergent in an attempt to make it wet enough to achieve film-wise condensation if this is appropriate for the test. The water beaker (steam generator) is filled and placed on the heating plate. The DL is inserted in double plastic bags to keep it in a dry environment and is set to run in the non-printing data mode. The DL is placed in the inner cylinder of the water bucket, then the flat plate assembly is fixed on the top of the DL and attached to the inner cylinder and leveled so that it is perpendicular to the gravity vector.
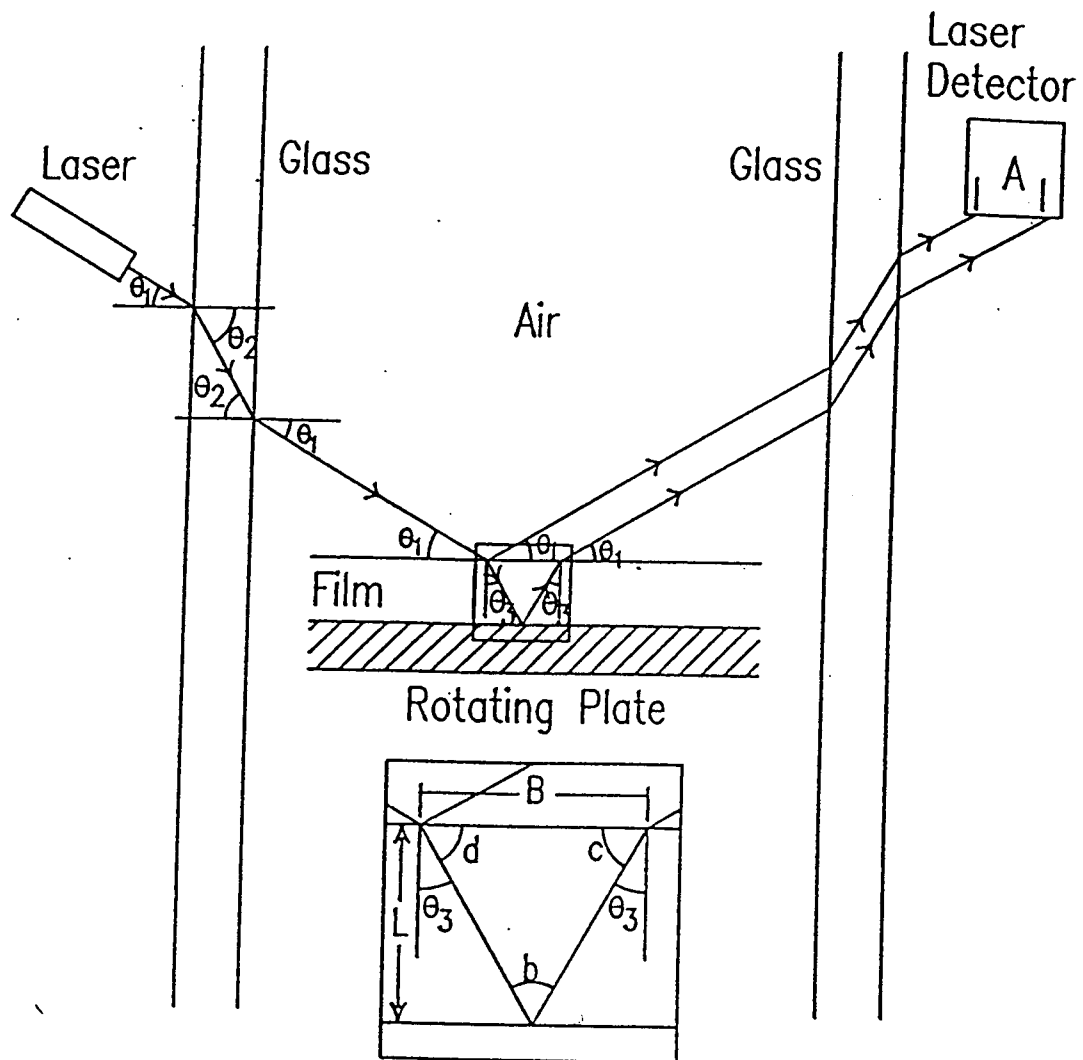
Figure (III.4) Fluid Film Thickness Measurement Using Laser Beam.

A sufficient amount of anti-fog treatment is put on the plastic window of the top glass pipe aluminum plate to allow for clear viewing then the top aluminum plate is placed on the top of the glass pipe and attached to its metal flange by the built in screws. The protection shield is placed on the outer side of the glass pipe. The heavy duty rubber hose between the water beaker and the steam valve is connected. The rubber stopper is placed on the top of the beaker. The steam valve is now opened. The vacuum hose is connected to the vacuum valve then the vacuum pump is turned on. The water in the beaker is watched, when it starts to boil, the steam valve is closed. When the vacuum gauge reaches approximately 6-7 kPa the vacuum pump is turned off. It typically takes about seven minutes to pump the chamber to this level.

The rotating motor is then started and set to the desired speed. The steam valve is opened fully and carefully. Rapid boiling of the water in the beaker may be noticed. This steam is transferred from the water beaker to the glass pipe through the heavy duty rubber hose.

The experiment is run for the time desired, usually until it reaches quasi steady state which takes about ten minutes from the time the steam is introduced. The steam valve is closed. The heater is turned off. The rotation speed is turned, slowly, to zero and then the motor is turned off. The data from the DL are loaded to the computer. The ice bucket is prepared for the next test by compressing the springs in the assembly by inserting the screw pin and fixing the teflon plate to its fully withdrawn position, then it is put in a freezer.

LASER CASE:

The precautions and procedures listed below are typical for the class of laser systems known as type III medium (also called III.b) laser systems. Thus, strict adherence to these precautions is required to avoid injury.

GENERAL PRECAUTIONS

1) No direct or reflected beam is to be viewed without appropriate eye protection.

2) Unplug the laser after each use and store it in its box.

3) Provide enclosures for beam paths whenever possible.

4) Beam stop should be in place at all times.

5) Place standard safety warning sign for class III laser on the outside of the doors of rooms A120 and A120B during operation. Be sure that the doors to rooms A120 and A120B are closed at the beginning of laser operation, and that the door to room A120B remains closed while the laser beam is exposed.

6) Wear appropriate eye protection in room A120B at all times the laser is plugged in.

OPERATIONAL PROCEDURES

Place the laser on its stand at the appropriate test angle with the stainless steel test plate. The laser should not be plugged in at this time, but the angle should be approximately set so that it will shine through the glass pipe. Be sure that the beam stop is placed in a position where it will be able to collect the scattered laser beam. Place a blank white piece of paper between the beam stop and the laser beam. All beam focusing and direction setting must be done on a blank white piece of paper before steam is introduced into the glass pipe or the stainless steel plate is rotated. Turn the laser beam off. Replace the focusing target with film (covered at this point). After the condensate film is consistently established on the rotating stainless steel plate, turn the dark room light on, the room lights off and uncover the receiver film to receive the reflected laser beams from the surface of the stainless steel plate and from the condensate film surface. Turn the laser beam on. Laser scanning is to start at one edge of the stainless steel plate, end at the other edge, and pass through the center point of the plate. This is to be done horizontally to maximize the separation of the film surface and mirror surface reflected beams. Turn the laser off. Cover the film. Turn the room lights on. Turn the red light off. Unplug and return the laser to its container.

FLOW PATTERN CASE: After the condensate film is consistently established on the rotating stainless steel plate, the video camera is placed on the top of the plexy glass window of the upper aluminum plate cover and turned on. The dark light is turned on with room light off. A solution of water

and fluorescent powder is introduced into the system through flexible plastic hose, by opening the controlling valve. Due to pressure difference the solution is driven into the chamber. The solution drops are meant to drip at the plate center so they spread with the condensate film towards the plate edge; a stick of brass is connected to the solution pipe end to direct the drops.

IV. RESULTS AND DISCUSSIONS

IV.1 Temperature Measurements :

In experimental heat transfer research, one of the first objectives, is to measure the temperature distribution on the tested surface. These temperature measurements form the basis for following calculations to obtain the final output from such a study which is usually heat transfer coefficients or related correlations.

After the system reaches a quasi steady state condition, the readings of the data logger temperatures were taken over a certain period of time and then averaged. The temperatures T_1, T_2, T_3, and T_4 are measured in this fashion. T_{Ali} and T_{Alo} were calculated by averaging the temperature readings of the two channels measuring the inner Aluminum temperatures and the other two channels measuring the outer Aluminum surface, respectively, at the quasi steady state conditions. Standard deviations for these temperatures were found using Quattro-Pro[47]. The temperature of the interfacial area between the steam and the condensate film was taken to be the saturation temperature corresponding to the pressure measured in the system. This saturation pressure varies very little once the system reaches a quasi steady state condition. As a result one temperature reading was recorded for T_{wv} and hence no standard deviation was obtained for it. It is worth while to note that for tests 9, 12, 15, and 16 the thermocouple locations were as follows: two channels, 1 and 3, at the plate center on opposite sides, and two

channels, 2 and 4, at 1.5" off the plate center, in both sides of the plate. For the rest of the tests the thermocouple locations were : two channels, 2 and 4, at 1.5" off the plate center on opposite sides, while channels 1 and 3 were located at 3.0" off the plate center in both sides too.

The log number of the adopted experimental raw data in the data logger software was mentioned in Tables IV.1.a,b, and c along with the average adopted temperature readings and their standard deviations where the system considered to behave as a quasi steady state condition.

Figure (IV.1) shows a typical example of an output profile of the temperature readings from the data logger. When the flat plate assembly is taken out of the freezer, temperatures of channels 1 through 4 start to increase due to their exposure to room temperature. When the flat plate assembly is inserted into the system the temperature profiles seemed to behave almost steady state and kept this profile until, all of the sudden, they started to increase rapidly. This sharp increase was when the thermocouples started to feel the effect of the introduction of steam. The thermocouple connected to channel 5 was used to watch the heat behavior in the system. Since this thermocouple can not read the right temperature of a water vapor in a system of low pressure, its readings were not used. The first part of the curve and the first steep decrease, in area (1), represent the period where the ice-bucket was not yet put in the system. The second steep decrease of the temperature profile of this thermocouple, in area (2), shows when the system was evacuated, while the increase after that was, due to the heat rejected from the motor. Then, in area (3), due to introducing the steam. By inspecting area (3), it is
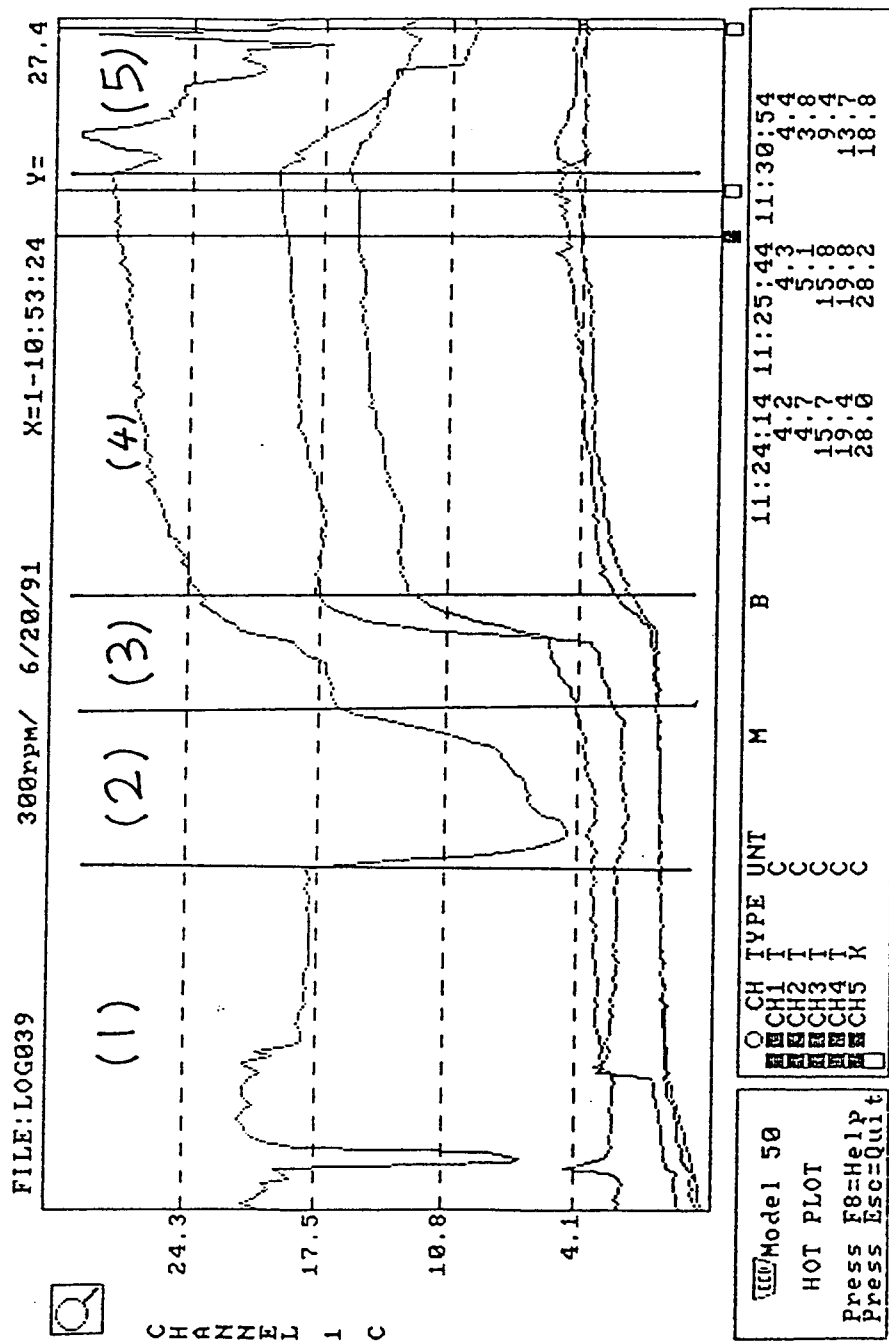
Figure (IV.1) A Typical Temperature Profile for Current Experiments.

seen that there was a short lag period between the time the steam was introduced, which is indicated by temperature increase of thermocouple of channel 5, and the time where thermocouples 3 and 4 felt the temperature increase. Due to the high thermal conductivity of aluminum no such time lag period was noticeable between thermocouples 3 and 4, and 1 and 2. After that the temperature profile started to behave as if it was in a quasi steady state condition, area (4). The last several temperature readings of this area were used. Then the decrease in these profiles, area (5), were due to turning the motor off and allowing air of a room temperature to enter the system.

Figure (IV.2) shows a magnification of the quasi steady state period, the black area in the bottom left shows the magnified area from the original whole curve. It is clear that the temperature profile throughout this minute and a half period represents a quasi steady state case. The temperature data was taken every ten seconds in this case.

Tables IV.1.a, b, and c show the measured temperatures over quasi steady state periods of all adopted tests, along with their standard deviations, for three flat plate angular speeds, namely 200, 300, and 400 rpm.
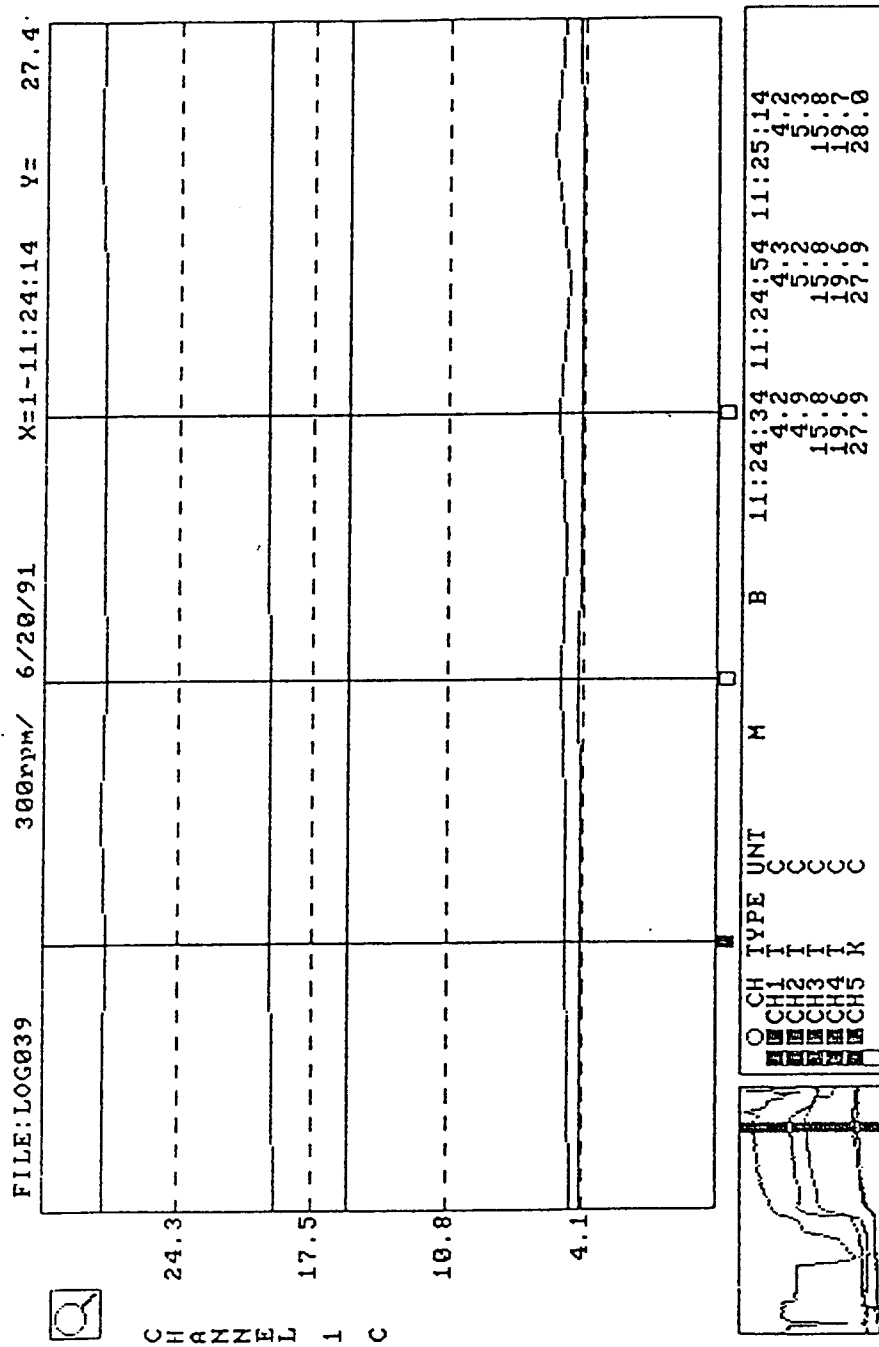
Figure (IV.2) A Typical Temperature Profile of a Quasi Steady
Period of Current Experiments.

TABLE IV.1.a

Averaged Temperatures Of Thermocouples Over Quasi Steady
State Period For Plate Angular Speed Of 200 rpm

Log No.	Raw Data No.	$T_1 \pm$ Std.	$T_2 \pm$ Std.	$T_3 \pm$ Std.	$T_4 \pm$ Std.	T_{wv}
		$T_{Ali} \pm$ St. Deviat.		$T_{Alo} \pm$ St. Deviat.		
9	119-126	9.44 ± 0.1	12.55 ± 0.1	4.24 ± 0.3	2.88 ± 0.1	49.07
		10.99 ± 1.56		3.56 ± 0.73		
12	145-159	8.21 ± 0.2	11.14 ± 0.3	3.54 ± 0.1	2.64 ± 0.1	62.03
		9.68 ± 1.48		3.09 ± 0.46		
15	234-243	19.03 ± 0.2	19.95 ± 0.2	15.32 ± 0.2	16.63 ± 0.2	43.60
		19.49 ± 0.51		15.98 ± 0.69		
16	215-221	15.26 ± 0.4	16.53 ± 0.4	9.84 ± 1.0	12.14 ± 0.5	43.60
		15.89 ± 0.75		10.99 ± 1.39		
25	207-214	6.75 ± 0.4	7.69 ± 0.5	14.28 ± 0.1	14.24 ± 0.2	47.44
		7.22 ± 0.62		14.26 ± 0.13		
43	174-180	3.84 ± 0.2	4.07 ± 0.1	16.01 ± 0.1	13.54 ± 0.1	47.44
		3.96 ± 0.20		14.78 ± 1.24		
60	252-259	24.80 ± 0.2	25.23 ± 0.3	27.51 ± 0.2	27.69 ± 0.2	50.71
		25.01 ± 0.33		27.60 ± 0.20		
62	144-151	16.88 ± 0.4	16.81 ± 0.4	21.39 ± 0.3	21.15 ± 0.3	55.19
		16.84 ± 0.36		21.27 ± 0.28		
66	300-306	10.46 ± 0.2	10.04 ± .1	15.81 ± 0.2	13.81 ± 0.1	61.04
		10.25 ± 0.21		14.81 ± 1.01		

TABLE IV.1.a (Continued)

67	258-264	9.64 ± 0.5	10.39 ± 0.1	14.74 ± 0.2	14.29 ± 0.1	65.80
		10.01 ± 0.53		14.51 ± 0.28		
68	168-174	4.24 ± 0.0	7.53 ± 0.1	14.59 ± 0.1	13.10 ± 0.0	47.44
		5.89 ± 1.65		13.84 ± 0.75		

TABLE IV.1.b

Averaged Temperatures Of Thermocouples Over Quasi Steady
State Period For Plate Angular Speed Of 300 rpm

Log No.	Raw Data No.	$T_1 \pm$ Std.	$T_2 \pm$ Std.	$T_3 \pm$ Std.	$T_4 \pm$ Std.	T_{wv}
		$T_{Ali} \pm$ St. Deviat.		$T_{Alo} \pm$ St. Deviat.		
26	202-209	3.74 ± 0.5	2.98 ± 0.1	11.64 ± 0.2	9.84 ± 0.1	47.44
		3.36 ± 0.52		10.74 ± 0.91		
29	201-209	3.77 ± 0.1	4.27 ± 0.1	14.51 ± 0.2	12.77 ± 0.1	47.44
		4.02 ± 0.28		13.64 ± 0.88		
30	174-181	3.75 ± 0.1	3.50 ± 0.1	11.71 ± 0.1	11.41 ± 0.1	45.81
		3.63 ± 0.16		11.56 ± 0.19		
39	185-193	4.21 ± 0.0	4.94 ± 0.2	15.78 ± 0.0	19.58 ± 0.1	47.44
		4.58 ± 0.39		17.68 ± 1.90		
60	222-228	21.03 ± 0.3	21.79 ± 0.3	25.06 ± 0.2	25.47 ± 0.2	49.07
		21.41 ± 0.47		25.26 ± 0.26		
66	240-246	4.53 ± 0.1	8.93 ± 0.1	14.23 ± 0.0	12.79 ± 0.1	55.19
		6.73 ± 2.20		13.51 ± 0.72		
67	198-204	4.40 ± 0.1	9.34 ± 0.0	13.13 ± 0.0	13.19 ± 0.0	58.84
		6.87 ± 2.47		13.16 ± 0.03		
68	228-234	5.47 ± 0.1	10.89 ± 0.1	16.67 ± 0.0	15.73 ± 0.1	49.07
		8.18 ± 2.71		16.20 ± 0.48		

TABLE IV.1.c

Averaged Temperatures Of Thermocouples Over Quasi Steady
State Period For Plate Angular Speed Of 400 rpm

Log No.	Raw Data No.	$T_1 \pm$ Std.	$T_2 \pm$ Std.	$T_3 \pm$ Std.	$T_4 \pm$ Std.	T_w
		$T_{Ali} \pm$ St. Deviat.		$T_{Alo} \pm$ St. Deviat.		
45	162-168	5.44 ± 0.2	4.29 ± 0.1	17.41 ± 0.0	19.23 ± 0.1	50.71
		4.86 ± 0.59		18.32 ± 0.91		
47	162-168	4.53 ± 0.1	4.30 ± 0.1	17.14 ± 0.1	17.87 ± 0.1	49.07
		4.41 ± 0.14		17.51 ± 0.38		
51	198-204	5.69 ± 0.2	4.64 ± 0.1	16.89 ± 0.2	19.41 ± 0.1	47.44
		5.16 ± 0.54		18.15 ± 1.27		
53	210-217	17.15 ± 0.3	8.34 ± 1.1	23.25 ± 0.2	24.98 ± 0.2	55.19
		12.92 ± 4.58		24.11 ± 0.86		
55	203-208	23.38 ± 0.2	24.93 ± 0.2	25.60 ± 0.2	26.52 ± 0.1	49.07
		24.16 ± 0.78		26.11 ± 0.41		
57	198-204	23.24 ± 0.2	23.14 ± 0.2	25.64 ± 0.1	26.71 ± 0.1	50.71
		23.19 ± 0.21		26.18 ± 0.55		
60	180-187	12.31 ± 0.7	13.93 ± 0.6	20.26 ± 0.2	20.66 ± 0.3	47.44
		13.12 ± 0.81		20.46 ± 0.34		
62	180-187	21.54 ± 0.3	21.91 ± 0.3	24.95 ± 0.2	24.23 ± 0.2	60.06
		21.73 ± 0.32		24.59 ± 0.41		
66	180-186	3.77 ± 0.2	5.79 ± 0.2	12.99 ± 0.1	11.04 ± 0.1	49.07
		4.78 ± 1.02		12.01 ± 0.98		

TABLE IV.1.c (Continued)

67	138-144	3.64 ± 0.1	6.64 ± 0.2	11.77 ± 0.1	11.93 ± 0.1	49.07
		5.14 ± 1.51		11.85 ± 0.12		
68	286-292	8.31 ± 0.6	14.1 ± 0.1	19.84 ± 0.1	19.24 ± 0.1	50.71
		11.22 ± 2.94		19.54 ± 0.31		

IV.2 Heat Flux And Overall Heat Transfer Coefficient Calculations :

It is found from Tables IV.1.a, b, and c that the film condensate temperature is on the order of a few tens of degrees celsius. C_p varies very slowly for water in this temperature range, e. g. it goes from 4226 J/Kg.°K at 0°C to 4175 J/Kg.°K for 40°C[40]. Also h_{fg} varies slowly, it is 2.5×10^6 J/Kg for 0.01°C and 2.4×10^6 for 40°C[48]. Since it is very difficult to get the exact temperature of the film condensate, the values of the C_p and h_{fg} were used for a temperature of 20°C, i. e. predicted mean value of the condensate, throughout the calculations, i. e. 4182 J/Kg.°K and 2.45×10^6 J/Kg respectively. The results are expected to be insensitive to this assumption.

Using $C_p \Delta T / h_{fg}$ values and equations 2.1, 3.2 where $K_{Al} = 167$ W/m/°C , 3.3, and 3.4, where the local heat transfer coefficient in the correlation developed by Sparrow and Gregg, i. e. equation 2.1, has been replaced with U1 and the temperature difference across the condensate with ($T_{wv} - T_{Ali}$), Tables IV.2.a, b, and c were formed, and with U2 and ($T_{wv} - T_{Alo}$), Tables IV.3.a, b, and c were formed. The errors, i.e. standard deviations, shown in these tables were calculated using equations 3.8 through 3.12.

TABLE IV.2.a[1]

Heat Transfer Coefficient Correlation Using U1 For Plate
Angular Speed Of 200 rpm

log #	$T_{Alo} - T_{Ali}$ (°C)	q" (W/m^2)	$T_{wy} - T_{Ali}$ (°C)	U1 (W/m^2/°C)	$C_p \Delta T / h_{fg}$	Correl. (using U1)
9	7.44 1.7	195613 45193	45.52 0.7	4298 995	0.080 0.001	0.86 0.20
12	6.59 1.6	173233 40767	58.94 0.5	2939 692	0.103 0.001	0.63 0.15
15	3.52 0.9	92442 22644	27.63 0.7	3346 824	0.048 0.001	0.59 0.15
16	4.90 1.6	128866 41611	32.61 1.4	3952 1287	0.057 0.002	0.73 0.24
25	7.04 0.6	185068 16696	40.22 0.6	4601 415	0.070 0.001	0.90 0.08
43	10.82 1.3	284610 32960	43.49 0.2	6545 781	0.076 0.000	1.30 0.15
60	2.59 0.4	68036 10017	25.69 0.3	2648 390	0.045 0.001	0.46 0.07
62	4.43 0.5	116374 11900	38.34 0.4	3035 311	0.067 0.001	0.58 0.06
66	4.56 1.0	120030 27063	50.79 0.2	2363 535	0.089 0.000	0.49 0.11
67	4.50 0.6	118346 15634	55.78 0.5	2122 280	0.098 0.001	0.45 0.06
68	7.96 1.8	209263 47561	41.56 1.6	5036 1148	0.073 0.003	0.99 0.23

[1] Lower value denotes the Standard Deviation.

TABLE IV.2.b[2]

Heat Transfer Coefficient Correlation Using U1 For Plate
Angular Speed Of 300 rpm

log #	$T_{ALo}-T_{ALi}$ (°C)	q" (W/m^2)	$T_{Wo}-T_{ALi}$ (°C)	U1 (W/m^2/°C)	$C_p \Delta T / h_{fg}$	Correl. (using U1)
26	7.38 1.1	194141 27607	44.09 0.5	4404 628	0.077 0.001	0.72 0.10
29	9.62 0.9	253051 24395	43.41 0.3	5830 563	0.076 0.001	0.94 0.09
30	7.94 0.2	208763 6527	42.19 0.2	4949 156	0.074 0.000	0.80 0.03
39	13.10 1.9	344520 51062	42.86 0.4	8038 1193	0.075 0.001	1.30 0.19
60	3.86 0.5	101436 14054	27.67 0.5	3666 512	0.048 0.001	0.53 0.07
66	6.78 2.3	178282 60894	48.46 2.2	3679 1268	0.085 0.004	0.61 0.21
67	6.29 2.5	165317 65016	51.97 2.5	3181 1260	0.091 0.004	0.54 0.21
68	8.02 2.7	210946 72306	40.90 2.7	5158 1801	0.072 0.005	0.82 0.29

[2]Lower value denotes the Standard Deviation.

TABLE IV.2.c[3]

Heat Transfer Coefficient Correlation Using U1 For Plate
Angular Speed Of 400 rpm

LOG #	$T_{Alo}-T_{Ali}$ (°C)	q'' (W/m^2)	$T_{Wo}-T_{Ali}$ (°C)	U1 (W/m^2/°C)	$C_p \Delta T / h_{fg}$	Correl. (using U1)
45	13.46 1.1	353908 28558	45.84 0.6	7720 631	0.080 0.001	1.10 0.09
47	13.09 0.4	344335 10590	44.7 0.2	7710 238	0.078 0.000	1.09 0.03
51	12.99 1.4	341521 36380	42.28 0.5	8078 867	0.074 0.001	1.13 0.12
53	11.19 4.7	294393 122596	42.27 4.6	6965 2997	0.074 0.008	0.97 0.42
55	1.95 0.9	51310 23046	24.92 0.8	2059 927	0.044 0.001	0.25 0.11
57	2.99 0.6	78529 15526	27.51 0.2	2854 565	0.048 0.000	0.36 0.07
60	7.34 0.9	193141 22955	34.32 0.8	5627 682	0.060 0.001	0.74 0.09
62	2.86 0.5	75295 13579	38.34 0.3	1964 355	0.067 0.001	0.27 0.05
66	7.24 1.4	190275 37165	44.30 1.0	4296 845	0.078 0.002	0.61 0.12
67	6.71 1.5	176389 39741	43.93 1.5	4015 915	0.077 0.003	0.57 0.13
68	8.32 3.0	218862 77730	39.49 2.9	5543 2011	0.069 0.005	0.76 0.28

[3]Lower value denotes the Standard Deviation.

TABLE IV.3.a[4]

Heat Transfer Coefficient Correlation Using U2 For Plate
Angular Speed Of 200 rpm

LOG #	$T_{wy}-T_{Alo}$ ($^\circ$C)	U2 (W/m^2/$^\circ$C)	$C_p \Delta T/ h_{fg}$	Correl. (using U2)
9	38.1 1.6	5137 1205	0.067 0.003	0.99 0.23
12	52.3 1.5	3309 784	0.092 0.003	0.69 0.16
15	24.1 0.5	3834 943	0.042 0.001	0.66 0.16
16	27.7 0.8	4651 1507	0.048 0.001	0.82 0.27
25	33.2 0.1	5577 504	0.058 0.000	1.03 0.09
43	32.7 1.2	8714 1062	0.057 0.002	1.61 0.20
60	23.1 0.2	2945 434	0.040 0.000	0.50 0.07
62	33.9 0.3	3431 352	0.059 0.001	0.64 0.07
66	46.2 1.0	2597 588	0.081 0.002	0.52 0.12
67	51.3 0.3	2308 305	0.090 0.001	0.48 0.06
68	33.6 0.8	6228 1422	0.059 0.001	1.16 0.26

[4]Lower value denotes the Standard Deviation.

TABLE IV.3.b[5]

Heat Transfer Coefficient Correlation Using U2 For Plate
Angular Speed Of 300 rpm

LOG #	$T_{wy}-T_{Alo}$ ($^{\circ}$C)	U2 (W/m^2/$^{\circ}$C)	$C_p \Delta T/ h_{fg}$	Correl. (using U2)
26	36.7 0.9	5289 764	0.064 0.002	0.82 0.12
29	33.8 0.9	7486 748	0.059 0.002	1.14 0.11
30	34.2 0.2	6096 194	0.060 0.000	0.93 0.03
39	29.8 1.9	11575 1868	0.052 0.003	1.71 0.28
60	23.8 0.3	4260 592	0.042 0.001	0.59 0.08
66	41.7 0.7	4277 1463	0.073 0.001	0.69 0.23
67	45.7 0.0	3619 1423	0.080 0.000	0.59 0.23
68	32.9 0.5	6417 2201	0.058 0.001	0.97 0.33

---

[5]Lower value denotes the Standard Deviation.

TABLE IV.3.c[6]

Heat Transfer Coefficient Correlation Using U2 For Plate
Angular Speed Of 400 rpm

LOG #	$T_w - T_{Alo}$ (°C)	U2 (W/m^2/°C)	$C_p \Delta T / h_{fg}$	Correl. (using U2)
45	32.4 0.9	10928 934	0.057 0.002	1.42 0.12
47	31.6 0.4	10908 360	0.055 0.001	1.41 0.05
51	29.3 1.3	11659 1342	0.051 0.002	1.48 0.17
53	31.1 0.9	9474 3954	0.054 0.002	1.22 0.51
55	23.0 0.4	2234 1004	0.040 0.001	0.27 0.12
57	24.5 0.6	3202 637	0.043 0.001	0.39 0.08
60	27.0 0.3	7159 855	0.047 0.001	0.89 0.11
62	35.5 0.4	2123 384	0.062 0.001	0.28 0.05
66	37.1 1.0	5134 1012	0.065 0.002	0.69 0.14
67	37.2 0.1	4739 1068	0.065 0.000	0.64 0.14
68	31.2 0.3	7023 2495	0.055 0.001	0.91 0.32

---

[6]Lower value denotes the Standard Deviation.

The heat flux was plotted against two dimensionless temperature difference groups, namely $C_p (T_{wv}-T_{Ali}) / h_{fg}$ and $C_p (T_{wv}-T_{Alo}) / h_{fg}$, and for the three tested speeds individually. Figure (IV.3) shows the heat flux verses $C_p (T_{wv}-T_{Ali}) / h_{fg}$ for rotational speed of 200 rpm, all data point are shown with their standard deviations in X-axis and Y-axis. Figures (IV.4) and (IV.5) show same things for rotational speeds 300 rpm and 400 rpm, respectively. Figure (IV.7) shows the heat flux verses $C_p (T_{wv}-T_{Alo})$ / h_{fg} for rotational speed of 200 rpm, all data point are shown with their standard deviations in X-axis and Y-axis. Figures (IV.8) and (IV.9) show same things for rotational speeds 300 rpm and 400 rpm, respectively. The least square fit of all data together is shown in one plot, i. e. Figure (IV.6) for the heat flux verses $C_p (T_{wv}-T_{Ali}) / h_{fg}$ and Figure (IV.10) for the heat flux verses $C_p (T_{wv}-T_{Alo}) / h_{fg}$. Since it is well known that when there is no temperature difference there is no driving force for heat transfer available, and q" is zero when ΔT approaches zero. The least squares fits were all therefore forced to pass through the origin. The slopes (m) for these three curves for the heat flux verses $C_p (T_{wv}-T_{Ali})$ / h_{fg} were found to be :

$$m_{200 \; rpm} = 2.05 \times 10^6 \quad W/m^2$$

$$m_{300 \; rpm} = 2.75 \times 10^6 \quad W/m^2$$

$$m_{400 \; rpm} = 3.21 \times 10^6 \quad W/m^2$$

While those slopes for heat flux verses $C_p (T_{wv}-T_{Alo}) / h_{fg}$ were found to be :

$$m_{200 \; rpm} = 2.31 \times 10^6 \quad W/m^2$$

$$m_{300 \; rpm} = 3.27 \times 10^6 \quad W/m^2$$

$$m_{400 \; rpm} = 3.89 \times 10^6 \quad W/m^2$$

Figure (IV.3) Heat Flux Verses Dimensionless Temperature Difference,
Used in Calculating U1, for rotational speed of 200 rpm.

Figure (IV.4) Heat Flux Verses Dimensionless Temperature Difference,
Used in Calculating U1, for rotational speed of 300 rpm.

Figure (IV.5) Heat Flux Verses Dimensionless Temperature Difference, Used in Calculating Ul, for rotational speed of 400 rpm.

Figure (IV.6) Least Square Fit for the Three Tested Rotational Speeds of Heat Flux Verses Temperature Difference Used in U1.

Figure (IV.7) Heat Flux Verses Dimensionless Temperature Difference,
Used in Calculating U2, for rotational speed of 200 rpm.
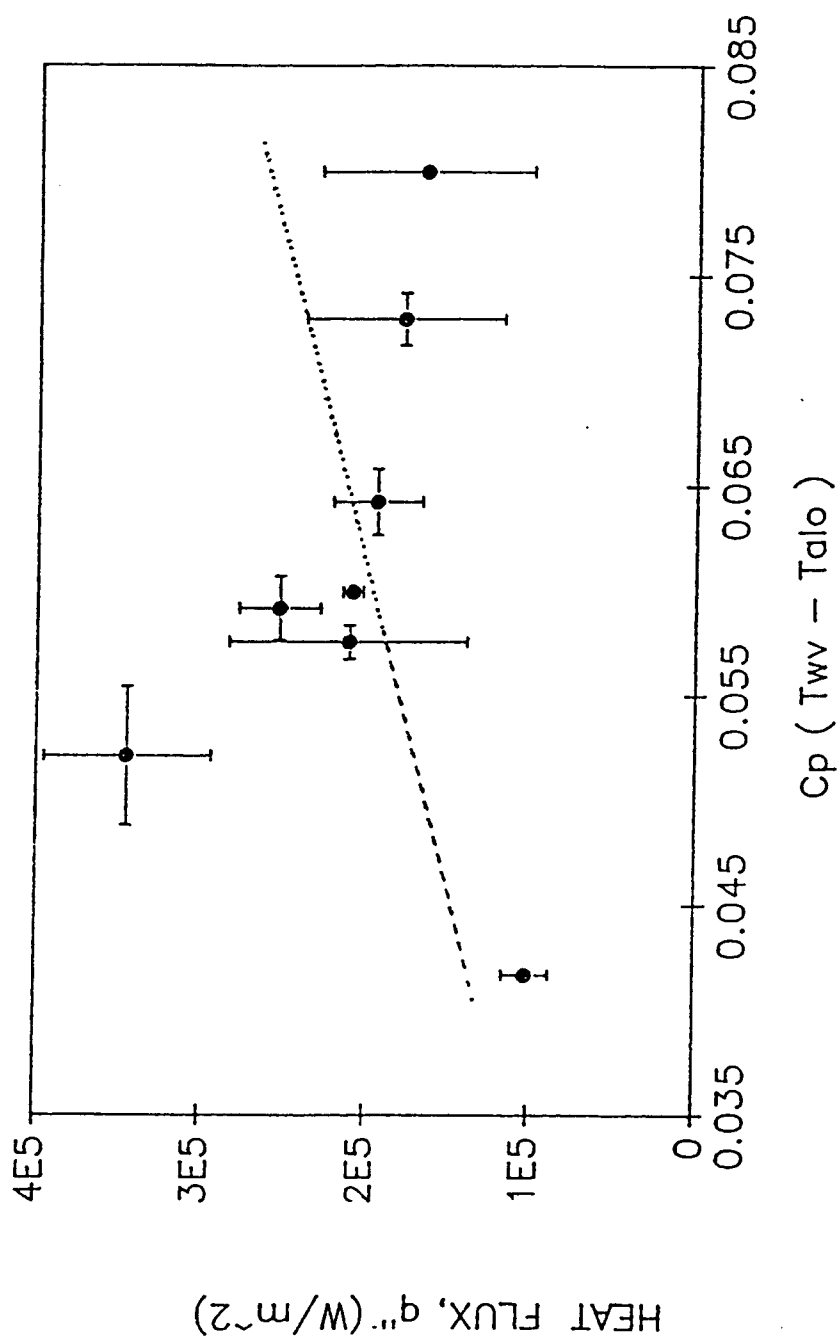
Figure (IV.8) Heat Flux Verses Dimensionless Temperature Difference, Used in Calculating U2, for rotational speed of 300 rpm.
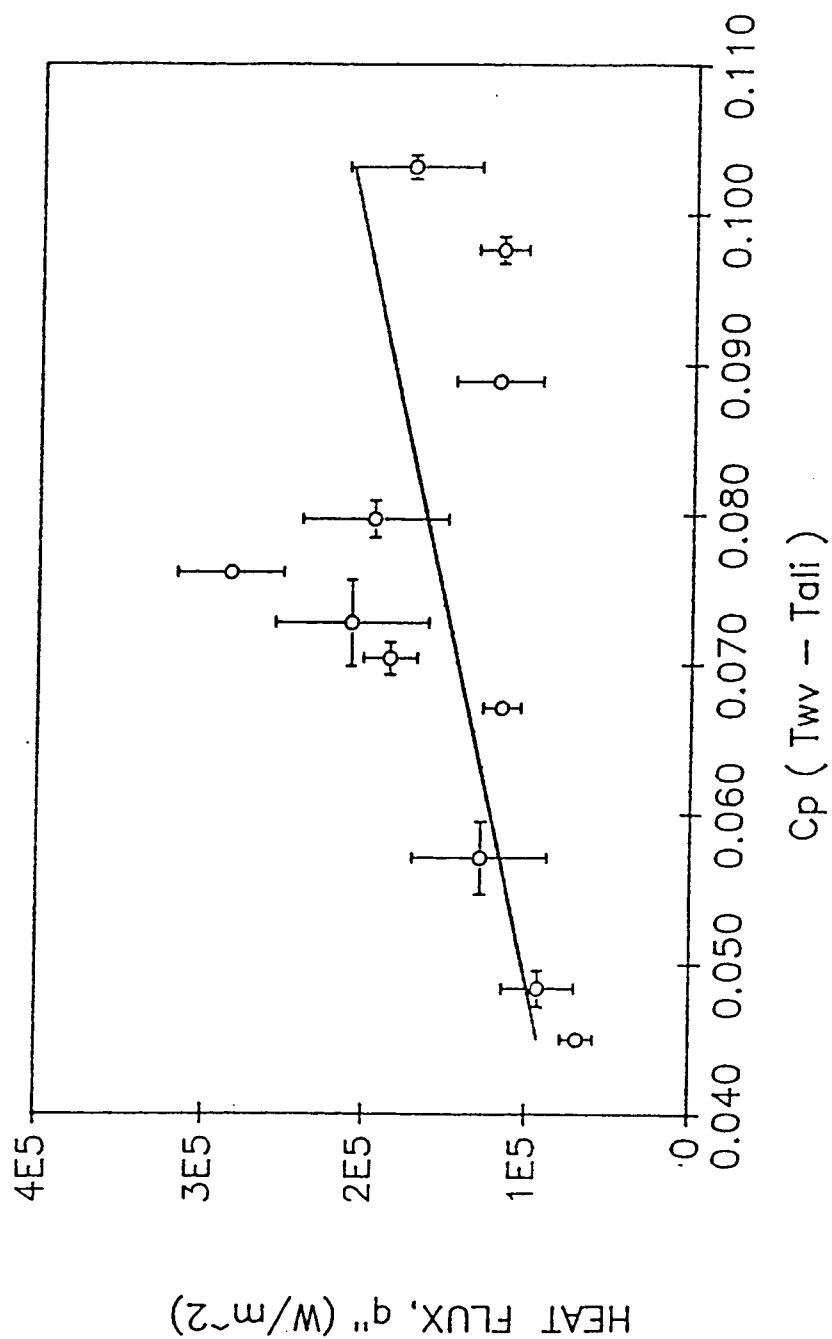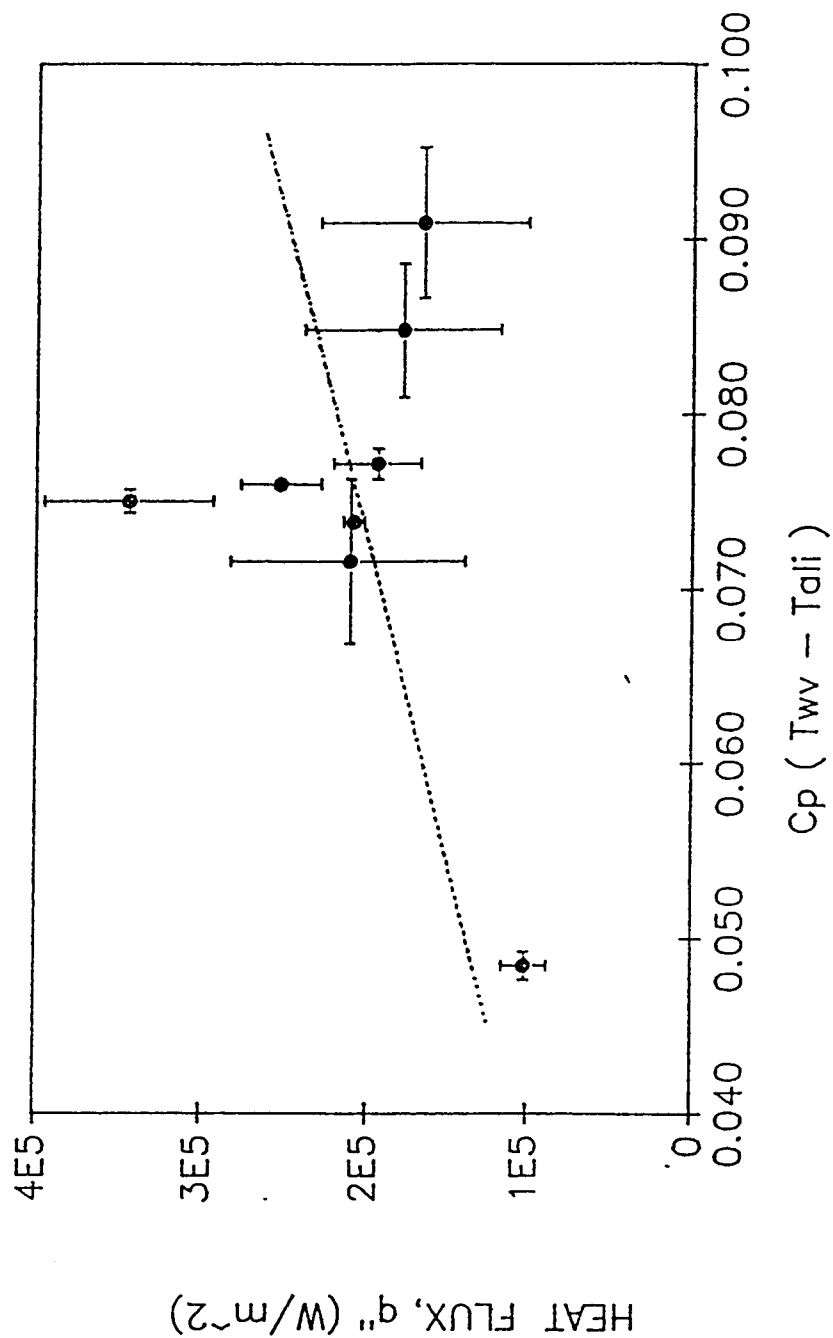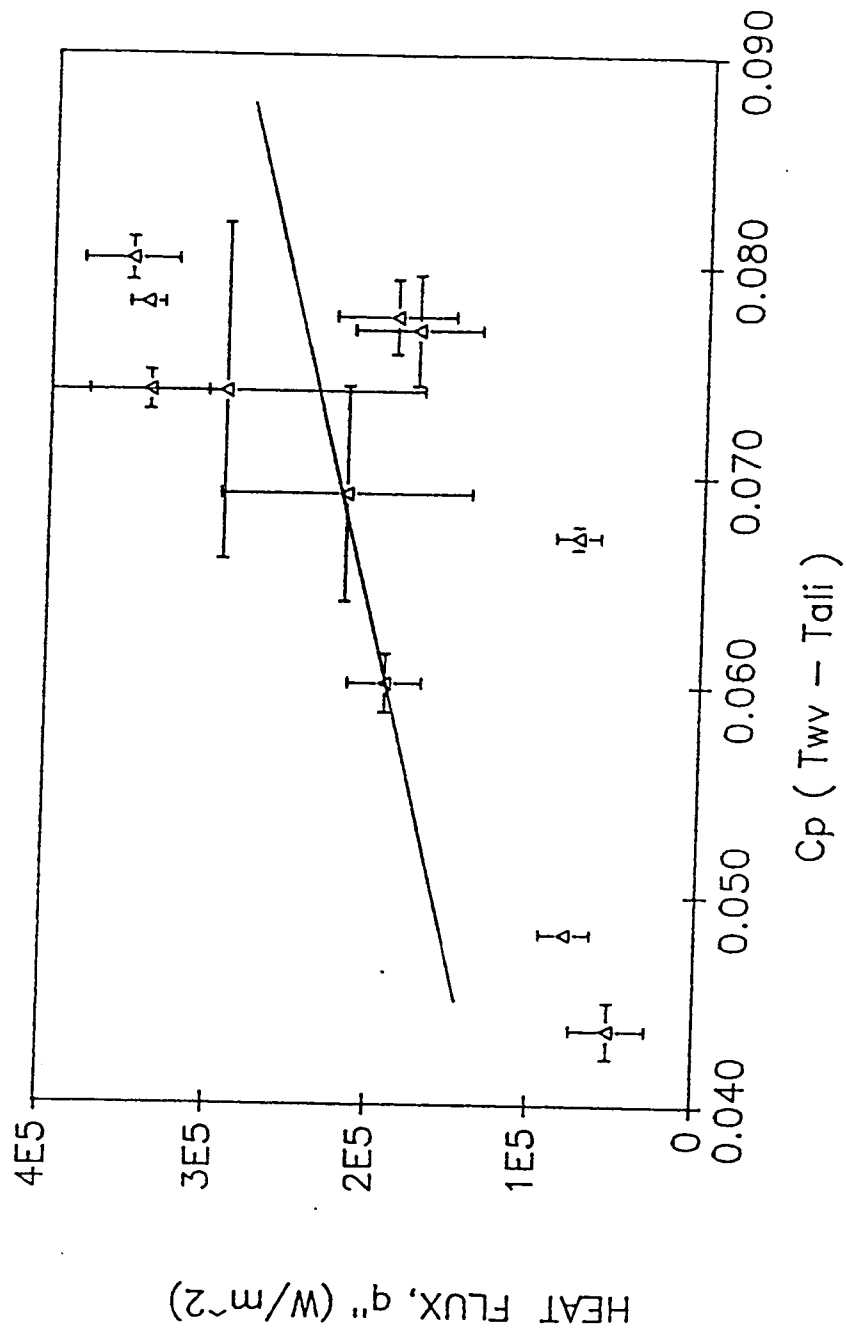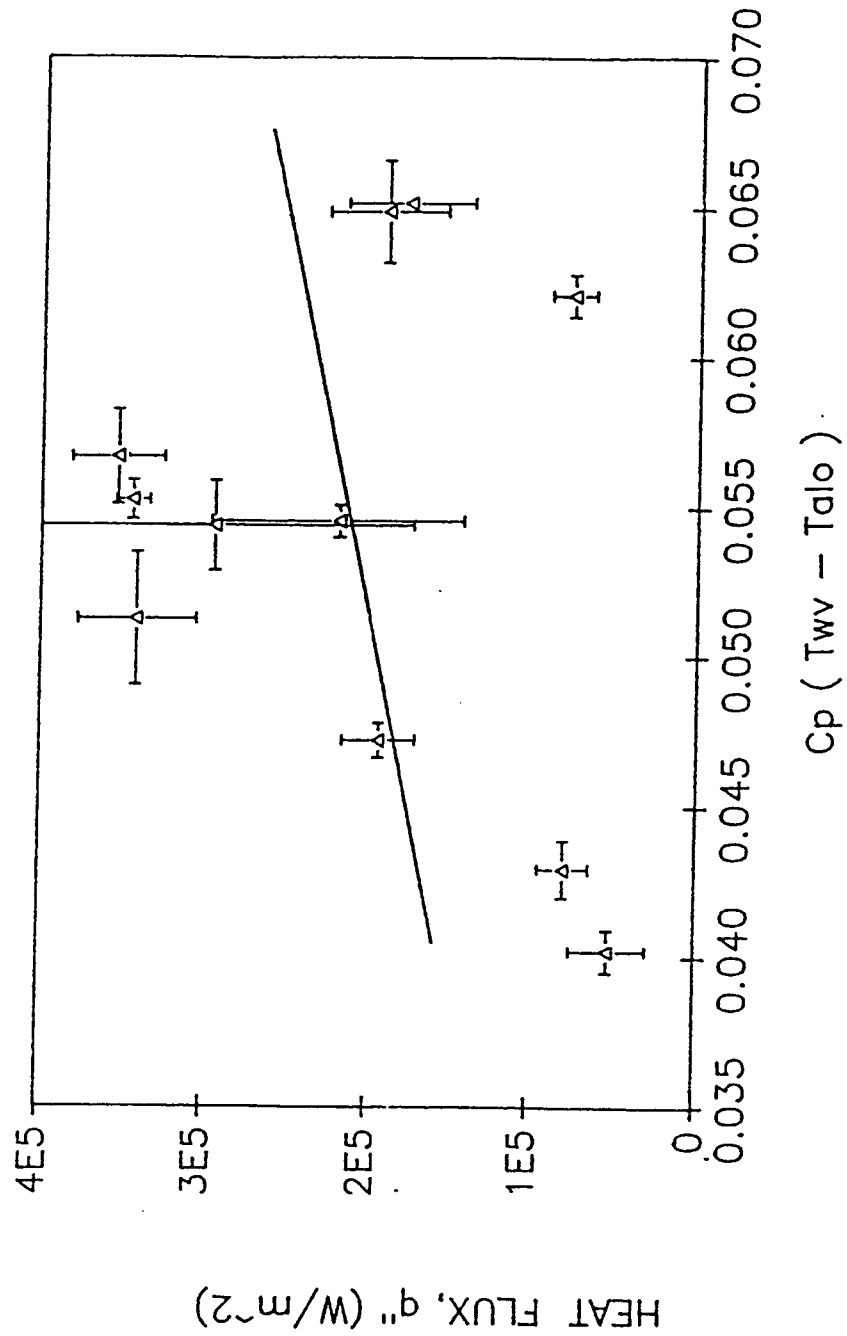
Figure (IV.9) Heat Flux Verses Dimensionless Temperature Difference, Used in Calculating U2, for rotational speed of 400 rpm.
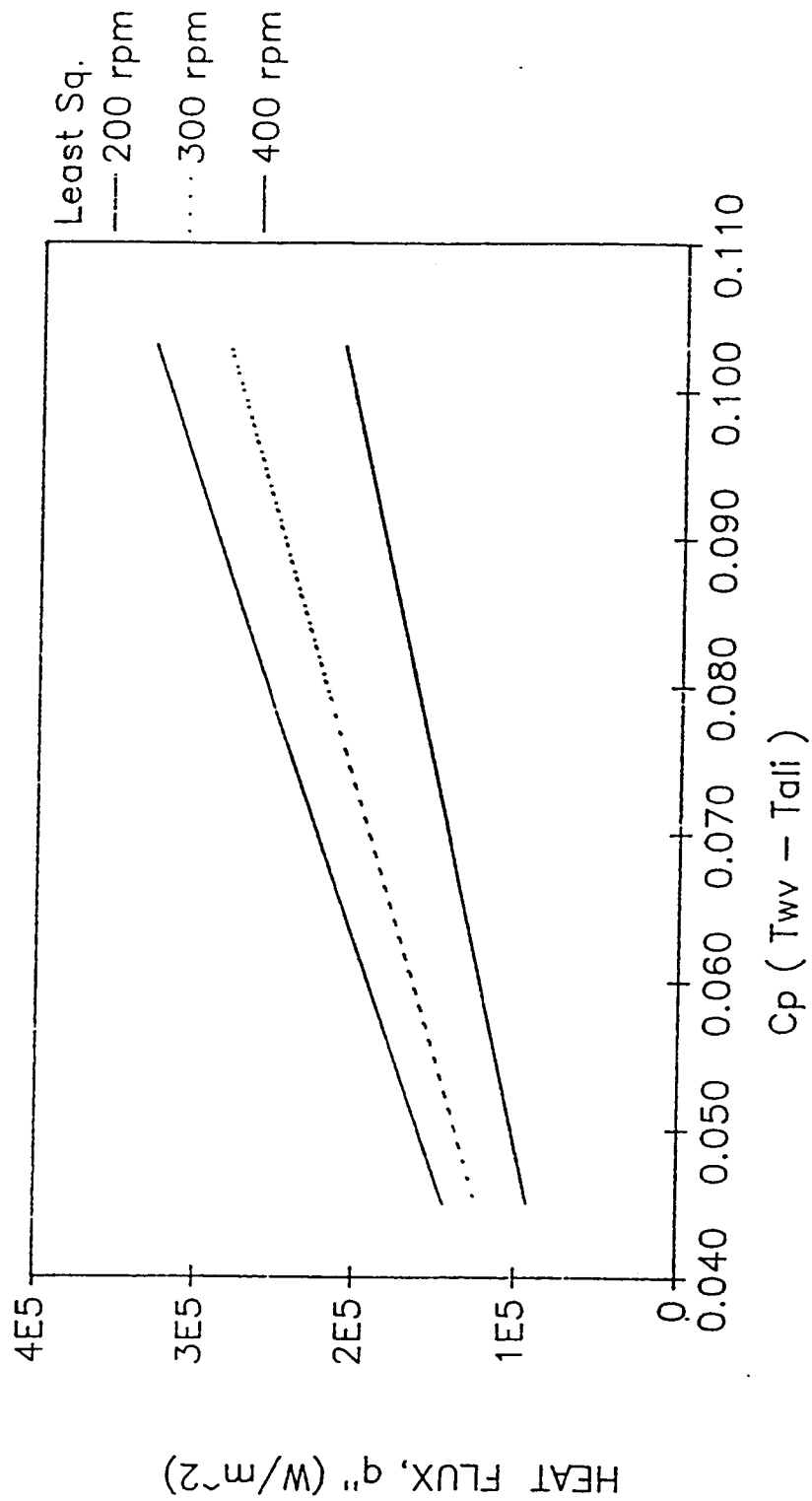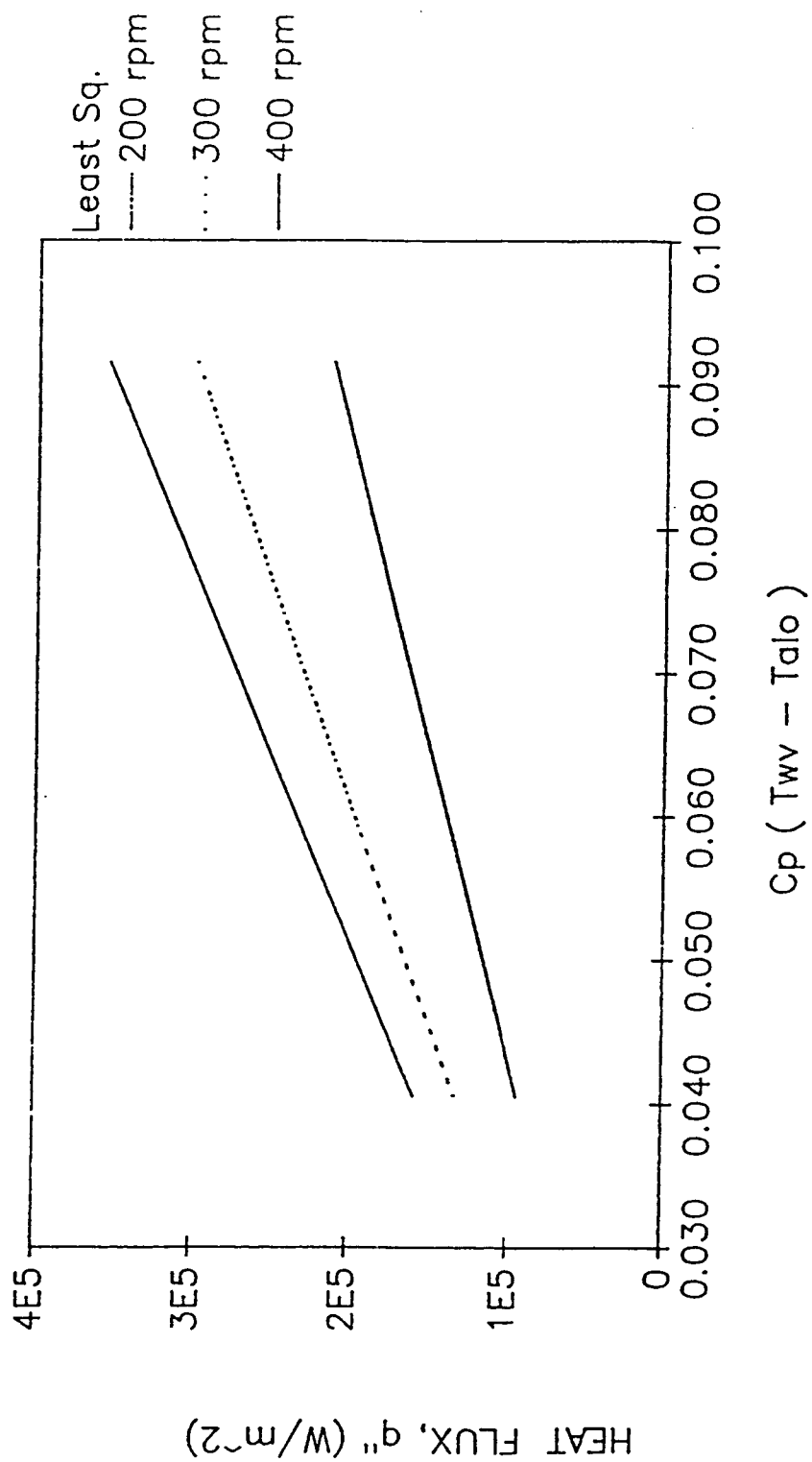
Figure (IV.10) Least Square Fit for the Three Tested Rotational Speeds of Heat Flux Verses Temperature Difference Used in U2.
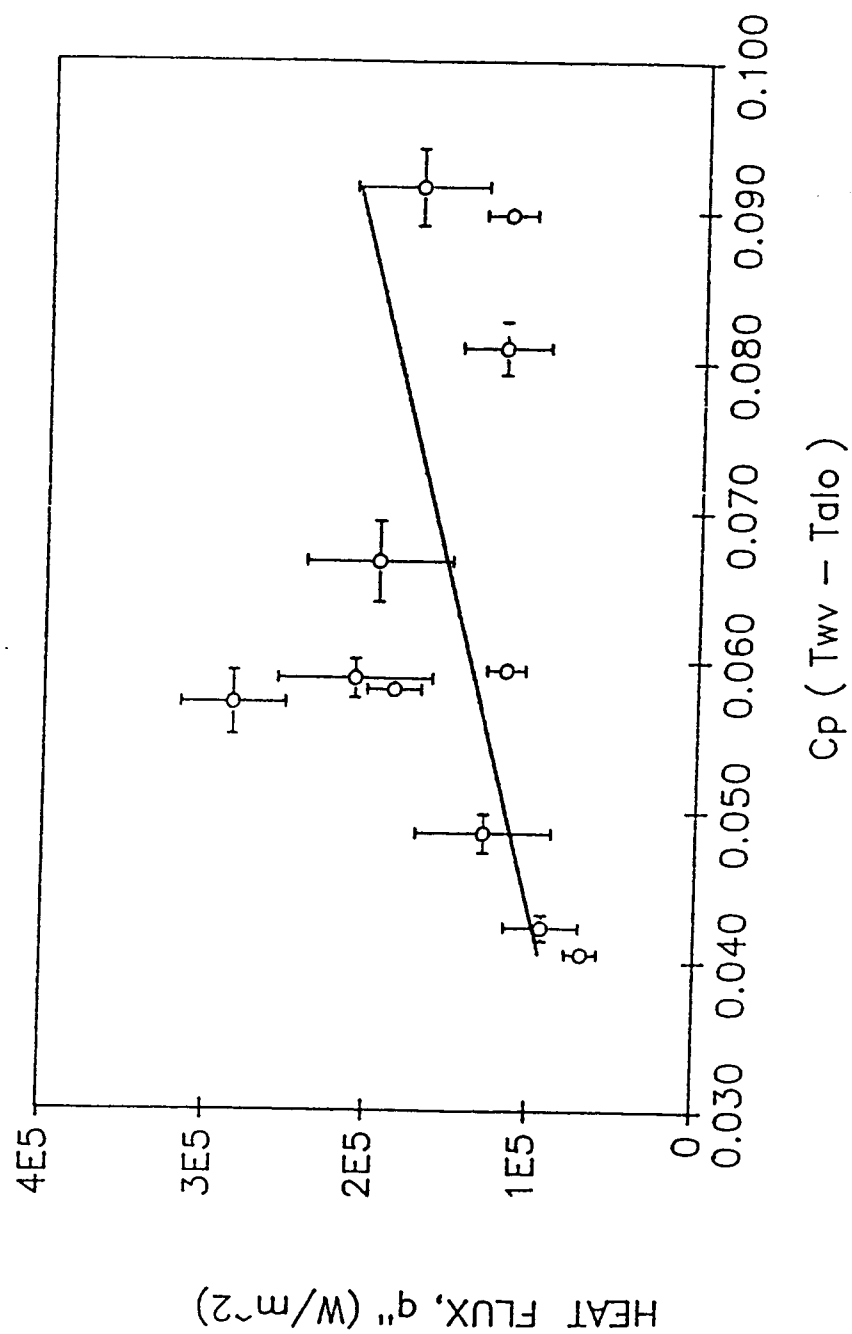
All slopes of the least square curves are positive. Since increasing temperature difference will increase the heat flux, positive slopes are expected.

According to the theory of Sparrow and Gregg[17] for a particular liquid and a fixed temperature difference, the local heat-transfer rate per unit area is proportional to the square root of the disk angular velocity and the relationship should be[17]

$$q'' \propto \omega^{1/2}$$

This relation implies that :

$$\left(\frac{q''_{400rpm}}{q''_{300rpm}}\right) = \left(\frac{\sqrt{400}}{\sqrt{300}}\right) = 1.155$$

$$\left(\frac{q''_{400rpm}}{q''_{200rpm}}\right) = \left(\frac{\sqrt{400}}{\sqrt{200}}\right) = 1.414$$

$$\left(\frac{q''_{300rpm}}{q''_{200rpm}}\right) = \left(\frac{\sqrt{300}}{\sqrt{200}}\right) = 1.225$$

The following tables show the comparison between the theoretical predictions and the experimental results :

TABLE IV.4.a

Comparison Between Theoretical And Experimental Results Of The
Rotational Speed Effect On Heat Flux Using $(T_{wv}-T_{Ali})$

EQUATION (m_{rpm})	THEORETICAL PREDICTION	EXPERIMENTAL RESULT	ERROR %
m_{400} / m_{300}	1.155	1.168	1.105
m_{400} / m_{200}	1.414	1.565	10.661
m_{300} / m_{200}	1.225	1.340	9.384

TABLE IV.4.b

Comparison Between Theoretical And Experimental Results Of The
Rotational Speed Effect On Heat Flux Using $(T_{wv}-T_{Alo})$

EQUATION (m_{rpm})	THEORETICAL PREDICTION	EXPERIMENTAL RESULT	ERROR %
m_{400} / m_{300}	1.155	1.188	2.884
m_{400} / m_{200}	1.414	1.565	18.794
m_{300} / m_{200}	1.225	1.340	15.534

The errors shown in these tables are acceptable for a system which has several sources of error. These will be discussed later. It is noticed that the lowest errors were at the higher rotational speeds where the effect of drop-wise condensation is lowest. The experimental results are in a good agreement with the theory, and the heat flux behaved with the rotational speeds as it should. This result is very important since the heat flux is the basis for the following heat transfer parameters in this research.

The overall heat transfer coefficients verses corresponding temperature difference were plotted for each speed individually, i. e. Figures (IV.12), (IV.13), (IV.14), (IV.16), (IV.17), and (IV.18), and then for the three speeds together, i. e. Figures (IV.11) and (IV.15). On the same plots, theoretical correlation results found by E. M. Sparrow and J. L. Gregg, and the experimental results of S. S. Nandapurkar and K. O. Beatty, Jr., for local heat transfer coefficients were also plotted in order to compare the current results with their results. Two types of curve fitting were used in this study, the least square and a line representing the average data point. All previous studies were plotted for the same dimensionless groups in order to facilitate the comparisons. It is worthwhile to mention that for the S. S. Nandapurkar and K. O. Beatty, Jr. study the lowest rotational speed was 400 rpm, which is the maximum in this study, and they have 5 data points at this speed for methanol and ethanol cases and 4 data points for Freon-113. However their results were found to be consistently 25-30% below the predictions of the E. M. Sparrow and J. L. Gregg correlation for all speeds. Data points of this study were plotted with their standard deviation to show the probable amount of fluctuation in this particular data point. In all cases, curve fittings used in the current study were very close to the analytical curve developed by E. M. Sparrow and J. L. Gregg and also closer to it than the experimental results which were obtained by S. S. Nandapurkar and K. O. Beatty, Jr.
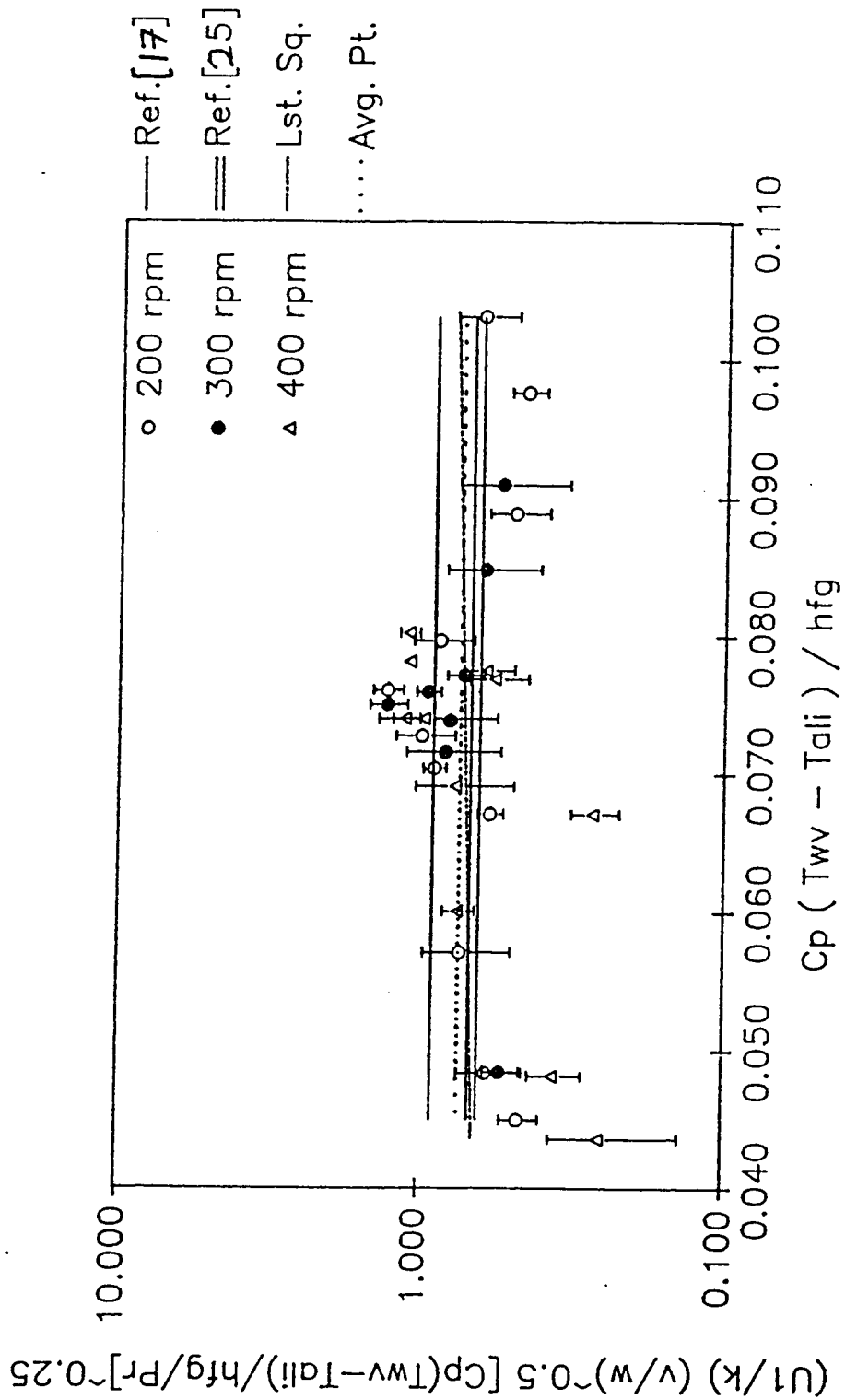
Figure (IV.11) Overall Heat Transfer Coefficient, U1, Correlation Verses
Temperature Difference of Working Fluid and Cold Surface.
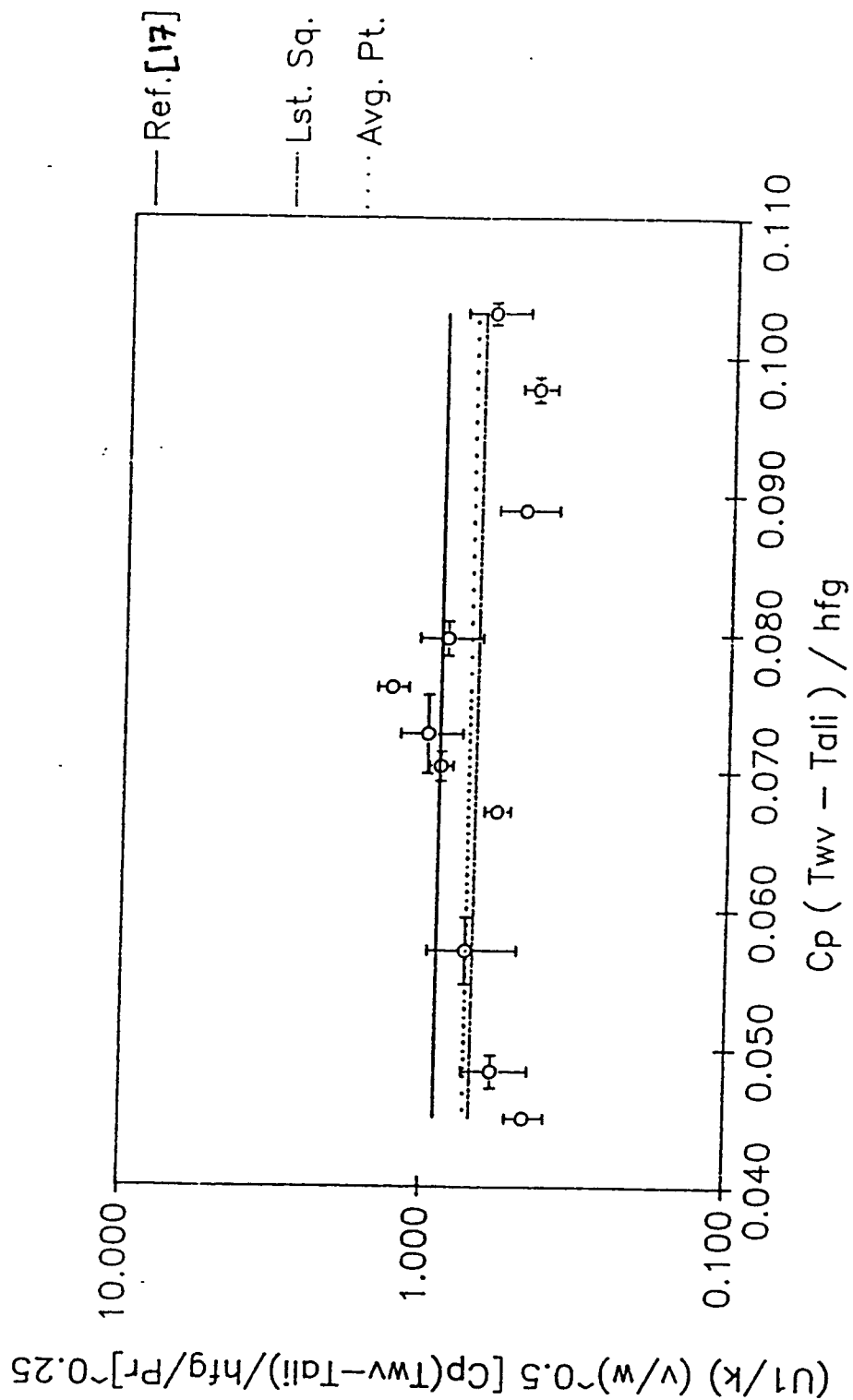
Figure (IV.12) Overall Heat Transfer Coefficient, U1, Correlation Verses
Corresponding Temperature Difference for Rotational Speed
of 200 rpm.
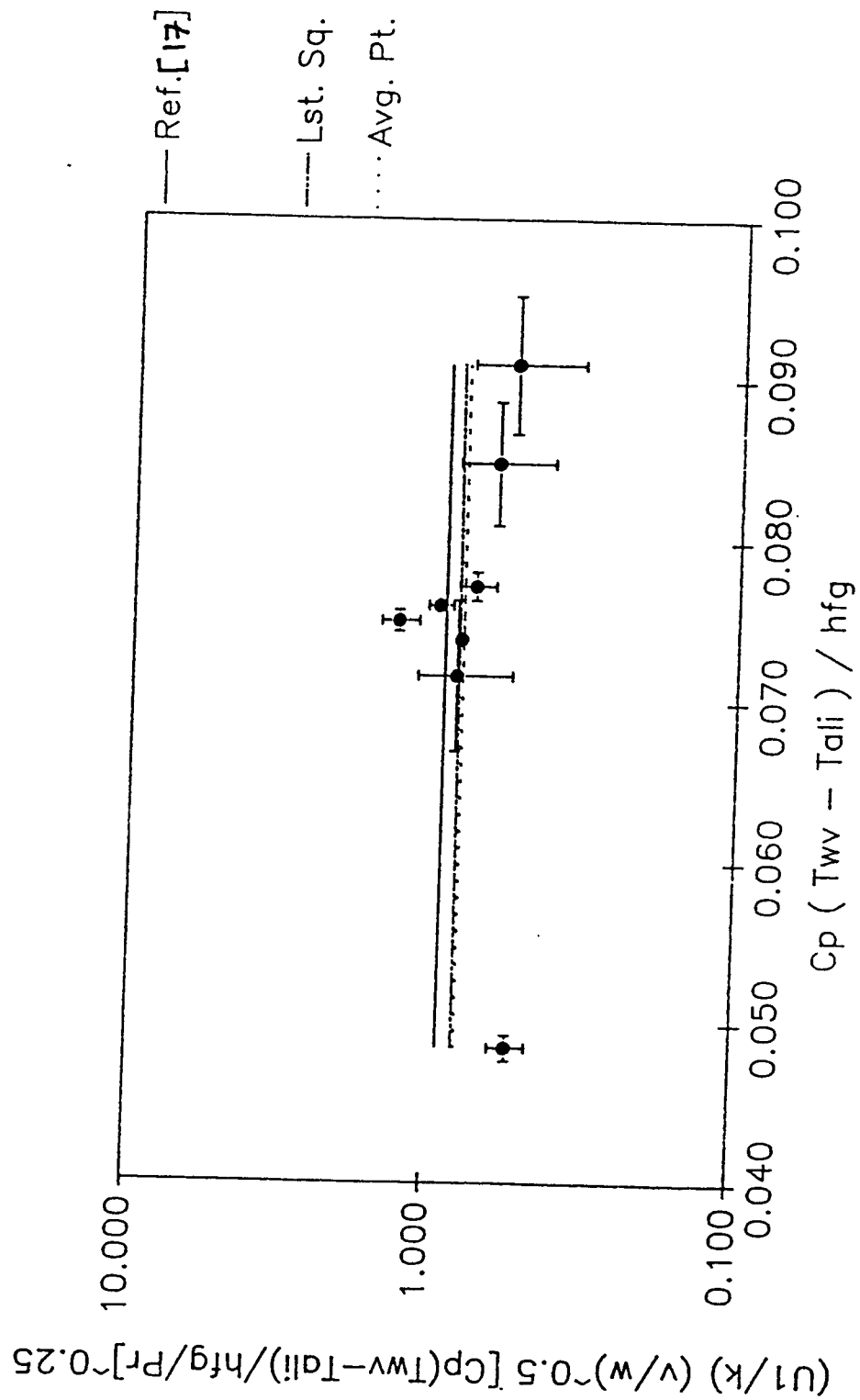
Figure (IV.13) Overall Heat Transfer Coefficient, Ul, Correlation Verses Corresponding Temperature Difference for Rotational Speed of 300 rpm.
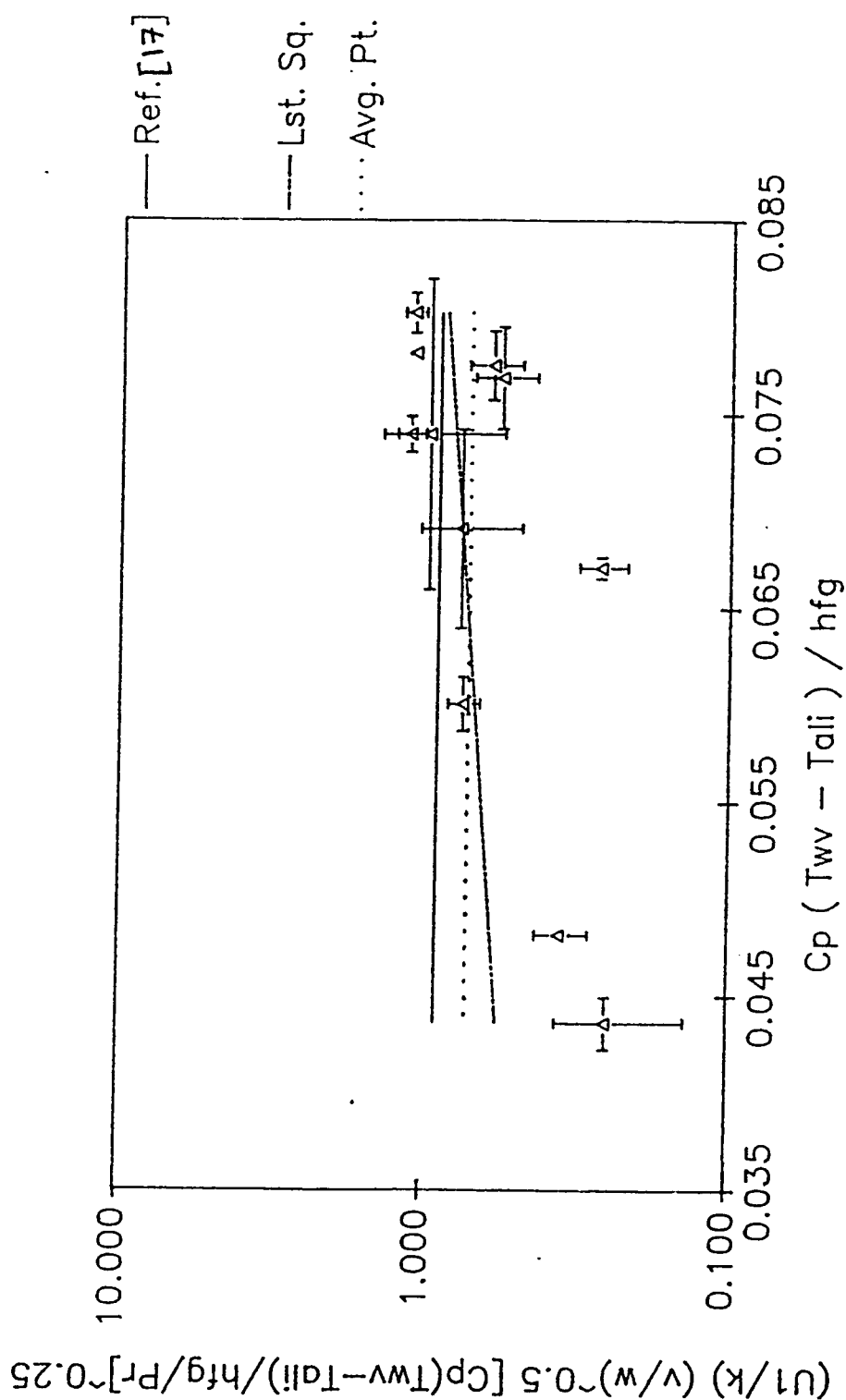
Figure (IV.14) Overall Heat Transfer Coefficient, Ul, Correlation Verses
Corresponding Temperature Difference for Rotational Speed
of 400 rpm.
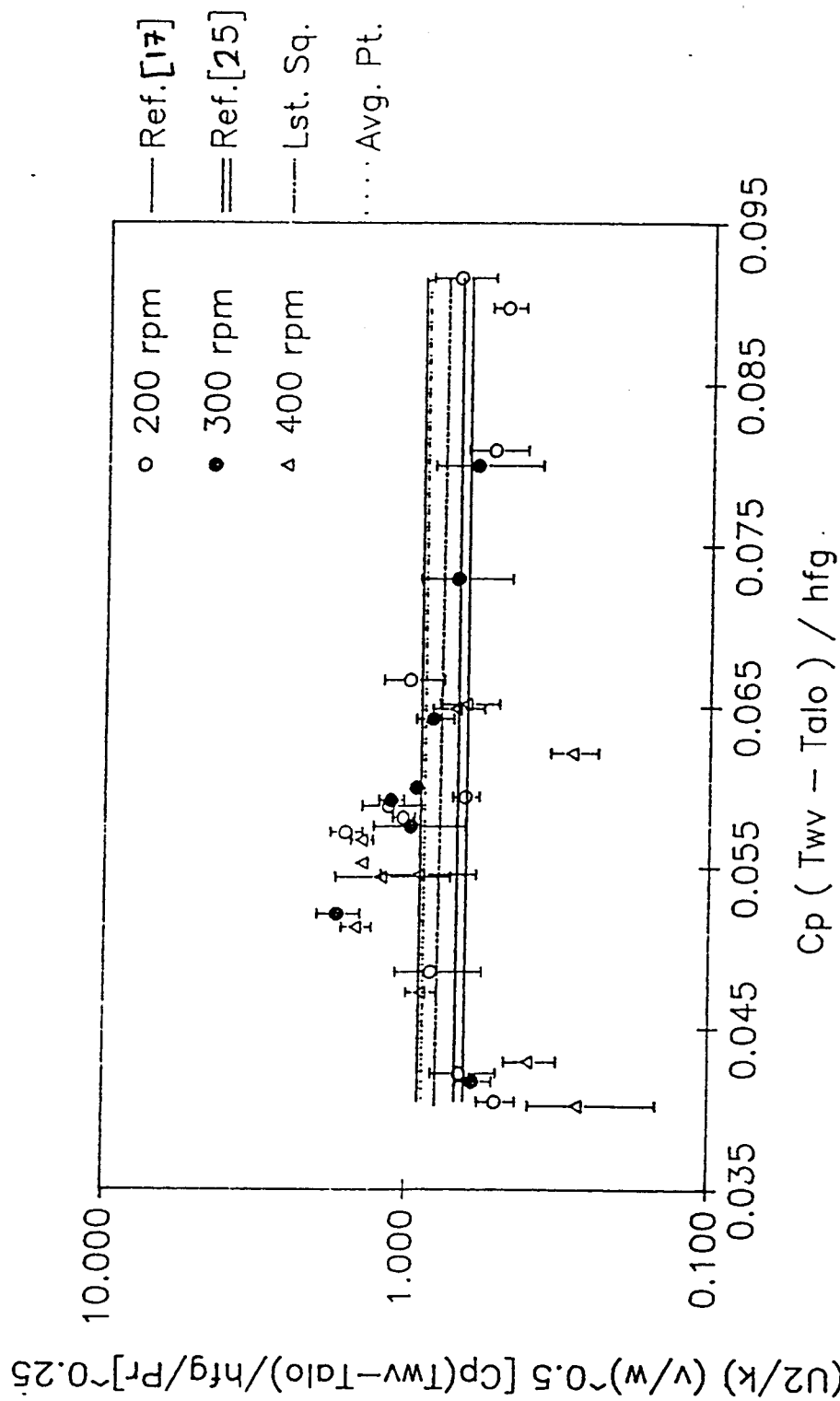
Figure (IV.15) Overall Heat Transfer Coefficient, U2, Correlation Verses
Temperature Difference of Working Fluid and Cold Surface.
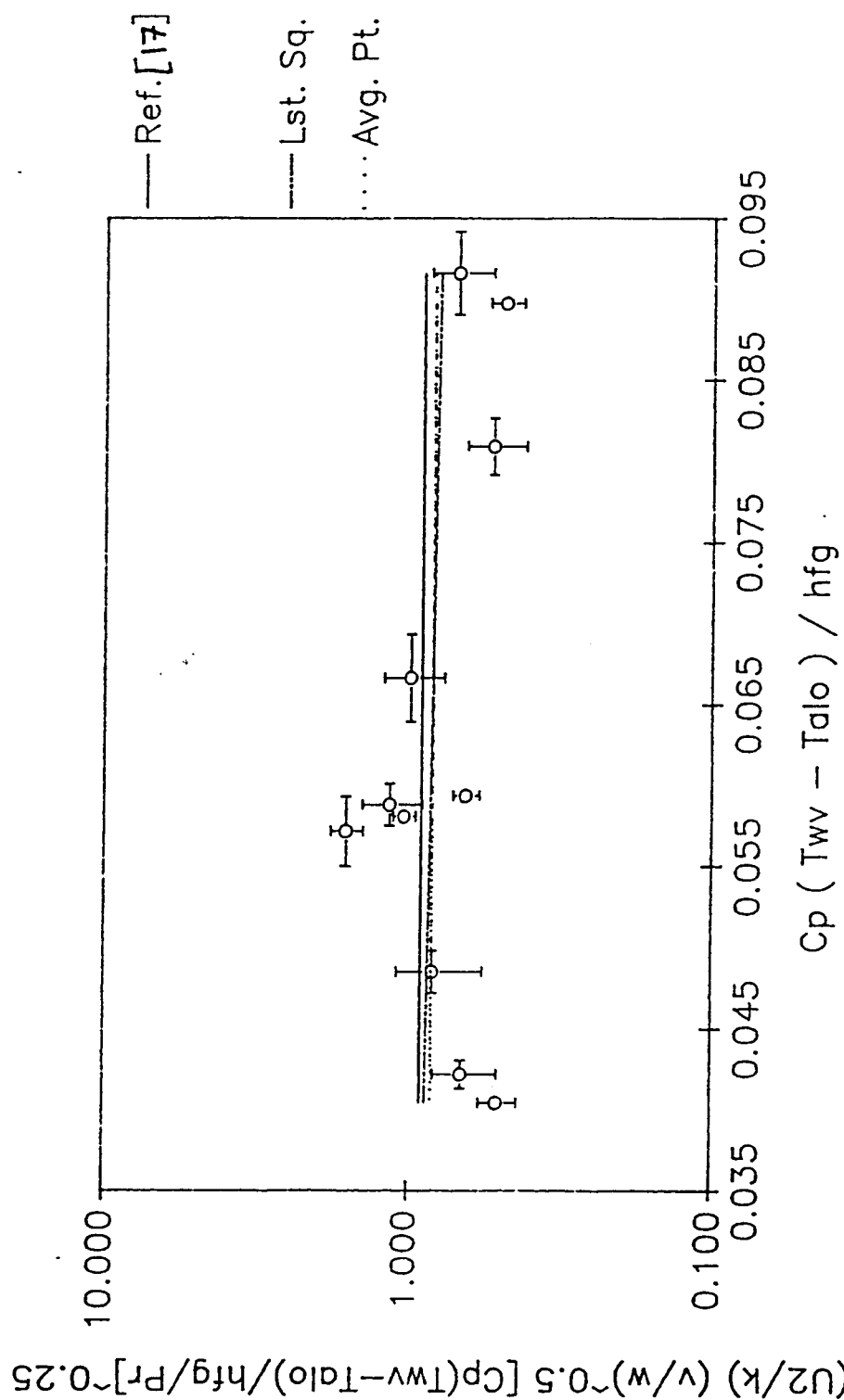
Figure (IV.16) Overall Heat Transfer Coefficient, U2, Correlation Verses
Corresponding Temperature Difference for Rotational Speed
of 200 rpm.
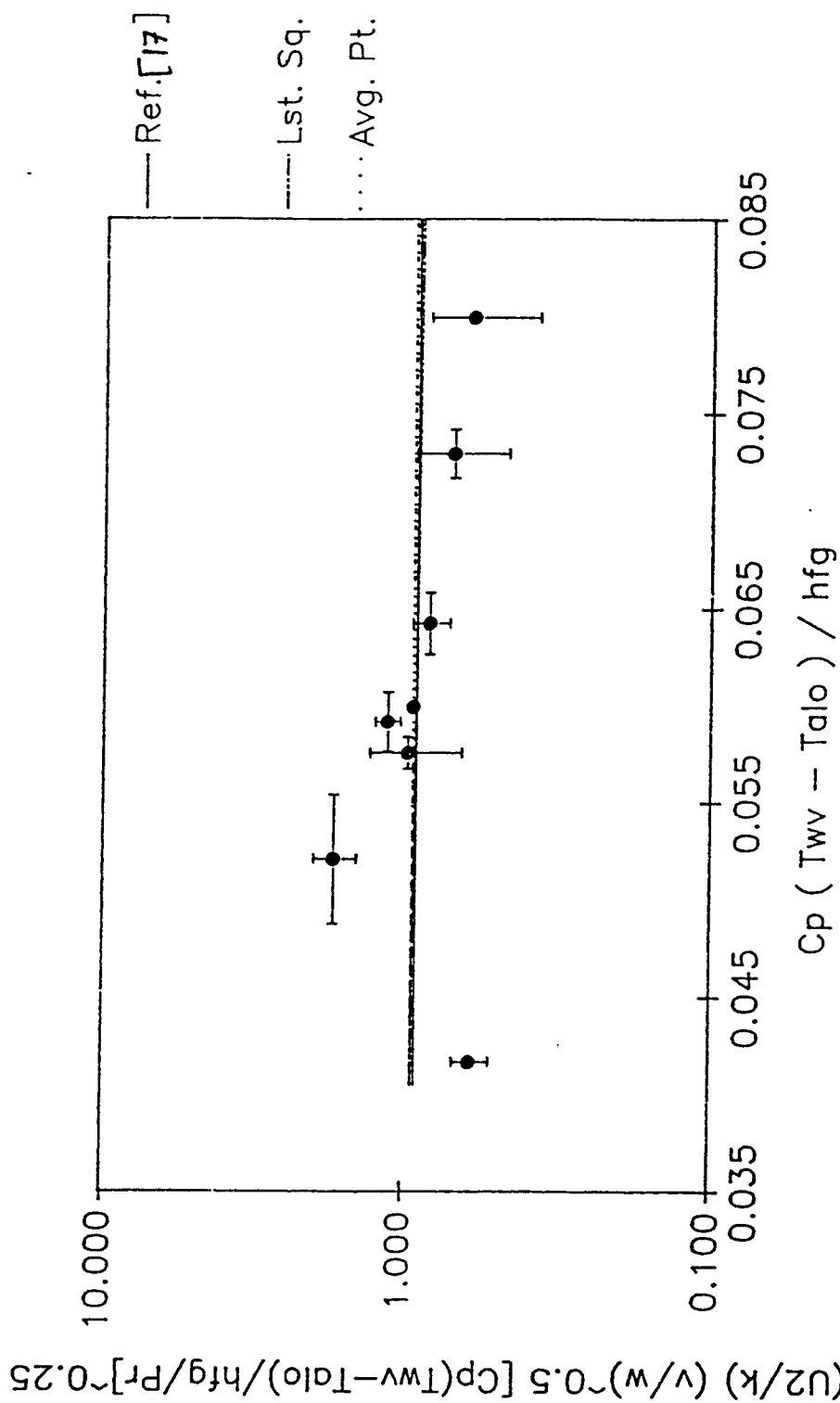
Figure (IV.17) Overall Heat Transfer Coefficient, U2, Correlation Verses
Corresponding Temperature Difference for Rotational Speed
of 300 rpm.
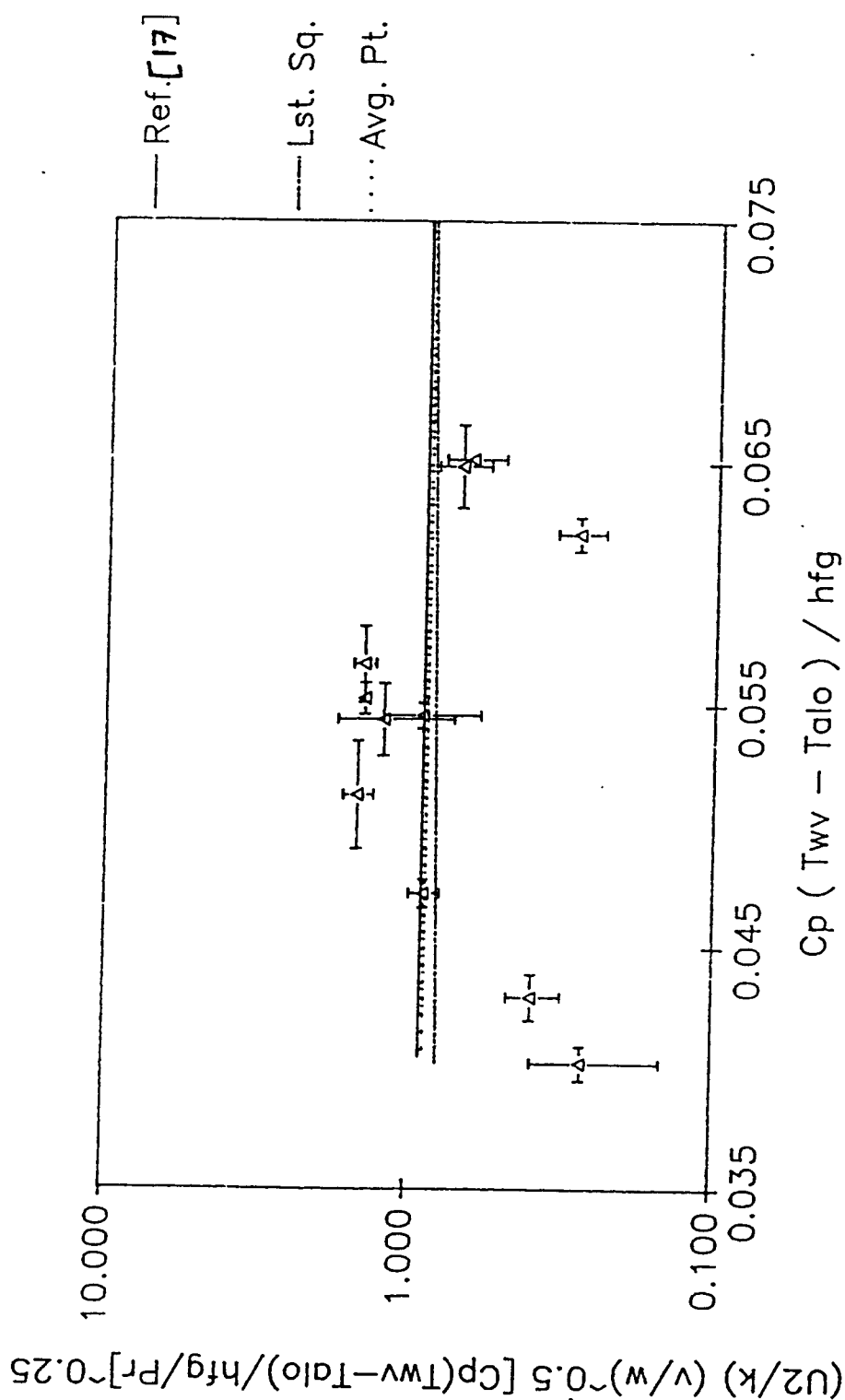
Figure (IV.18) Overall Heat Transfer Coefficient, U2, Correlation Verses Corresponding Temperature Difference for Rotational Speed of 400 rpm.

The average local heat transfer coefficients were calculated using equation 3.5, and the corresponding average condensing surface temperatures were found using equation 3.6. Their standard deviations were found using methods mentioned in Section III.2.4. The results are shown in Tables IV.5.a, b, and c.

The accumulation of errors, during error propagation calculations, for the average local heat transfer coefficients resulted in some negative values of h_{avg}, which is theoretically wrong. These values were dropped from consideration. This is the reason why less data points were mentioned in table IV.5 than in the previous Tables.

TABLE IV.5.a[7]

Heat Transfer Coefficient Correlation Using h_{avg} For Plate
Angular Speed Of 200 rpm

Log No.	T_c (°C)	$T_w - T_c$ (°C)	h_{avg} (W/m²/°C)	$C_p \Delta T / h_{fg}$	Correl. (using h_{avg})
9	42.88 7.5	6.20 7.5	31572 39055	0.011 0.013	3.85 4.90
12	37.91 6.8	24.11 6.8	7184 2641	0.042 0.012	1.23 0.46
15	34.56 3.7	9.04 3.7	10221 4899	0.016 0.007	1.37 0.67
16	36.89 6.8	6.70 6.8	19221 20526	0.012 0.012	2.39 2.62
25	44.42 2.7	3.02 2.7	61267 55530	0.005 0.005	6.24 5.83
60	38.69 1.6	12.02 1.6	5662 1138	0.021 0.003	0.82 0.17
62·	40.24 2.0	14.95 2.0	7784 1294	0.026 0.003	1.18 0.20
66	34.38 4.5	26.66 4.5	4502 1270	0.047 0.008	0.79 0.23
67	33.80 2.6	31.99 2.6	3699 572	0.056 0.005	0.68 0.11

[7]Lower value denotes the Standard Deviation.

TABLE IV.5.b[8]

Heat Transfer Coefficient Correlation Using h_{avg} For Plate Angular Speed Of 300 rpm

Log No.	T (°C)	$T_w - T_c$ (°C)	h_{avg} (W/m²/°C)	$C_p \, \Delta T / h_{fg}$	Correl. (using h_{avg})
26	35.00 4.6	12.44 4.6	15604 6171	0.022 0.008	1.85 0.75
29	45.26 4.1	2.18 4.1	116150 217451	0.004 0.007	8.90 17.17
30	37.65 1.1	8.16 1.1	25592 3485	0.014 0.002	2.73 0.38
60	37.94 2.3	11.13 2.3	9111 2270	0.019 0.004	1.05 0.27
66	35.79 10.0	19.40 10.0	9190 5664	0.034 0.017	1.22 0.77
67	33.82 10.6	25.02 10.6	6606 3818	0.044 0.019	0.93 0.55
68	42.56 11.8	6.51 11.8	32395 59722	0.011 0.021	3.26 6.20

[8]Lower value denotes the Standard Deviation.

TABLE IV.5.c[9]

Heat Transfer Coefficient Correlation Using h_{avg} For Plate
Angular Speed Of 400 rpm

Log No.	T_c (°C)	T_w-T_c (°C)	h_{avg} (W/m²/°C)	$C_p \Delta T/ h_{fg}$	Correl. (using h_{avg})
55	32.52 3.8	16.55 3.8	3100 1562	0.029 0.007	0.34 0.17
57	35.99 2.6	14.71 2.6	5337 1413	0.026 0.005	0.57 0.15
60	44.60 3.8	2.84 3.8	67967 90212	0.005 0.007	4.82 6.59
62	34.00 2.3	26.06 2.3	2889 578	0.046 0.004	0.36 0.07
66	35.79 6.1	13.28 6.1	14327 7186	0.023 0.011	1.49 0.77
67	33.89 6.5	15.18 6.5	11620 5608	0.026 0.011	1.25 0.62
68	46.89 12.7	3.81 12.7	57424 192036	0.007 0.022	4.38 15.10

[9]Lower value denotes the Standard Deviation.

The average local heat transfer coefficients were plotted against the average calculated temperature difference across the film condensate, both in dimensionless groups, for the flat plat rotational speeds of 200, 300, and 400 rpm, together. The best curve fit for all data points is shown in Figure (IV.19). In Figure (IV.20), only values of $C_p \Delta T / h_{fg} \geq$ 0.105 were considered and then same comparing curves and best fittings used in analyzing data for overall heat transfer coefficients were used too.

The high errors shown in low values of $C_p \Delta T / h_{fg}$, i.e. for values $\leq$ 0.015, should be attributed to neglecting the heat resistance due to the gap effect between the Aluminum plate and the Stainless steel plate in equation 3.5. Low ΔT tends to have higher errors, while when ΔT increases, the assumption of neglecting the gap effect on heat transport seems to be reasonable. It was not easy to precisely measure the tiny gap for each experiment.
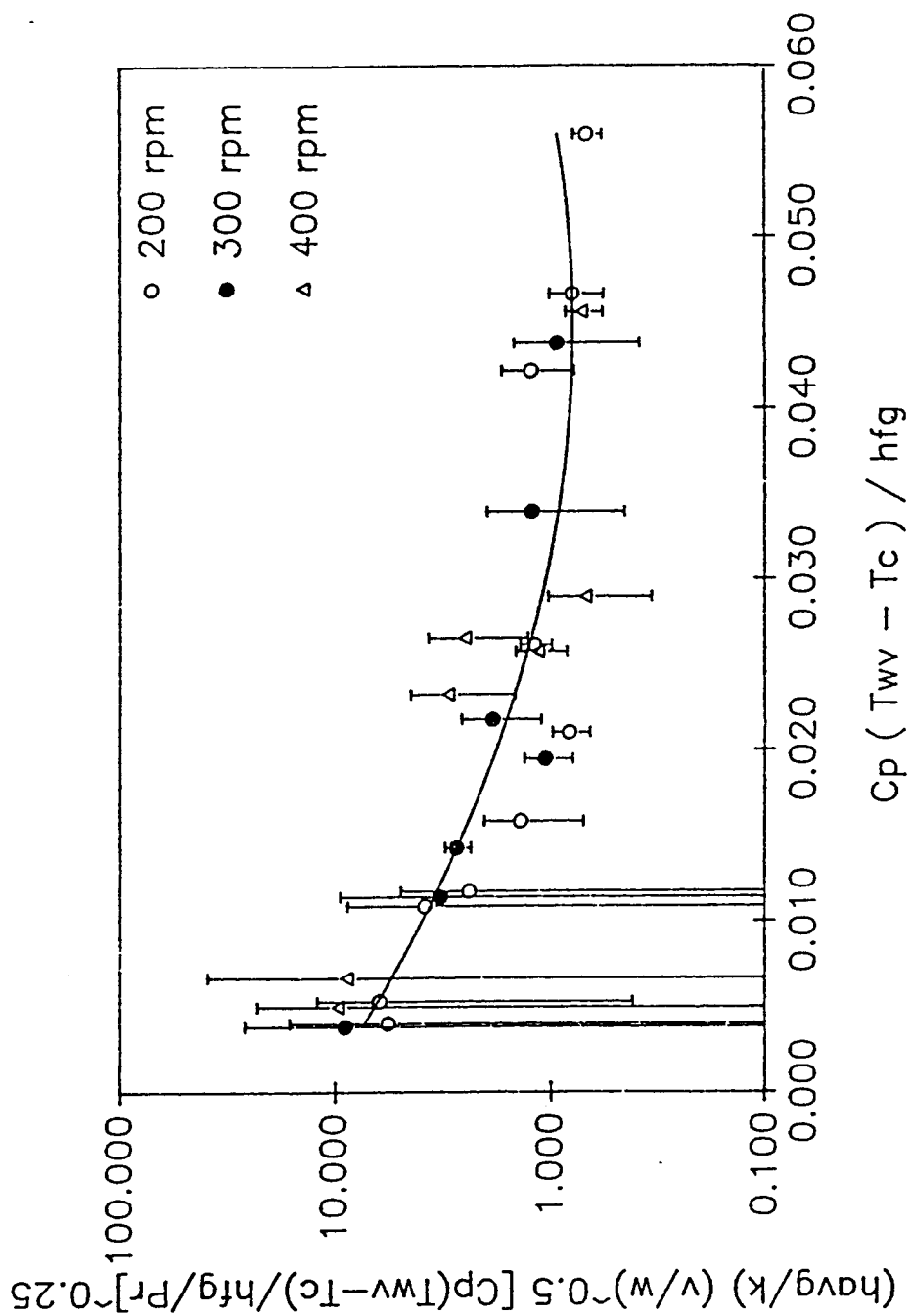
Figure (IV.19) Best Fit of the Average Heat Transfer Coefficient
Correlation Data Points.
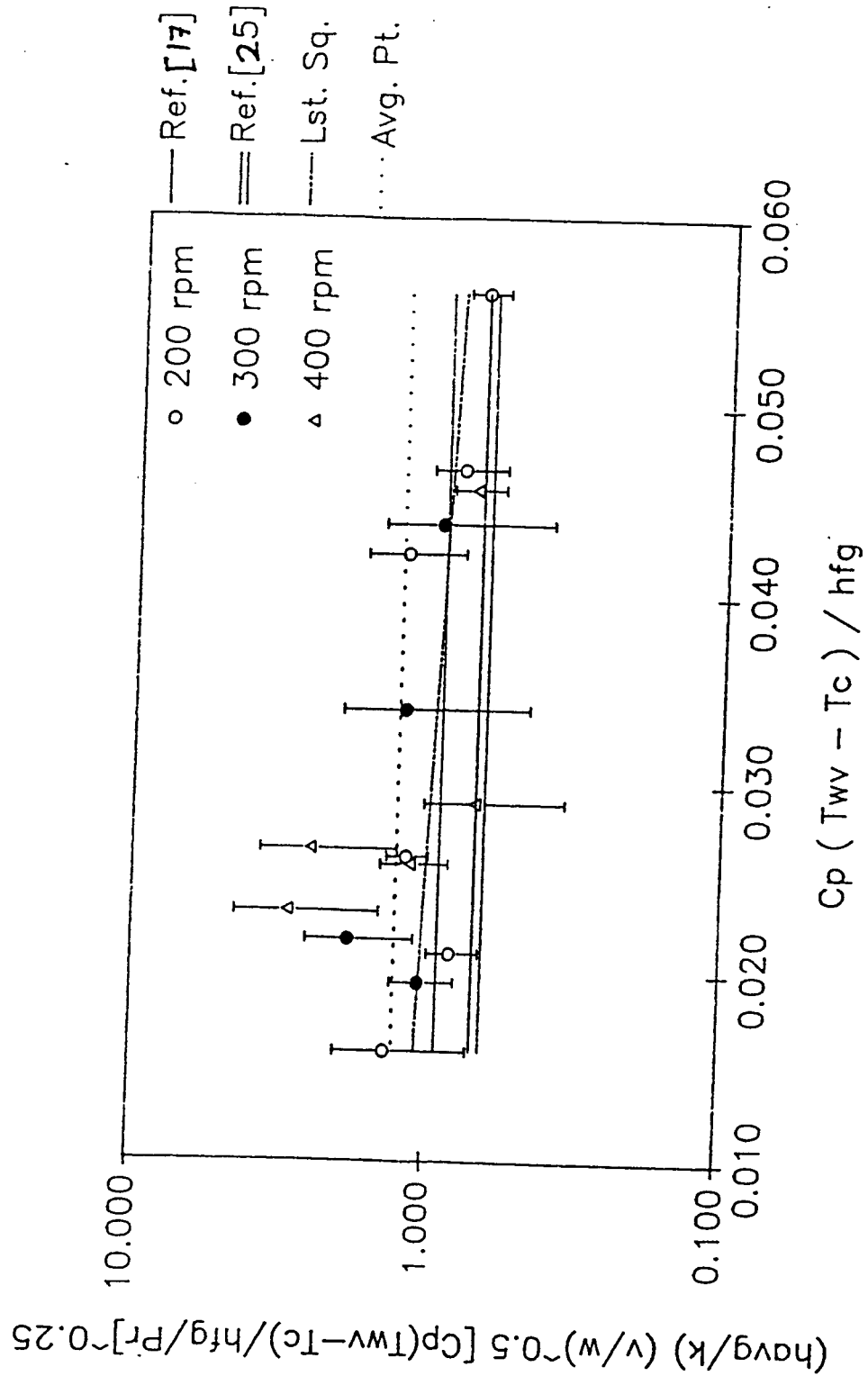
Figure (IV.20) Average Heat Transfer Coefficient Correlation Verses
Temperature Difference across the condensate film.

IV.3 Thickness Measurement And Flow Patterns :

Several experiments were performed attempting to find the film condensate thickness at all tested rotational speeds using expected resolution of reflected laser beam, from the condensing surface and the condensate film, on laser receivers.

A few problems were faced in measuring the condensate film thicknesses. The first major problem was the system vibration that develops wavy films in the condensate which let the laser beam to look like a fuzzy moving point at the laser receiver. A second problem, the laser beam diameter was wider than the condensate film thickness which causes overlapping points at the laser receiver. This gets worse as the rotational speed increases. Less important reasons why the measurements of the thickness were difficult were drop-wise condensation at the center of the condensing surface, and condensation on the inside surface of the glass pipe.

When the technique was tested for 0 rpm under standard pressure and temperature with water film thicknesses greater than the laser beam diameter, the technique worked nicely; this is shown in Figure (IV.21). As mentioned in section II.3, no study has been found dealing experimentally with the condensate film thickness measurements on rotating geometries; and the current study fails to contribute. Figure (IV.22) shows pictures of the laser receivers where laser beams could not be recognized from each other as desired or too fuzzy to be noticed. None of

these preliminary results were considered, and additional research is needed in this area.

Few preliminary results to investigate the change of flow patterns with the rotational speeds were videotaped at all tested rotational speeds. The technique and results looked to be working nicely. Since most of the problems that were faced in measuring the condensate thickness were also faced in studying condensate flow patterns, no further experiments were performed. It was set as a proposed future work. Since reasonable efforts were spent on this study, it is worth to be mentioned. These preliminary results showed curved flow patterns which gave the expected result.
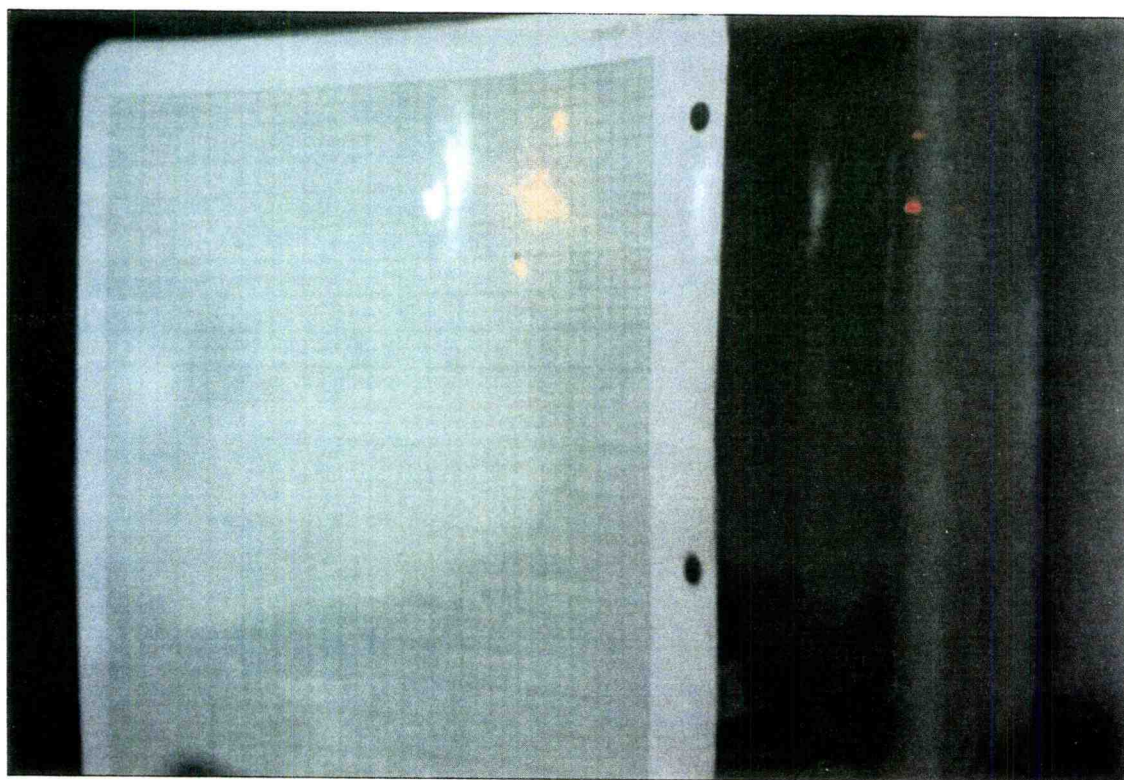
Figure (IV.21) A Picture of Laser Receiver While Flat Plate is Stationary.
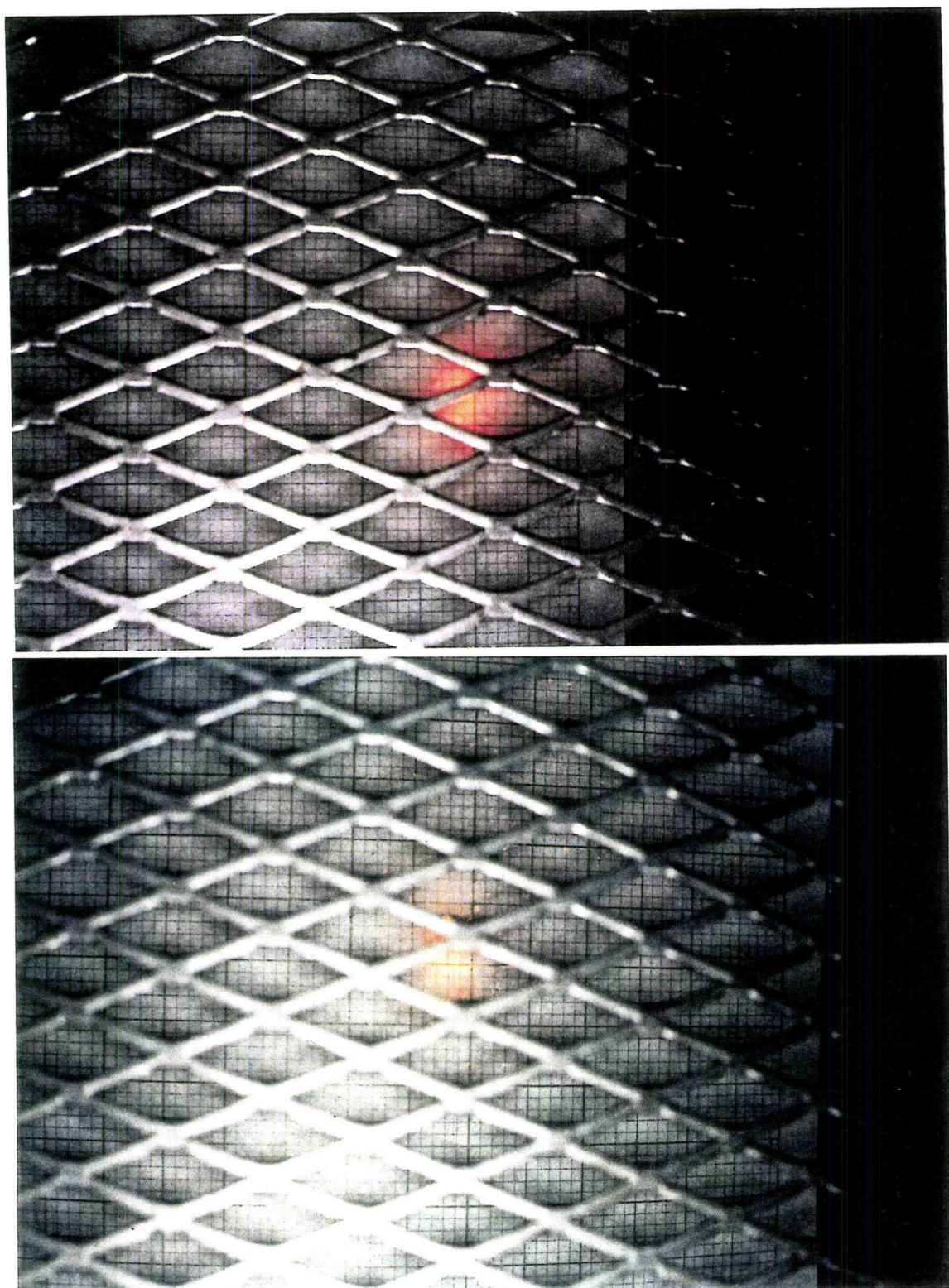
Figure (IV.22) Pictures of Laser Receivers While Flat Plate is Rotating.

IV.4 General Error Sources Discussion :

A number of specific errors were mentioned in different places in this chapter for specific results. The following sources of errors are common between all tests and cause some degree of uncertainty in the results.

1) One-Dimension Heat Transfer Assumption :

By inspecting Tables IV.1.a,b, and c, one can compare the temperature difference (T_{wv} - T_{Ali}) which causes the heat to be transferred in the Z-direction, and the temperature difference of (T_1 - T_2) or (T_3 - T_4) which causes the heat to be transferred in the R-direction. T_{wv} represents the temperature of the interface area between the water vapor and condensate films, and T_{Ali} represents the average temperature of the inner aluminum plate surface. The distance between these two locations in Z-direction equals the aluminum plate thickness (0.635 cm), the stainless steel plate thickness (0.265 cm), the gap between the plates, plus the film condensate thickness. The last two thicknesses were very small and difficult to measure, being conservative, it could be assumed that both of these thicknesses together equal to 0.2 cm. As a result, the total thickness in Z-direction was about 1.1 cm. The distance between the thermocouples on each side of the aluminum plate, which is in R-direction, was 3.81 cm.

A simple way to compare the amount of heat transfer in the Z-direction to that in R-direction is to look at the temperature gradient, in both directions. By inspecting Tables IV.1.a,b, and c, one can conclude that the temperature drop per centimeter in R-direction is very

much lower than that of Z-direction. An example, randomly chosen, for each rotational speed is shown in Table V.6. As a result, the one-dimension, i. e. Z-direction, heat transfer assumption seems to be reasonably accepted.

TABLE IV.6

Comparison Of Temperature Drop Per Centimeter
In R And Z Direction

Log # (rpm)	R-direction (°C/cm)	Z-direction (°C/cm)	(R-dir./Z-dir.)%
25 (200)	1.85	36.57	5.1
30 (300)	2.08	38.35	5.4
47 (400)	3.44	40.60	8.5

2) Steady State Condition Assumption :

Figures (IV.1) and (IV.2) have shown a typical sample of the output data. It is clear that a complete steady state condition in which the temperature does not change with time was not strictly achieved. But, the Figures also showed that the temperature change with time was not too large. It was claimed that a quasi steady state condition was achieved where the temperature changes very slowly with time. A complete steady state problem could not be reached even for long time runs due to the fact that the ice block melts.

Assuming a fully steady state problem should add an error to the results. The amount of error depends solely on how much the temperatures change with time. Smaller change means less error and vice versa. In almost all of the adopted cases of this study, the change was very small

and Figure (IV.2) a typical result. Those runs that did not satisfy this condition were rejected. Thus, the assumption is reasonable and the error resulting from it should be acceptable.

3) Drop-Wise Condensation :

As was discussed in Section II.4, drop-wise condensation is associated with much higher heat transfer rates than film-wise condensation. Since the theoretical model used for comparison assumed film-wise condensation, it is required to obtain film-wise condensation for a good comparison. Even though surface treatment was used to get film-wise condensation over the entire condensing surface, drop-wise condensation was noticed at the center area in several cases. It was noticed also that higher rotational speeds tend to decrease this area of drop-wise condensation. This seems logical since more force would be applied on the droplets to push them outward to join with other droplets forming a film.

However, it was thought that for some cases this source of error had the highest effect on the results where they tend to increase the heat transfer. Therefore, no run which had drop-wise condensation on areas other than the center area was included in the analysis.

4) Non-Condensable Gases :

In all experiments, the glass pipe was evacuated to 6-7 KPa (the maximum which could be reached using the available system) before introducing the steam. This is expected to reduce the effect of non-condensable gases dramatically. As mentioned in section II.5, this source of error tends to reduce the heat transfer coefficient.

5) System Vibration :

In all tests it was observed that as the rotational speed increased the system vibration increased. This might affect the expected condensate thickness shape which in order affects the expected distribution of the heat transfer along the condensing surface. Even though this source of error was thought to have the least effect, it is worth mentioning.

IV.5 Special Experiment Run Cases :

Several other experiments were made to see the effects of various parameters on the experimental results. The main two parameters were the effect of evacuation and the effect of zero rotational speed. Two experiments were conducted, one for standard pressure and the other for 85 KPa, each one of them used the three tested speeds. Comparing the results of these two experiments with the other ones where the starting operating pressure was 6-7 KPa, it was found that the heat flux was much lower in these two cases than in the others. This was attributed to the following: less steam could enter the system in these two experiments than in cases where the vacuum was low enough to draw in a sufficient amount of superheated water vapor to fill the system. As a result not enough steam was available to simulate the tested model where the system is full of steam to accommodate the maximum demand of the condensing surface. One other reason could be the presence of air, i.e. non-condensable gases, in the system which tends to reduce the heat transfer coefficient. The results of these two experiments, are shown in Table IV.6.a ad IV.6.b.

TABLE IV.7.a

Heat Transfer Correlation For U1 And U2 At Standard Pressure (T_{wv}=100°C)

Speed (rpm)	$T_{\Delta l i}$ (°C)	$T_{\Delta l o}$ (°C)	q" (W/m²)	$C_p\Delta T_{U1}/h_{fg}$	Corr. using U1	$C_p\Delta T_{U2}/h_{fg}$	Corr. using U2
200	8.73	12.06	87458	0.16	0.23	0.15	0.24
300	4.08	8.74	122725	0.17	0.25	0.16	0.26
400	1.18	4.98	99923	0.17	0.17	0.17	0.18

TABLE IV.7.b

Heat Transfer Correlation For U1 And U2 At 85 KPa (T_{wv}=95°C)

Speed (rpm)	$T_{\Delta l i}$ (°C)	$T_{\Delta l o}$ (°C)	q" (W/m²)	$C_p\Delta T_{U1}/h_{fg}$	Corr. using U1	$C_p\Delta T_{U2}/h_{fg}$	Corr. using U2
200	8.87	12.28	89641	0.15	0.25	0.15	0.25
300	6.38	9.78	89430	0.16	0.20	0.15	0.20
400	2.45	6.28	100594	0.16	0.18	0.16	0.19

In addition, three experiments were conducted at 0 rpm in exactly the same way as the other experiments were conducted. As it is shown in Table IV.7, the measured heat transfer parameters are much higher than those supposed to be, for film-wise condensation, at 0 rpm. It was visually clear that drop-wise condensation was obtained in these experiments which explains why more heat was transferred. This supports the need to put more force on the condensate droplets to join each other forming a film. Creating centrifugal forces through rotating the flat plate at higher rotational speeds is the easiest way to get such a force in such a system.

TABLE IV.8

Heat Transfer Measurements At 0 rpm

T_{HW} (°C)	T_{Ali} (°C)	T_{Alo} (°C)	q'' (W/m^2)	Cp1	U1 (W/m^2/ °C)	Cp2	U2 (W/m^2/ °C)
47.44	3.06	11.04	197770	0.08	4456	0.06	5433
45.81	2.22	8.48	152798	0.08	3505	0.07	4093
47.44	4.26	11.93	203950	0.08	4723	0.06	5742

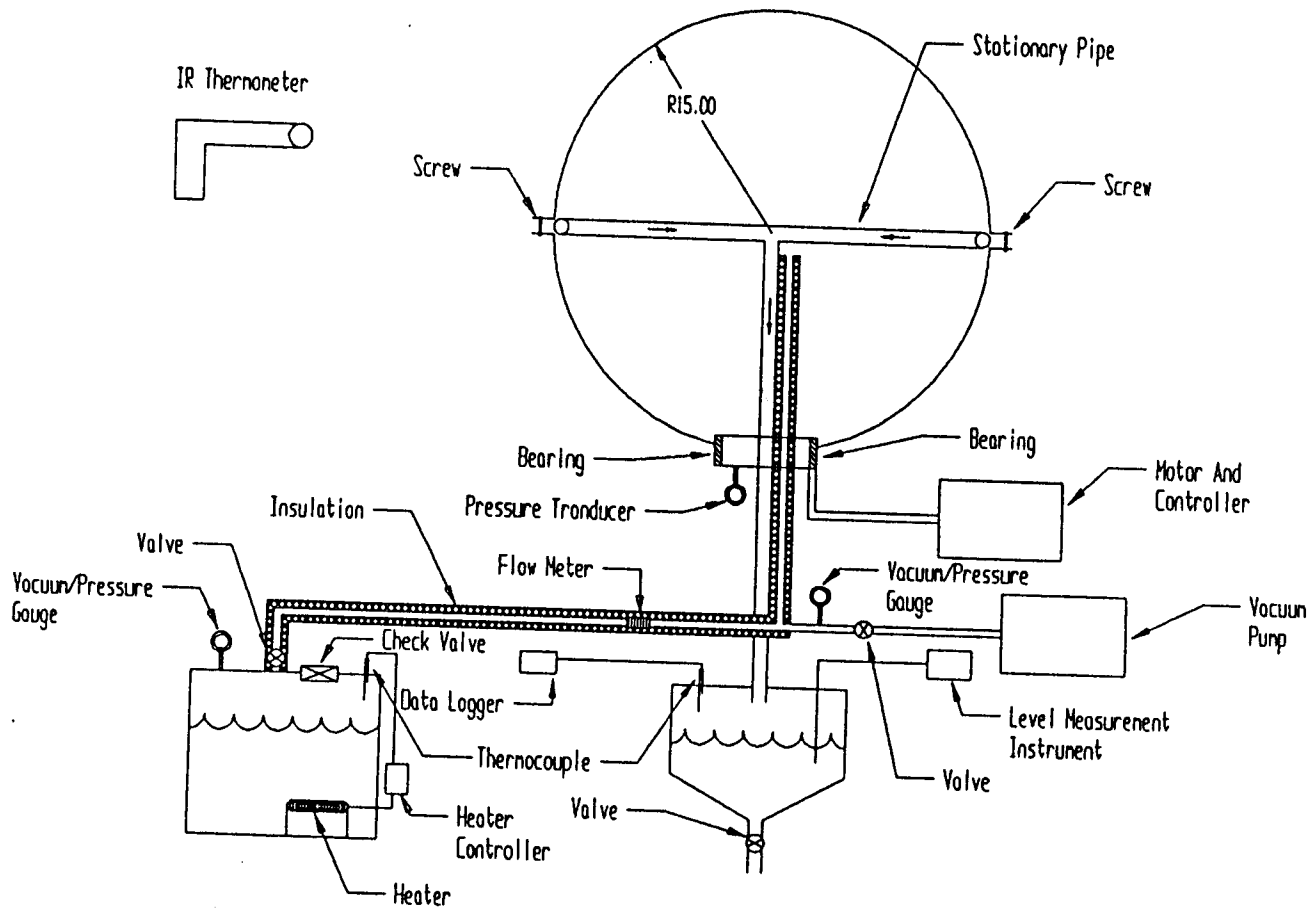## V. RBMR Prototype Design and Construction

V.1 Introduction :

A full sphere RBMR test stand was designed and constructed to simulate one of the proposed configurations of the RBMR. Figure (V.1) shows a schematic drawing of major parts and equipment of this RBMR test.

An investigation was made to compare the effect of various rotational speeds on a working fluid droplet on a rotating flat plate and on the inner surface of a rotating sphere. Both droplets were assumed to have the same size, are swept on perfect frictionless surfaces, and in a micro-gravity environment, i.e. gravitational forces were neglected. Results of this study are shown in Figures (V.2) , (V.3), and (V.4). Detailed calculations are shown in Appendix II.

Since the normal force on droplets inside the sphere will be canceled with the reaction from the sphere wall, it will not have any effect on moving the droplet. Analysis, from Figures (V.2) and (V.3), has shown that the tangential force on a droplet of the working fluid on the inner surface of a RBMR with a one meter radius located at 45° angle from the equator and rotating at 45 rpm is equal to the force acting on the same quantity of working fluid located 7.0 cm from the center of a flat plate rotating at about 330 rpm. This is also the same amount of force exerted on that droplet located on the inside of a sphere of 4.2 meter radius at about 10 rpm and 10.0 centimeter from the center of a flat plate

IR Thermometer

Stationary Pipe

R15.00

Screw

Screw

Bearing

Bearing

Motor And Controller

Insulation

Pressure Tranducer

Valve

Vacuun/Pressure Gauge

Flow Meter

Vacuun/Pressure Gauge

Vacuun Pump

Check Valve

Data Logger

Level Measurenent Instrument

Thernocouple

Heater Controller

Valve

Valve

Heater

Figure (V.1) Schematic Diagram of the RBMR Prototype.

rotating at 300 rpm. Thus, as it is shown in Figure (V.3), in order to simulate the fluid and convective heat transport of a droplet of an in-space RBMR with a 4.2 meter radius at 45° angle from the equator, to that at 10.0 centimeter from the center of the flat plate, operating with rotational speeds from 2 to 16 rpm, the flat plate must rotate at speeds from 50 to 400 rpm. These Figures show examples where many similar studies may be made for comparison or simulation goals on normal gravity.

Testing a prototype of the RBMR in microgravity is a very important step to validate the concept for future considerations. The prototype that was built through the efforts of this research can be modified for use in a microgravity flight to test the operational principles of the RBMR.
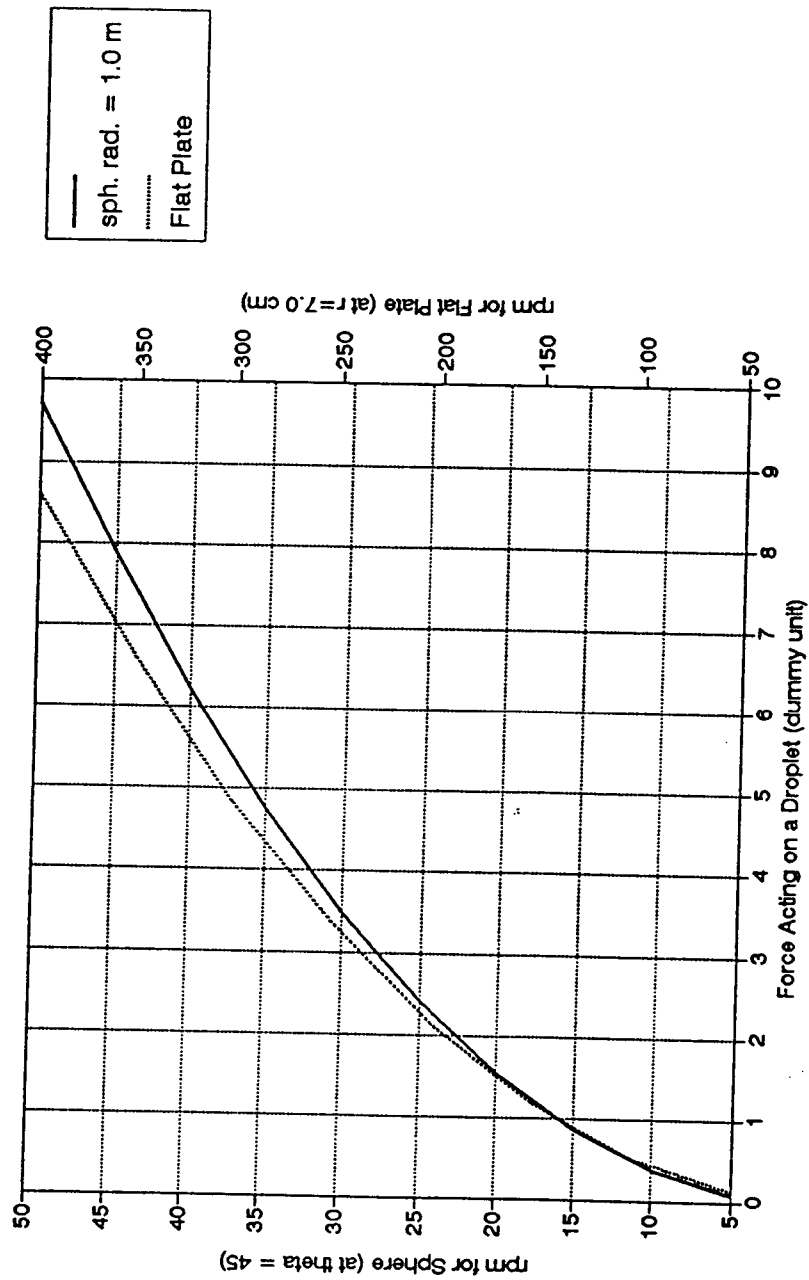
Figure (V.2) Sphere of One Meter Radius and Flat Plate rpm
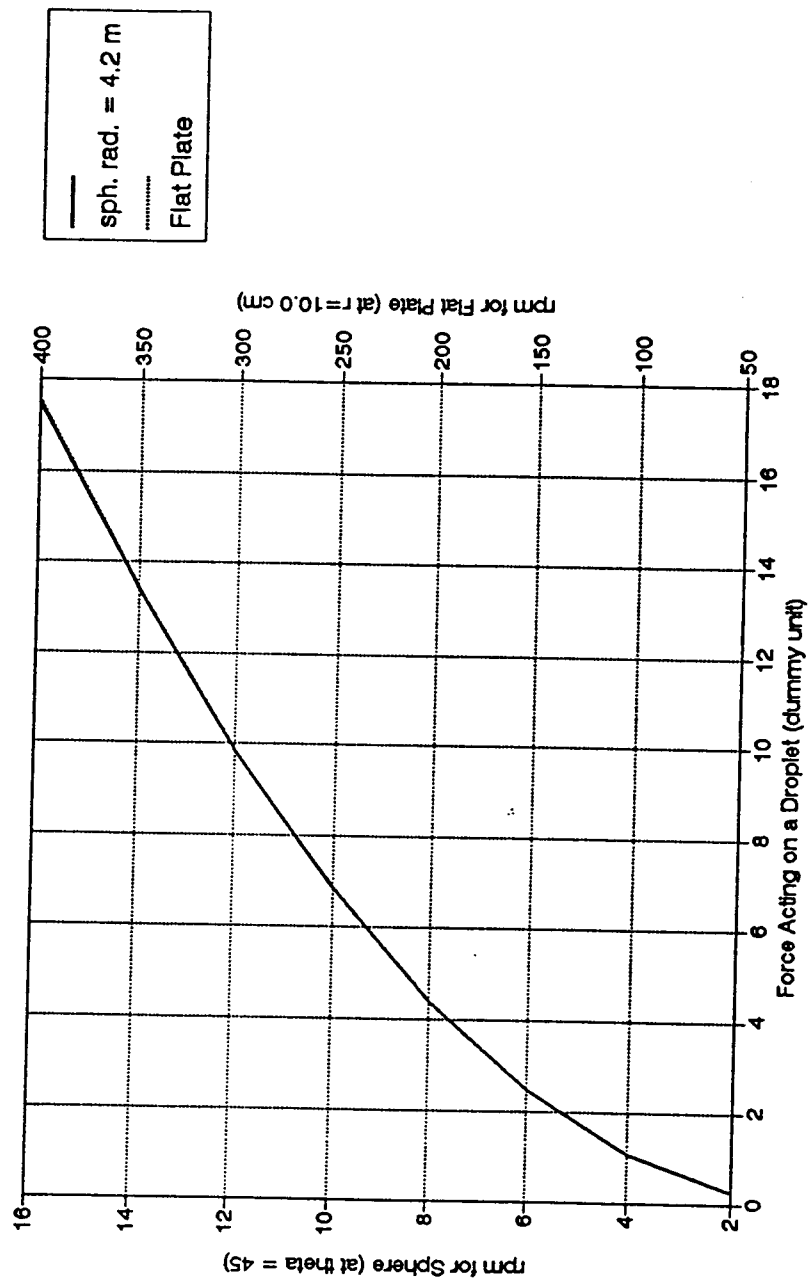Verses Force Acting on a Droplet.

Figure (V.3) Sphere of 4.2 Meter Radius and Flat Plate rpm
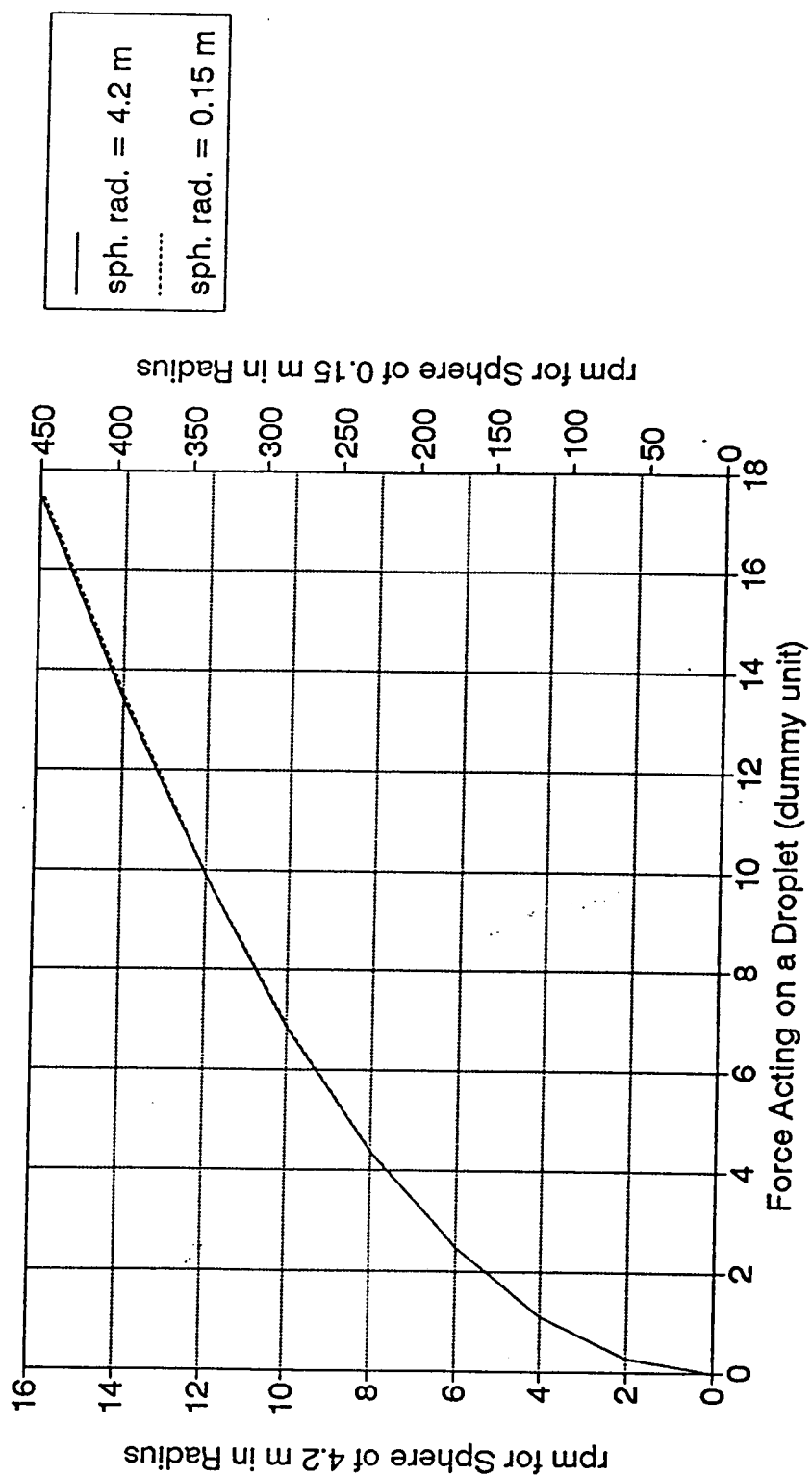Verses Force Acting on a Droplet.

Figure (V.4) Spheres of 4.2 Meter and 0.15 Meter Radius
Verses Force Acting on a Droplet (at theta = 45°).

V.2 Methodology And Design :

The primary components of the RBMR Condensation Experiment are shown in Figure (V.1). Their purposes are described as follows :

1) A spherical shell made of Aluminum 6061-T6 with a 0.638 cm (0.25") thickness. It consists of two hemispheres attached to each other with screws. The bottom hemisphere has a stationary base where instrumentation and pipes may be inserted to the inside of the sphere. This stationary base is well sealed against vacuum leakage with suitable bearings. A schematic drawing of these bearings is shown in Figure (V.4).

The main function of the sphere is that the outer surface should be cooled enough to condense the working fluid vapor on the inner surface.

2) Instrumentation :

Several measuring instruments are used. The data logger mentioned in Section III.2 with different types of thermocouples are used to measure the temperatures of the condensate working fluid in the condensate collecting tank. The temperature of the sphere environment during operation is taken from the saturation temperature for the pressure transducer, model 891.23.560 from WIKA, Klingenberg, Main, reading for the inside sphere.

Some other vacuum/pressure gauges are used in various locations in the system as shown in Figure (V.1). Also relief valves are used in the steam generator tank in order that the pressure inside the tank does not exceed 30 psi for safety purposes.

A level measuring instrument, model CAP ANALOG/4100, from DELAVAN Process Instrumentation, Scottsdale, Arizona, is used in the condensate collecting tank to measure the mass flow rate which is needed in calculating the overall heat transfer coefficient used in Equation (3.1). An Infra-Red (IR) thermometer of model OS52 from OMEGA Engineering, Inc., is used to measure the outer surface temperature of the sphere while it is rotating. This temperature is also needed in using Equation (3.1).

3) Control System :

A variable speed motor, model 4Z528 DC motor from DAYTON, with controlling current input, model 5X412C from DAYTON, is used to control the rotational speed of the spherical shell. A strobe light was used to determine the rotational speeds for corresponding knob settings. These data are shown in Appendix III.

4) Steam Generator System :

A cylindrical aluminum tank of 6061-T6 type is used to serve as a steam generator. It is filled with a working fluid. It is heated while the steam valve is closed to get a high saturation pressure with corresponding high saturation temperature. When the steam valve, which connects the steam generator to pipes reaching the low pressure environment inside the sphere, is opened, the steam is exposed to lower pressure resulting in high super heated steam. A 550 W heating cartridge, model TB5064TB1 from VULCAN, placed on the bottom base of the steam generator tank is used to heat the working fluid. It is connected to a thermocouple which turns the heating cartridge on/off according to pre set temperature limits.

5) Condensate Collecting System :

This system consists of a cylindrical Aluminum, 6061-T6 type, tank with a conical base where the condensate can be collected and then drained.

When the spherical shell rotates, the condensate is forced toward the sphere equator where stationary pipes are located with their open ends facing opposite the rotation direction of the sphere. The condensate is collected in these pipes and then transported to the collecting tank by gravitational forces.

Nearly the same methodology as explained in Section III.3 is to be used in these experiments. One main difference is using Equation (3.1), rather than Equations (3.2) and (3.3), to find the overall heat transfer coefficient. This coefficient is to be found between the vapor-condensate interface temperature, which represents the working fluid temperature, and the outer surface temperature of the sphere, which represents the cold environment. The spherical shell could be cooled by putting the whole experiment in a cold room especially when a high temperature difference is desired. If this is the case, the freezing point of the working fluid must be considered in order to keep the condensate from freezing. Since the steam generator of the RBMR can generate high temperature steam, room temperature may be considered for the initial testing.

V.3 Comments And Observations :

Several runs were made to assure that the system operated as it was designated. It was noticed, after to a few operational testing runs, that at relatively high speeds, i.e. 500 rpm and above, the temperatures of the

outer surface of the sphere shell, as read by the IR thermometer, tends to read same every where, except at the poles, which indicates that at those speeds the effect of gravitational forces is negligible compared to centrifugal forces. Thus, a good simulation of the RBMR, using these high speeds, may be obtained in normal gravity.

Several considerations were taken into account in designing and constructing the RBMR prototype. Among these, the system should be self sustained, it should have a reasonably small size so that it can fit into several micro-gravity carriers, and that it should be easy to modify. Several additional modifications are possible in this design such as a full coolant loop, inserting a fiber optic camera in the spherical shell to watch the condensation process and document the flow patterns, and it is possible, with little effort, to replace the spherical shell with other geometries for the RBMR while all other systems, equipments, and instruments remain the same.

VI. CONCLUSIONS AND RECOMMENDATIONS

VI.1 General Remarks :

The first, second, and fourth objectives of the current study, mentioned in chapter I, were completely accomplished; these are designing, constructing, operating and demonstrating a heat rejection system using condensation on a rotating flat plate and on a full sphere, Appendix IV shows photographs of the hardware; and also the development of an empirical correlation to relate the overall heat transfer parameter of the rotating flat plate to the angular rotational speeds. Three rotational speeds were used in these experiments, namely 200, 300, and 400 rpm.

The third objective was partially achieved. The condensate film thickness was very difficult to precisely measure, primary because of the vibration in the entire system, the requirement of precise normality between the flat and the axis of rotation, and also the wide laser beam diameter comparing to the condensate film thickness. Condensate flow patterns for several experiments were recorded at the three rotational speeds by videotape but no more study seemed to be useful in the design of such heat rejection systems where the main concern is usually finding correlations for heat transfer coefficients. However, preliminary results obtained from experiments have proved both techniques, i.e. the concept of using laser beams in finding the thickness of transparent consistent objects and fluorescent fluid in recording fluid motions, are working well

and worthy to be considered in further experiments if these problems can be overcome.

Dimensionless groups developed by Sparrow and Gregg[17] were used in this study by replacing their local heat transfer coefficients with the overall heat transfer coefficients, and their temperature difference across the film condensate with the temperature difference corresponding to the overall heat transfer coefficients used. Two different overall heat transfer coefficients were inspected, namely U1 and U2. Two different kind of fittings were used in analyzing the experimental data, least square and average point line. One can conclude that using the same curve of Sparrow and Gregg for the overall heat transfer coefficient and its corresponding temperature difference will give satisfactory results. This conclusion was proved experimentally for intervals of $C_p \Delta T / h_{fg}$ from about 0.04 to about 0.105.

The heat flux measurements for the three tested rotational speeds verses dimensionless temperature difference were in a good agreement with the theoretical predictions.

Errors of the correlation including h_{avg} were high for low temperature difference, while they where reasonable for higher ones. This was attributed to neglecting the gap effect between the two plates where its effect could be minimized by higher temperature differences.

Possible sources of errors in these experiments were mentioned and discussed in detail throughout Chapter IV. It was found that the effects of these sources of errors on experiment results were minimal. The scattered nature of the data points should be attributed to these sources of errors. Statistical analysis was performed on all studied parameters to show the probable amount of fluctuation in the experimental data.

VI.2 The Significance of These Investigations :

Several significant conclusions were made from these current
investigations, among which :

*   The empirical correlation found in this study, which was found to be
similar to the one developed by Sparrow and Gregg[17], is useful for
choosing the optimum rotational speed for the flat plate radiator given a
desired heat rejection load. Since the working fluid properties, system
temperatures, and the temperature of the environment are usually known,
this correlation will give the relationship between the rotational speed
and the overall heat transfer coefficient. Then the designer can choose
the optimum rotational speed to reject a certain amount of heat from the
system.

*   Since the current study is compared to the analytical work of
Sparrow and Gregg[17], which is insensitive to working fluid Prandtl
numbers for $C_p \Delta T / h_{fg}$ less than or equal 0.1, the results of this study
are not necessarily restricted to materials with Prandtl numbers similar
to that of water.

*   This study also provides the basis for designing new heat rejection
systems utilizing centrifugal forces and condensation phenomena in both
space and ground applications.

*   The first RBMR ever built was designed, constructed, operated, and
is ready for future investigations.

VI.3 Future Work And Recommendations :

Using the same available apparatus and instruments, and pretty much similar procedures and methodology of these experiments, more studies can be performed and investigated. The present ground based investigation is considered as a first step in a series of experiments using different working fluids and surface configurations, such as the available RBMR prototype, and concludes with experimental tests in microgravity. Testing different working fluids with various Prandtl numbers will help in generalizing the results and hence broadening the applications of the correlations to other fluids. Investigating different geometries is a very important step in choosing the optimum configuration of the RBMR which allows the best heat transport and is suitable for other design parameters.

Further study is also needed to extend the testing interval beyond $C_p \Delta T / h_{fg}$ equal to 0.105. According to the analytical work of Sparrow and Gregg[17], the straight correlation line of 0.904 for the flat plate condensation experiments starts to curve below and above its original value depending on Prandtl numbers (see Figure II.1). Increasing this interval experimentally could be achieved by increasing the temperature difference between the cooled surfaces and the operating temperatures. The existing apparatus of the steam generator system of the RBMR prototype is suitable for this purpose because it was made of aluminum which can tolerate reasonably high pressures, and hence high temperatures. The glass beaker used in the flat plate experiments must be replaced by

another high pressure chamber to be suitable in generating high temperatures.

Using higher rotational speeds is highly recommended for future work. This will help in applying more force on condensate droplets to join each other and hence to get film-wise condensation, and also in assuring the conclusion of generalizing the correlation to other rotational speeds. These same experiments could be performed along with the flow pattern study, with no change in major procedures, to investigate and document the change of flow patterns with the rotational speeds.

REFERENCES

[1] S. S. Voss, *SNAP Reactor Overview*, Final Report, AFWL-TN-84-14, 1984.

[2] R. A. Johnson and M. Shirbacheh, " Low Power DIPS Design for NASA Missions ", Proceedings of 8th Symposium on Space Nuclear Power Systems, p. 916, DOE CONF-910116, Albuquerque, NM, 1991.

[3] M. E. Lisano and M. F. Rose, " An Isotope-Powered Thermal Storage Unit for Space Applications ", Proceedings of 8th Symposium on Space Nuclear Power Systems, p. 928, DOE CONF-910116, Albuquerque, NM, 1991.

[4] R. F. Hartman, J. R. Peterson and W. Barnett, " Modular RTG Status ", Proceedings of 9th Symposium on Space Nuclear Power Systems, p. 177, DOE CONF-920104, Albuquerque, NM, 1992.

[5] R. B. Harty, " Comparison of DIPS and RFCs for Lunar Mobile and Remote Power Systems ", Proceedings of 9th Symposium on Space Nuclear Power Systems, p. 202, DOE CONF-920104, Albuquerque, NM, 1992.

[6] V. C. Truscello and L. L. Rutger, " The SP-100 Power System ", Proceedings of 9th Symposium on Space Nuclear Power Systems, p. 1, DOE CONF-920104, Albuquerque, NM, 1992.

[7] T. J. Miller and G. L. Bennett, " Nuclear Propulsion for Space Exploration ",Proceedings of 9th Symposium on Space Nuclear Power Systems, p. 24, DOE CONF-920104, Albuquerque, NM, 1992.

[8] G. L. Bennett and T. J. Miller, " Planning for the Space Exploration Initiative: the Nuclear Propulsion Option ", Proceedings of 8th Symposium on Space Nuclear Power Systems, p. 1, DOE CONF-910116, Albuquerque, NM, 1991.

[9] W. G. Huber, " Requirements for Advanced Space Transportation Systems ", Proceedings of 9th Symposium on Space Nuclear Power Systems, p. 64, DOE CONF-920104, Albuquerque, NM, 1992.

[10] J. Tournier, M. S. El-Genk and A. Juhasz, " Heat-Pipe Transient Model for Space Applications ", Proceedings of 8th Symposium on Space Nuclear Power Systems, p. 857, DOE CONF-910116, Albuquerque, NM, 1991.

[11] R. D. Rovang, R. A. Holzel and R. B. Dirling,Jr., " SP-100 High-Temperature Advanced Radiator Development ", Proceedings of 8th Symposium on Space Nuclear Power Systems, p. 702, DOE CONF-910116, Albuquerque, NM, 1991.

[12] A. C. Klein, *Fabric Composite Radiators for Space Nuclear Power Applications*, Proposal to United States Department of Energy, Grant Number DE-FG07-89ER12901, September, 1989.

[13] B. J. Webb, Z. I. Antoniac, A. C. Klein and K. A. Pauley, *Preliminary Design and Analysis of Rotating Bubble Membrane Radiator for Space Applications*, Report to NASA Johnson Space Center prepared by Battelle Pacific Northwest Laboratory under USDOE contract DE-AC06-76RL01830, Richland, WA, March, 1989.

[14] A. G. Williams, S. S. Nandapurkar and F. A. Holland, " Condensation on a Vertical Rotating Finned Tube ", The Canadian Journal of Chemical Engineering, Vol. 49, p. 51, February, 1971.

[15] E. M. Sparrow and J. P. Hartner, " Condensation on a Rotating Cone ", Journal of Heat Transfer, p. 101, February, 1961.

[16] M. M. Rahman, A. Faghri, W. L. Hankey and T. D. Swanson, " Computation of The Free Surface Flow of a Thin Liquid Film at Zero and Normal Gravity ", Numerical Heat Transfer, Part A, Vol. 17, p. 53, 1990.

[17] E. M. Sparrow and J. L. Gregg, " A Theory of Rotating Condensation ", Journal of Heat Transfer, p. 113, May, 1959.

[18] E. M. Sparrow and J. L. Gregg, " A Boundary-Layer Treatment of Laminar-Film Condensation ", Journal of Heat Transfer, p. 13, February, 1959.

[19] J. W. Yang, " Laminar Film Condensation on a Sphere ", Transactions of the ASME, p. 174, May, 1973.

[20] W. Roetzel, " Laminar Film Surface Evaporation With Uniform Heat Flux in a Fast Rotating Drum ", Int. J. Heat Mass Transfer, Vol. 20, p. 549, 1977.

[21] M. A. Osei-Bonsu and M. J. Holgate, " Condensation on Rotating Axisymmetric Curved Bodies ", Journal Mechanical Engineering Science, Vol. 17, No. 6, p. 301, 1975.

[22] A. Faghri and L. C. Chow, " Forced Condensation in a Tube With Suction at the Wall for Microgravitational Applications ", Transactions of the ASME, Vol. 110, p. 982, November, 1988.

[23] R. Chandran and F. A. Watson, " Condensation on Static and Rotating Pinned Tubes ", Transactions Instn Chem. Engrs, Vol. 54, p. 65, 1976.

[24] A. I. Butuzov and V. F. Rifert, " An Experimental Study of Heat Transfer During Condensation of Steam at a Rotating Disk ", Heat Transfer-Soviet Research, Vol. 4, No. 6, November-December, 1972.

[25]   S. S. Nandapurkar and K. O. Beatty, Jr., " Condensation on a Rotating Disk ", Chemical Engineering Progress Symposium Series, Vol. 56, No. 30, p. 129, 1960.

[26]   E. M. Sparrow and J. L. Gregg, " The Effect of Vapor Drag on Rotating Condensation ", Journal of Heat Transfer, p. 71, February, 1960.

[27]   P. M. Beckett, P. C. Hudson and G. Poots, " Laminar Film Condensation Due a Rotating Disk ", Journal of Engineering Mathematics, Vol. 7, No. 1, January 1973.

[28]   V. Dhir and J. Lienhard, " Laminar Film Condensation on Plane and Axisymmetric Bodies in Nonuniform Gravity ", Journal of Heat Transfer, p. 97, February, 1971.

[29]   C. S. Wang and R. Grief, " The Effect of Impingement on Heat Transfer in Rotating Condensation ", Int. J. Heat Mass Transfer, Vol. 24, No. 7, p. 1097, 1981.

[30]   S. P. Chary and P. K. Sarma, " Condensation on a Rotating Disk With Constant Axial Suction ", Transactions of the ASME, p. 682, November, 1976.

[31]   C. S. Wang, R. Greif and A. D. Laird, " Heat Transfer in a Rotating Disk Evaporator ", Desalination, Vol. 33, p. 259, 1980.

[32]   D. Salinas and P. J. Marto, " Analysis of an Internally Finned Rotating Heat Pipe ", Numerical Heat Transfer, Part A, Vol. 19, p. 255, 1991.

[33]   A. R. Alansari and J. A. Edwards, " Numerical Study of the Three-Dimensional Laminar Film Condensation ", Proceedings of International Conference on Alternative Energy Sources, Vol. 5, p. 535, CONF-851201, Miami, FL, 1985.

[34]   A. A. Muzhilko, V. G. Rifert and P. A. Barabash, " Flow of Liquid Film Over the Surface of a Rotating Disk ", Heat Transfer-Soviet Research, Vol. 15, No. 5, September-October, 1983.

[35]   B. G. Higgins, " Film Flow on a Rotating Disk ", Phys. Fluids, Vol. 29, No. 11, p. 3522, November, 1986.

[36]   A. F. Charwat, R. E. Kelly and C. Gazley, " The Flow and Stability of Thin Liquid Films on a Rotating Disk ", J. Fluid Mech., Vol. 53, Part 2, p. 227, 1972.

[37]   S. Matsumoto, K. Saito and Y. Takashima, " The Thickness of a Viscous Liquid Film on a Rotating Disk ", Journal of Chemical Engineering of Japan, Vol. 6, No. 6, p. 503, 1973.

[38]   S. Thomas, *Numerical and Experimental Analysis of a Thin Liquid Film on a Rotating Disk*, Master's Thesis, Department of Mechanical and Materials Engineering, Wright State University, Dayton, OH, 1989.

[39]   D. Fultz, R. Long, G. Owens, W. Bohan, R. Kaylor and J. Weil, *Studies of Thermal Convection in a Rotating Cylinder With Some Implications for Large Scale Atmospheric Motions*, Meteorological Monographs, Vol. 4, No. 21, Boston American Meteorology Society, Boston, MA, December, 1959.

[40]   J. Welty, C. Wicks and R. Wilson, *Fundamentals of Momentum, Heat, and Mass Transfer*, John Wiley & Sons, New York, NY, 1984.

[41]   M. M. El-Wakil, *Nuclear Heat Transport*, American Nuclear Society, La Grange Park, IL, 1978.

[42]   T. Fujii, *Theory of Laminar Film Condensation*, Springer-Verlag, New York, NY, 1991.

[43]   V. P. Carey, *Liquid-Vapor Phase-Change Phenomena*, Hemisphere Publishing Corporation, 1992.

[44]   D. Azbel, *Fundamentals of Heat Transfer for Process Engineering*, NOYES Publications, 1984.

[45]   J. L. Devore, *Probability & Statistics for Engineering and the Sciences*, Brooks/Cole Publishing Company, 1982.

[46]   G. F. Knoll, *Radiation Detection and Measurements*, John Wiley & Sons, New York, NY, 1979.

[47]   Borland, " Quattro-Pro 3.0 Superior Spreadsheet Power ", 1991.

[48]   G. J. Van Waylen and R. E. Sonntag, *Fundamentals of Classical Thermodynamics*, John Wiely & Sons, 1985.

APPENDICES

Appendix I

Flat Plate Experimental Procedures Checklist :

- --- Put the water bucket on the rotating shaft, in the glass pipe, then use two screws to attach the bucket to the shaft.

- --- Take out the ice bucket from the freezer.

- --- Connect the thermocouple (TC) wires to the data logger (DL), then start the data logger, on the print data mode, to read the temperature at this time to assure that the TC's are working properly as well as the DL.

- --- Turn the DL off. Cut the print out data sheet, attach it to the corresponding page in the lab note book.

- --- Treat the flat plate surface if this is appropriate for the test.

- --- Fill the water beaker to between 1000 ml and 1400 ml. Place the beaker on the heating plate. Turn the heater on.

- --- Insert the DL in double plastic bags to keep it in a dry environment, then seal it. Set it to run in the non-printing data mode.

- --- Place the DL in the inner cylinder of the water bucket, then place the ice-bucket on the top of the DL (try to match the marks in order to reduce the possibility of cutting the thermocouple wires).

- --- Use two screws to attach the ice-bucket to the inner cylinder and to level the condensing surface. Check the level by the leveling instrument.

- --- Put a sufficient amount of anti-fog treatment on the plastic window of the top aluminum plate to allow for clear viewing, then wipe the window clean.

- --- Place the top aluminum plate on the top of the glass pipe, then attach it to its metal flange by the built in screws.

- --- Place the protection shield on the outer side of the glass pipe.

- --- Connect the rubber hose between the water beaker and the steam hose. Place the rubber stopper on the top of the beaker. No boiling must occur at this point, if there is boiling, try to cool it down until no boiling is noticed. Be sure the steam valve is open.

- --- Connect the vacuum hose to the vacuum valve. Turn the vacuum pump on. Turn the vacuum valve handle to evacuate the chamber.

- --- Watch the water in the beaker, when it starts to boil, close the steam valve.

--- Watch the vacuum gauge, when it reaches to 6-7 kPa turn the vacuum pump off, it takes usually seven minutes to pump the chamber to this level. Turn the vacuum pump off.

--- Start the rotating motor. Increase the speed of the rotating shaft to the desired speed. Watch the voltmeter to set the desired speed (14 V corresponds to 1000 rpm).

--- Open the steam valve carefully. Rapid boiling of the water in the beaker should be noticed. This steam will transfer from the water beaker to the glass pipe through the hose.

--- Run the experiment for the time desired. Close the steam valve. Turn the heater off. Reduce the rotation speed to zero. Turn the motor off.

--- Measure the water collected. Download the data from the DL to the computer.

--- Prepare the ice bucket for the next test by compressing the springs in the assembly by inserting the screw pin and fixing the teflon plate to its fully withdrawn position.

PRECAUTIONS AND PROCEDURES FOR THE USE OF THE 10 mW LASER SYSTEM IN ROOM A120B AT THE RADIATION CENTER AT OREGON STATE UNIVERSITY

The precautions and procedures listed below are typical for the class of laser systems known as type III medium (also called III.b) laser systems. The laser system has a power level of 10 mW and its wave-length is in the visible region. Thus, strict adherence to these precautions is required to avoid injury. Each person who needs to have access to room A120B during laser operation must read and sign a copy of these precautions and procedures signifying that they have read, understand, and will comply with them.

GENERAL PRECAUTIONS

1) No direct or reflected beam is to be viewed without appropriate eye protection.

2) Unplug the laser after each use and store it in its box.

3) Provide enclosures for beam paths whenever possible.

4) Beam stop should be in place at all times.

5) Place standard safety warning sign for class III laser on the outside of the doors of rooms A120 and A120B during operation. Be sure that the doors to rooms A120 and A120B are closed at the beginning of laser operation, and that the door to room A120B remains closed while the laser beam is exposed.

6) Wear appropriate eye protection in room A120B at all times the laser is plugged in.

OPERATIONAL PROCEDURES

1) Inform the Radiation Center Director's office when a test is to be conducted which will use the laser system during normal working hours (from 8:00 A.M. to 5:00 P.M.).

2) Display the standard warning signs on the doors of A120 and A120B during operations using the laser system. The doors to both A120 and A120B are to be closed when beginning use of the laser system, and the door to room A120B is to remain closed while the laser system is operating to reduce the chance that the laser beam will escape out of the operating area. Place rope barrier with warning sign in front of the door to room A120B.

3) Place the laser on its stand at the appropriate test angle with the stainless steel test plate. The laser should not be

plugged in at this time, but the angle should be approximately set so that it will shine through the glass pipe. Be sure that the beam stop is placed in a position where it will be able to collect the scattered laser beam.

4) Place a blank white piece of paper between the beam stop and the laser beam.

5) All beam focusing and direction setting must be done on a blank white piece of paper before steam is introduced into the glass pipe or the stainless steel plate is rotated.

6) Turn the laser beam off. Replace the focusing target with film (covered at this point).

7) After the condensate film is consistently established on the rotating stainless steel plate, turn the dark room light on, the room lights off and uncover the receiver film to receive the reflected laser beams from the surface of the stainless steel plate and from the condensate film surface. Turn the laser beam on.

8) Laser scanning is to start at one edge of the stainless steel plate, end at the other edge, and pass through the center point of the plate. This is to be done horizontally to maximize the separation of the film surface and mirror surface reflected beams.

9) Turn the laser off. Cover the film. Turn the room lights on. Turn the red light off. Unplug and return the laser to its container.

10) Notify the Radiation Center Director's office that the test has been completed.

I have read, understand and agree to comply with these precautions and procedures concerning the use of the laser system in room A120B at the Radiation Center. I acknowledge that it is important that these precautions be followed to avoid any potential injury.

_____   _____
              Signature   Date

Appendix II

Forces Acting on a Working Fluid Droplet Inside a Rotating Sphere

Assumptions : 1) Perfect frictionless surface.
2) Gravitational force is neglected.

$$\sum \vec{F} = \int\int_{c.s.} \vec{v}\rho\,(\vec{v}\cdot\vec{n})\,dA + \frac{\partial}{\partial t}\int\int\int_{c.v.} \rho\vec{v}\,dv$$

For steady state case

$$\sum \vec{F} = \int\int_{c.s.} \vec{v}\rho\,(\vec{v}\cdot\vec{n})\,dA$$

But,

$$\vec{F}=f(\theta) \quad only \quad [\vec{F}\neq f(\varphi,R)]$$

This means

$$\vec{v} = v_\theta\,\hat{i}_\theta$$

where,

$$v_\theta=(r\omega)\,(2\Pi) \qquad r=R\cos\theta$$

Therefore,

$$F = v_\theta^2\,\rho\,A$$

$$F = F_T + F_N$$

Where,

$$F_N = \vec{F}\cos\theta \qquad F_T = \vec{F}\sin\theta$$

Let $\rho = A = 1$ dummy unit (for simplicity), then
$$F = 4\Pi^2R^2\omega^2\cos^3\theta + 4\Pi^2R^2\omega^2\sin\theta\cos^2\theta$$

OR

$$F = 4\Pi^2 R^2 \omega^2 (\cos\theta + \sin\theta) \cos^2\theta$$

Forces Acting on a Working Fluid Droplet on the upper Surface of a Rotating Disk

Assumptions : 1) Perfect frictionless surface.
2) Gravitational force is neglected.

Steady state case

$$\sum \vec{F} = \int\int_{c.s.} \vec{v}\rho\,(\vec{v}.\vec{n})\,dA$$

But,

$$\vec{F} = f(r) \quad only \quad [\vec{F} \neq f(\theta), v_z \text{ is negligible}]$$

This means

$$\vec{v} = v_r\,\hat{i}_r$$

where

$$v_r = (r\omega)\,(2\Pi)$$

Therefore,

$$F = v_r^2\,\rho\,A$$

Let $\rho = A = 1$ dummy unit (for simplicity), then

$$F = 4\,\Pi^2\,r^2\,\omega^2$$

It is noticed that this equation is identical to the one that was derived for the full sphere case in the previous page when theta is equal to zero.

Appendix III

Knob Setting for the Rotating Motor Used in the Flat Plate Experiments
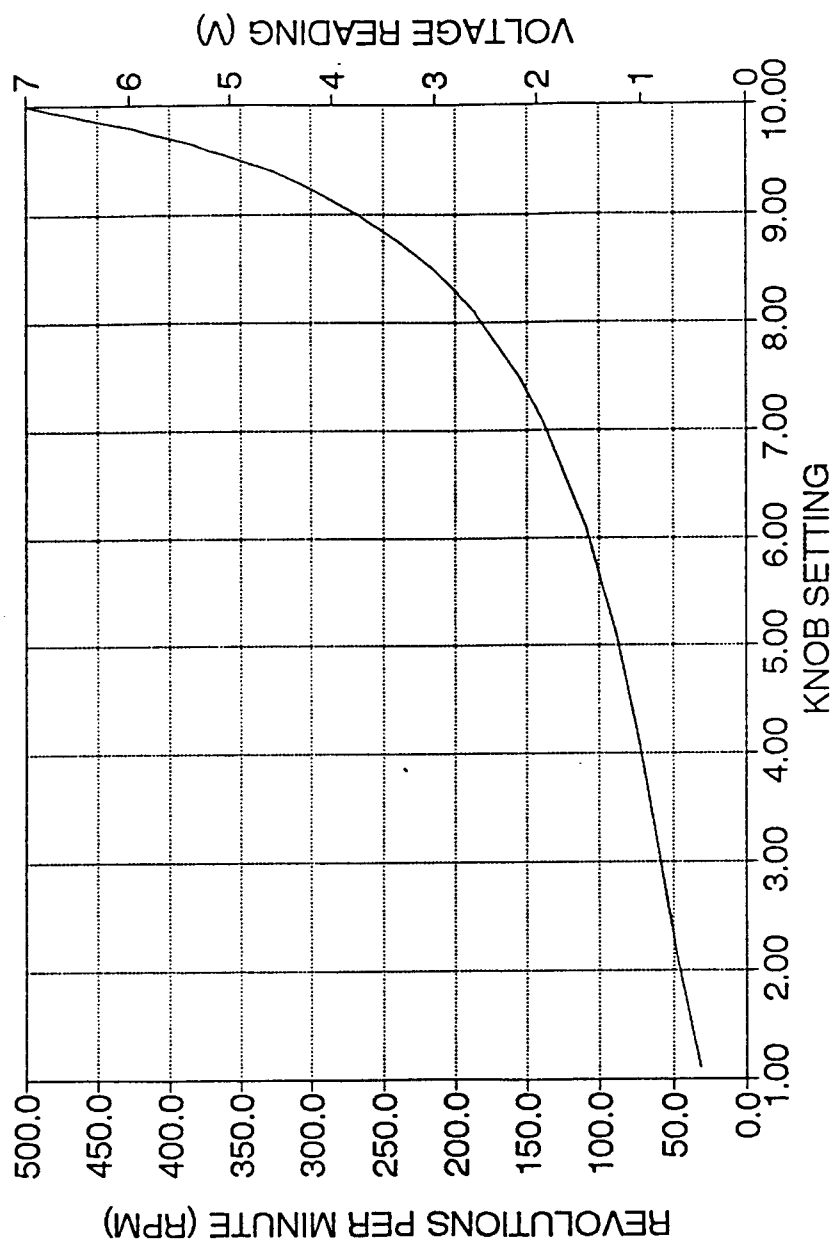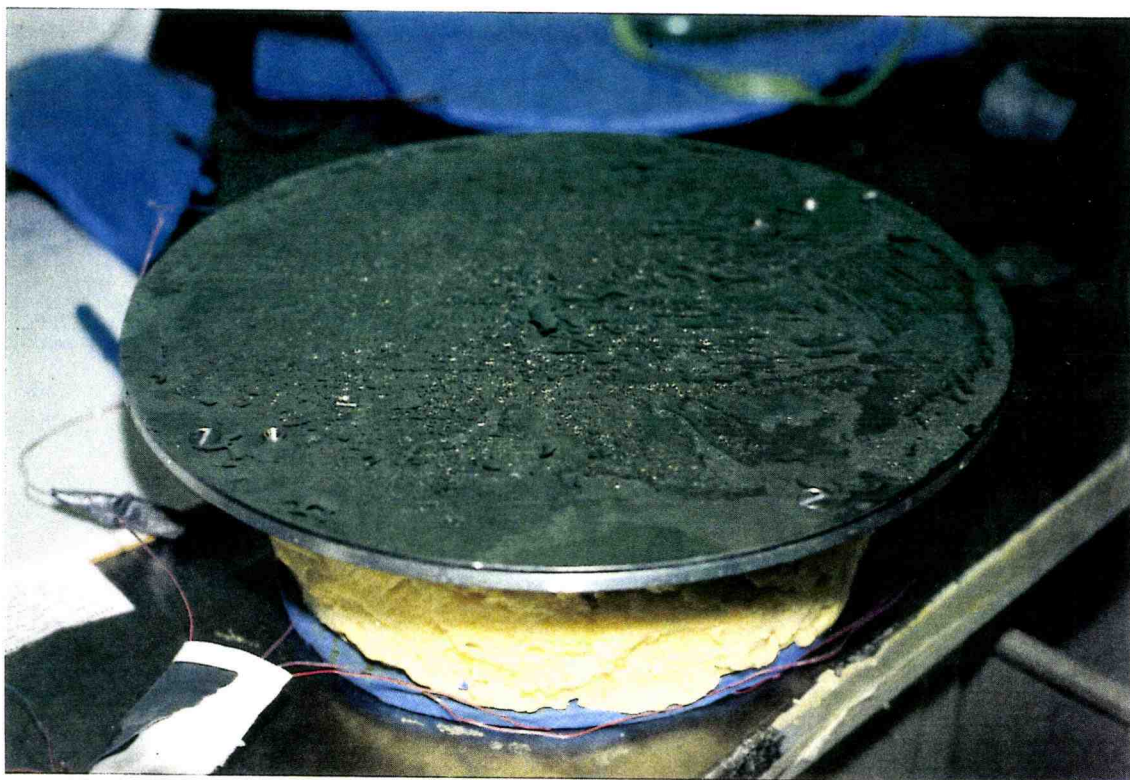
Knob Setting for the Rotating Motor Used in the RBMR Prototype Experiments
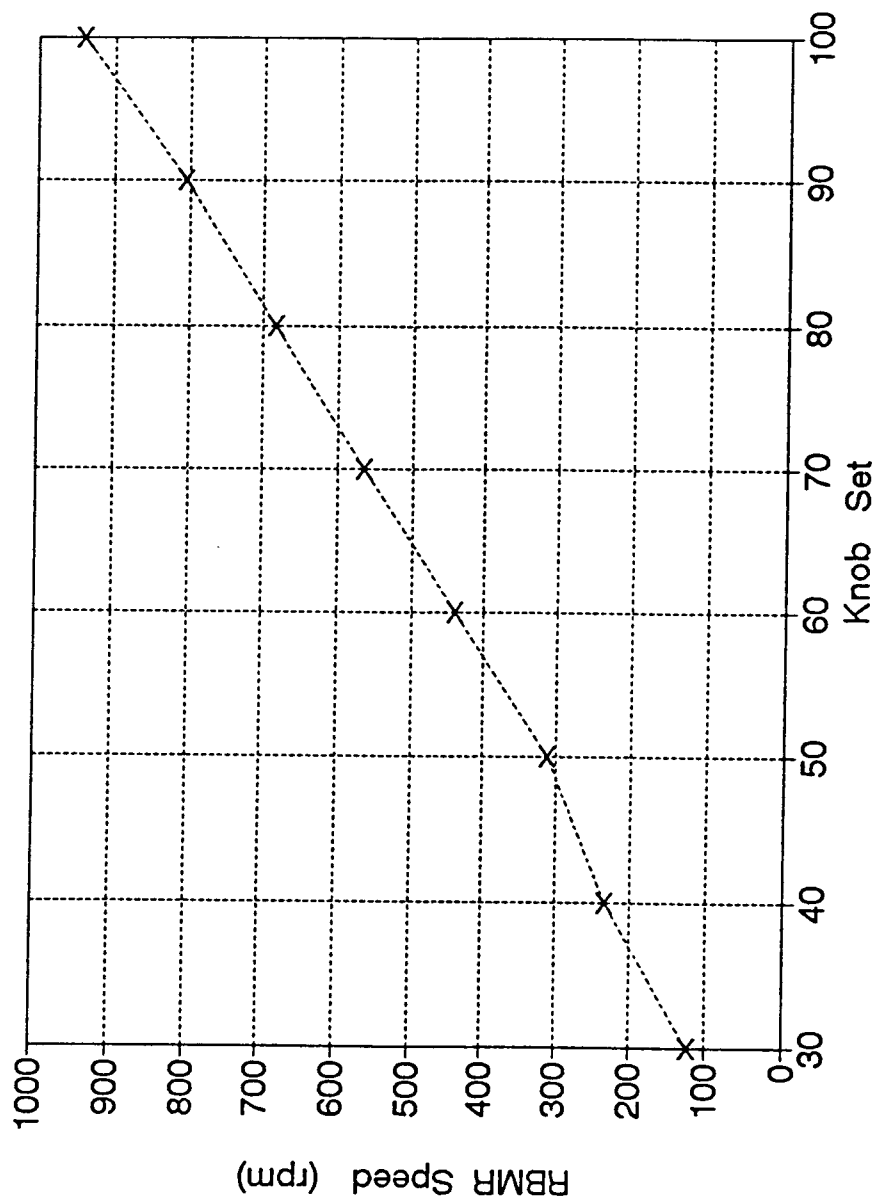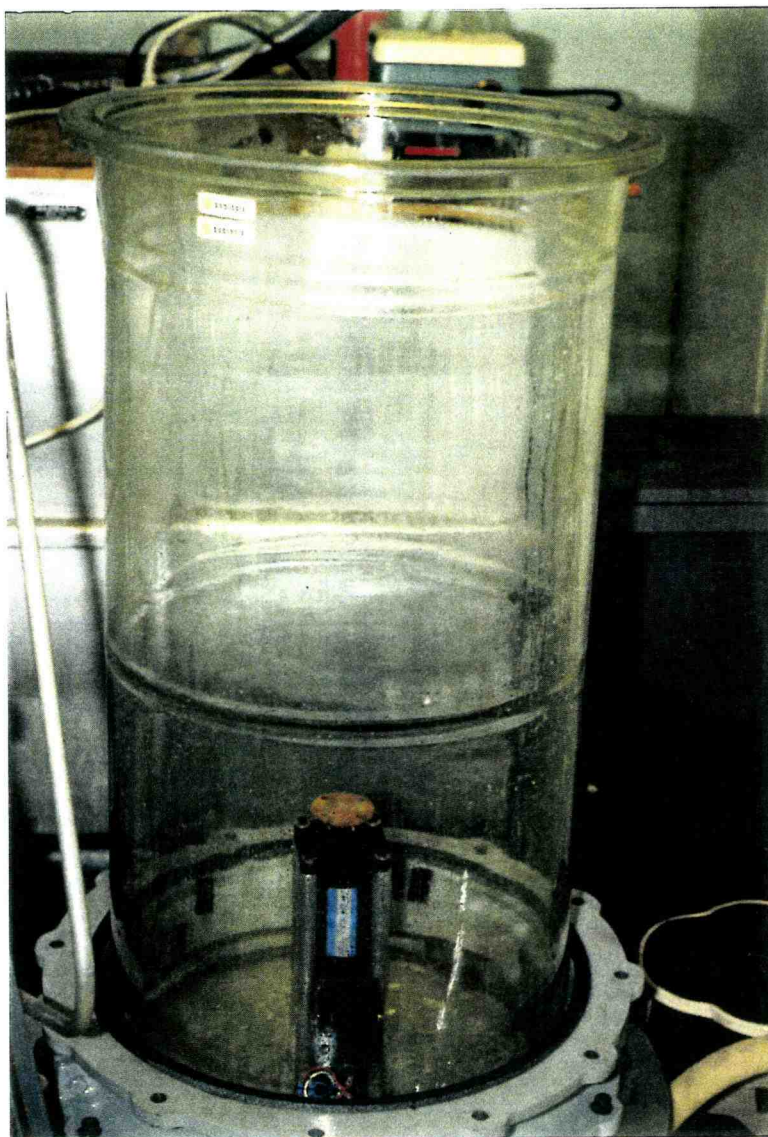
Appendix IV
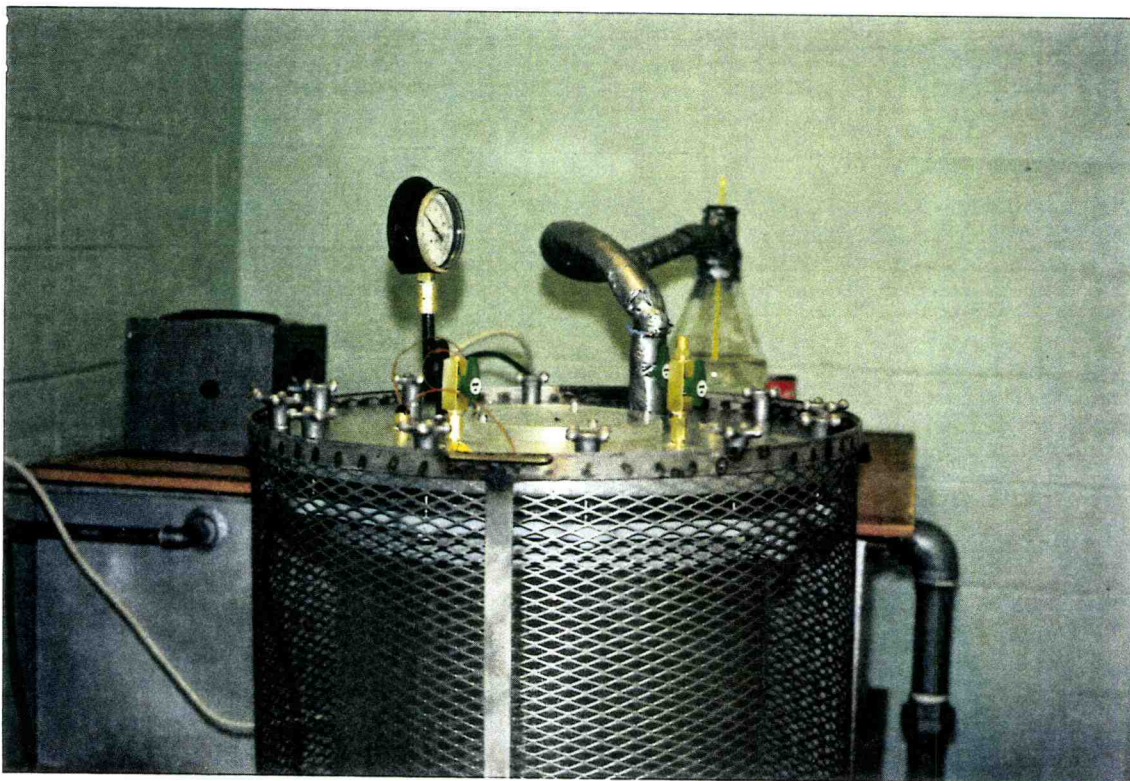
Photographic Pictures of the Experiment Hardware
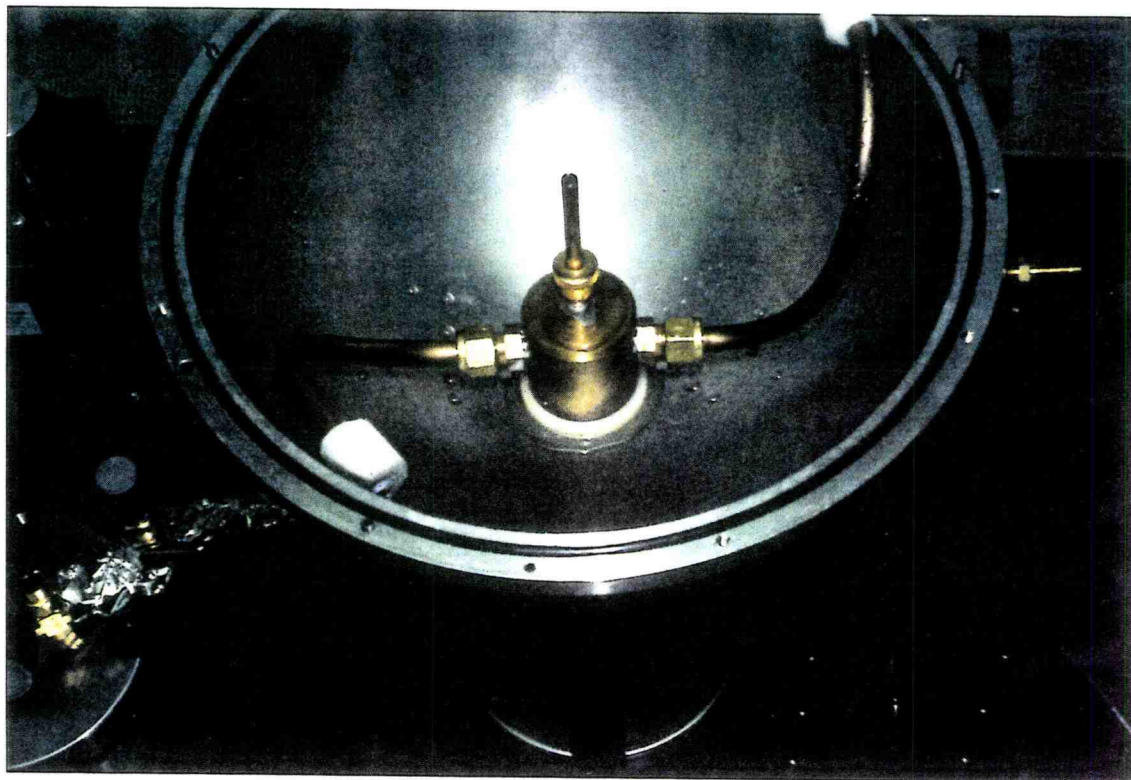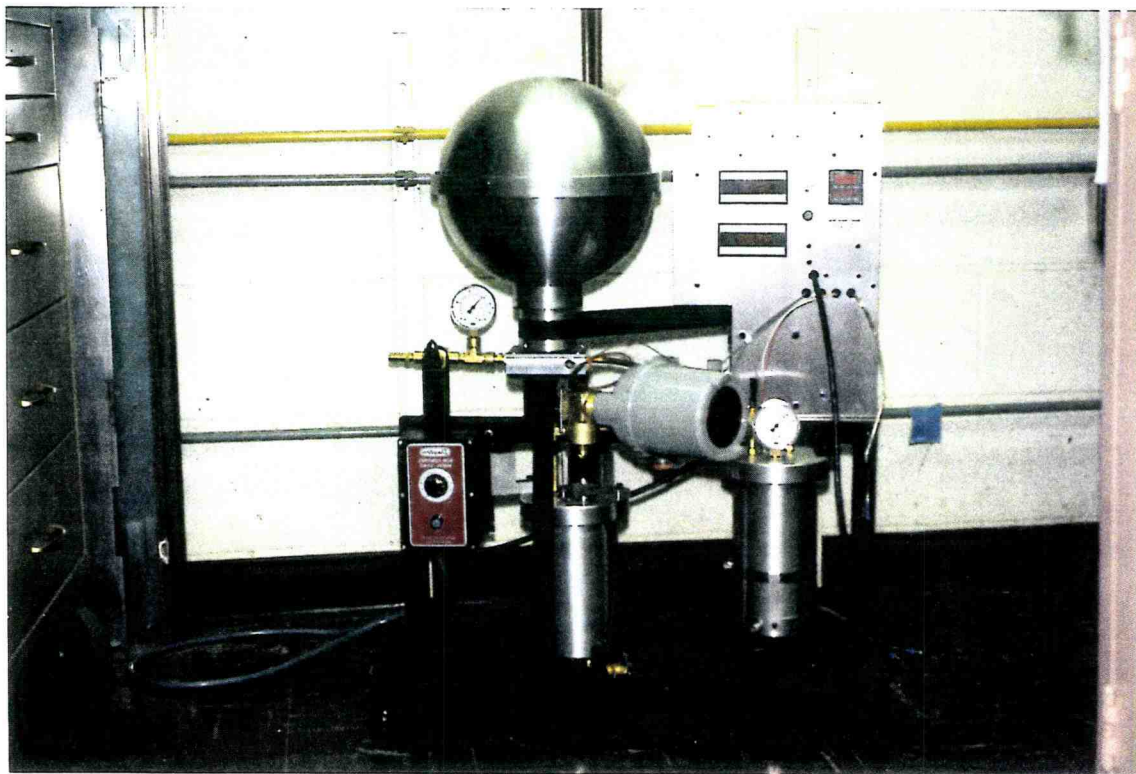

Ice Bucket Assembly

Water Bucket

Glass Pipe with the Rotating Motor and Vacuum Pump

Glass Pipe with Upper Aluminum Cover and Shield

Lower RBMR Hemisphere with Stationary Pipes

An Overall Picture of the RBMR Prototype